KTH ROYAL INSTITUTE
OF TECHNOLOGY

Doctoral Thesis in Chemical Engineering

Non-geological hydrogen storage for fossil-free steelmaking

JOAKIM ANDERSSON

Stockholm, Sweden 2022

Non-geological hydrogen storage for fossil-free steelmaking

JOAKIM ANDERSSON

Academic Dissertation which, with due permission of the KTH Royal Institute of Technology, is submitted for public defence for the Degree of Doctor of Philosophy on Friday the 8th of April 2022, at 2:00 p.m. in Kollegiesalen, Brinellvägen 8, KTH, Stockholm.

Doctoral Thesis in Chemical Engineering
KTH Royal Institute of Technology
Stockholm, Sweden 2022

ISBN 978-91-8040-162-3
TRITA-CBH-FOU-2022:21

Printed by: Universitetsservice US-AB, Sweden 2022

Abstract

In the last half-century, global steel use has increased more than threefold and further growth is expected, particularly in developing economies. However, steelmaking is currently responsible for 7% of the global net carbon dioxide (CO_2) emissions, and any substantial further optimization of existing processes that utilize fossil fuels for iron ore reduction is infeasible. Therefore, steelmaking must change for climate change mitigation targets to be achievable.

Hydrogen (H_2) steelmaking using H_2 produced via electrolysis is one way forward. A challenge is the substantial electricity demand of electrolysis. H_2 storage may lower the electricity cost of electrolysis by allowing a larger share of H_2 to be produced when the electricity price is low. Existing experience with large-scale H_2 storage is limited to salt caverns and the construction of such caverns requires suitable geological formations, which are neither ubiquitous nor well-distributed. However, geologically-independent H_2 storage technologies have not previously been evaluated for integration with H_2 steelmaking. This is the aim of this thesis.

H_2 storage technologies were reviewed and liquid H_2 carriers were identified as the most techno-economically feasible non-geological options. Out of these liquid carriers, methanol (CH_3OH) was found particularly promising for H_2 steelmaking due to the low heat demand of its dehydrogenation, its low-cost storage, and the high technological readiness of plants for both its production and dehydrogenation.

A complete CH_3OH-based H_2 storage concept was developed, including processes for CO_2 and heat supply. Its ability to reduce the H_2 production cost in a H_2 steelmaking process was evaluated via a deterministic optimization method based on historical electricity prices. Results indicate that CH_3OH-based storage may be competitive with geological storage options, especially for cases with long-duration electricity price patterns.

The option to also sell off accumulated CH_3OH from the storage was investigated. Such steel and CH_3OH co-production may improve storage utilization and reduce the risk of investment into H_2 storage as it allows for profitability to be reached under a more diverse set of electricity market conditions.

Keywords: hydrogen storage, fossil-free, steelmaking, industrial decarbonization, hydrogen direct reduction

Sammanfattning

Den globala stålanvändningen har mer än tredubblats under de senaste 50 åren och ytterligare tillväxt förväntas, framförallt i utvecklingsländer. Ståltillverkning står dock för 7 % av de globala nettoutsläppen av koldioxid (CO_2) och möjligheter till ytterligare optimering av nuvarande processer för järnmalmsreduktion baserade på fossila bränslen är begränsade. Nya ståltillverkningsmetoder krävs därför för att etablerade klimatmål ska kunna uppnås.

En väg framåt är järnmalmsreduktion med vätgas (H_2) producerad via elektrolys. En utmaning är elektrolysens stora elbehov. Ett H_2-lager kan reducera elkostnaden för elektrolys genom att tillåta att en större andel H_2 produceras när elpriset är lågt. Befintlig erfarenhet av storskalig H_2-lagring är helt begränsad till saltkaverner i geologiska saltformationer och dessa finns inte att tillgå överallt. Icke-geologiska H_2-lagringstekniker har dock inte tidigare utvärderats för H_2-baserad ståltillverkning, vilket är syftet med denna avhandling.

Flytande H_2-bärare identifierades som de mest tekno-ekonomiskt gångbara alternativen för icke-geologisk H_2-lagring. Av dessa bärare befanns metanol (CH_3OH) vara särskilt lovande för H_2-baserad ståltillverkning på grund av det låga värmebehovet för dess dehydrogenering, dess låga lagringskostnad och för att processer för både dess produktion och dehydrogenering har en hög teknisk mognadsgrad.

Ett komplett CH_3OH-baserat lagringskoncept för H_2-baserad ståltillverkning utvecklades, inklusive processer för CO_2- och värmeförsörjning. Detta koncepts förmåga att minska kostnaden för H_2-baserad ståltillverkning utvärderades via en deterministisk optimeringsmetod baserad på historiska elpriser. Resultat indikerar att H_2-lagring i CH_3OH kan vara konkurrenskraftigt med geologisk lagring, särskilt i särskilt i scenarier med ihållande perioder med höga elpriser.

Vidare undersöktes även möjligheter att inkludera försäljning av CH_3OH i lagringskonceptet. Resultat visar att sådan försäljning kan minska risken för investering i ett CH_3OH-baserat H_2-lager som en del av en H_2-baserad ståltillverkningsprocess då det gör det möjligt för lagret att nå lönsamhet under mer varierade elmarknadsförhållanden.

List of Appended Papers

I. *J. Andersson and S. Grönkvist, "Large-scale storage of hydrogen," International journal of hydrogen energy, vol. 44, no. 23, s. 11901-11919, 2019.

II. J. Andersson, A. Krüger and S. Grönkvist, "Methanol as a carrier of hydrogen and carbon in fossil-free production of direct reduced iron," Energy Conversion and Management: X, vol. 7, no. 100051, 2020.

III. A. Krüger, J Andersson, S. Grönkvist and A. Cornell, "Integration of water electrolysis for fossil-free steel production," International journal of hydrogen energy, vol. 45, no. 55, s. 29966-29977, 2020.

IV. J. Andersson, "Application of Liquid Hydrogen Carriers in Hydrogen Steelmaking," Energies, vol. 14, no. 5, s. 1392, 2021.

V. J. Andersson and S. Grönkvist, "A comparison of two hydrogen storages in a fossil-free direct reduced iron process," International journal of hydrogen energy, vol. 46, no. 56, s. 28657-28674, 2021.

VI. J. Andersson and S. Grönkvist, ”Improving the economics of fossil-free steelmaking via co-production of methanol” *submitted to Journal of Cleaner Production.*

*A corrigendum to this paper is also attached.

Related publications not included in the thesis:

Patent application: J. Andersson and S. Grönkvist, SE 2030072-9, “Methanol as hydrogen carrier in H-DRI process”

Contribution to the appended papers

Paper I: I conducted the literature review, performed all calculations, and wrote the paper.

Paper II: I wrote the paper and developed the process concept. I also performed all calculations, excluding the modeling of solid oxide electrolysis in Aspen, which was done by Andries Krüger.

Paper III: I helped define the process concepts and calculation methods. I also adapted the process model originally developed for paper II by me. I assisted Andries Krüger in writing the paper.

Paper IV: I am the sole author of this paper.

Paper V: I wrote the paper and performed all calculations.

Paper VI: I wrote the paper and performed all calculations.

The work in all papers was carried out under the supervision of Associate Professor Stefan Grönkvist.

Nomenclature

AEL	Alkaline electrolysis
AF	Annuity factor
ASU	Air separation unit
BF	Blast furnace
BECCS	Bioenergy carbon capture and storage
BOF	Basic oxygen furnace
CCS	Carbon capture and storage
CDRI	Cold direct reduced iron
CH_3OH	Methanol
CH_4	Methane
CO	Carbon monoxide
CO_2	Carbon dioxide
CRI	Carbon Recycling International
DAC	Direct air capture
DR	Direct reduction
DRI	Direct reduced iron
EAF	Electric arc furnace
EOC	Electrolyzer overcapacity
EU	European Union
EUROFER	European Steel Association
Fe	Iron
Fe_2O_3	Hematite (iron(III) oxide)
Fe_3C	Cementite
FeO	Wüstite (iron(II) oxide)
H_2	(Molecular) Hydrogen
H_2O	Water
HBI	Hot briquetted iron
H-DR	Hydrogen direct reduction
HHV	Higher heating value
HYBRIT	Hydrogen Breakthrough Ironmaking Technology
HyL	Hoyalata y Lamina S.A
IEA	International Energy Agency
IRENA	International Renewable Energy Agency
KOH	Potassium hydroxide
LHV	Lower heating value
LKAB	Luossavaara-Kiirunavaara Aktiebolag
LOHC	Liquid organic hydrogen carrier
LRC	Lined rock cavern
MSR	Methanol steam reforming
N_2	Nitrogen
NG	Natural gas
NH_3	Ammonia
NLP	Non-linear programming
O_2	(Molecular) Oxygen
PEMEL	Polymer electrolyte membrane electrolysis
SMR	Steam methane reforming
SOEL	Solid oxide electrolysis
TGR	Top gas recycling
ZR	Zero reformer
WACC	Weighted average cost of capital
WGS/rWGS	Water-gas shift/reverse water-gas shift

Contents

List of tables

List of figures

1 INTRODUCTION

It is difficult to exaggerate the importance of steel. Modern construction, transportation, agriculture, and electricity generation, to name a few examples, would simply be impossible without access to this inexpensive yet strong and durable material. Due to its importance for economic development, global steel use is expected to continue to grow up until and beyond 2050, largely driven by emerging economies [1]. However, steel is currently most commonly produced via the blast furnace-basic oxygen furnace (BF-BOF) process, which is inherently associated with significant emissions of carbon dioxide (CO_2). The majority of these emissions stem from the reduction of iron ore to iron via reaction with coke in the BF.

The second most common way to produce steel today is via scrap recycling in electric arc furnaces (EAFs). Although scrap-based EAF steelmaking is much less energy and CO_2-intensive than iron ore-based production, it is limited by the supply of high-quality steel scrap and this is expected to remain the case over the coming decades as steel demand continues to increase [2]. Therefore, iron ore-based steelmaking will persist for the foreseeable future and it is of utmost importance to find alternatives to the BF that allow the future steel demand to be met without endangering the fulfillment of climate change mitigation targets, most notably the 1.5 °C goal of the Paris Agreement [3, 4]. This requires rapid action. The recent 1.5 °C-compliant scenario by the International Energy Agency (IEA) suggests that steelmaking-related CO_2 emissions must be reduced by 91% by 2050 but also as much as 24% already by 2030 [5]. Consequently, due to the typically long investment cycles in the steel industry and the need for drastic process innovation, development and commercialization of near-zero CO_2 BF alternatives must occur during the 2020s [6, 7].

Although several pathways towards low-CO_2 iron ore-based steelmaking have received consideration from the steel industry over the last couple of decades—including approaches based around carbon capture and storage (CCS), increased use of biomass, and direct electrification—processes based on reducing iron ore by reaction with hydrogen (H_2) are increasingly the center of attention, particularly among European steelmakers [5, 8-11]. When iron ore is reduced with H_2, the only byproduct is water (H_2O). Consequently, the direct CO_2 emissions from such an ironmaking process may potentially be close to zero. However, this requires that H_2 can also be produced without significant emissions. The currently most mature technology that has the potential to achieve this is (H_2O) electrolysis, i.e., the electrochemical splitting of H_2O into H_2 and oxygen (O_2).

Perhaps the most prominent H_2-based steelmaking project is the HYBRIT (Hydrogen Breakthrough Ironmaking Technology) initiative, started in 2016 by Swedish steelmaker SSAB along with the state-owned mining company LKAB (Luossavaara-Kiirunavaara Aktiebolag), and the state-owned energy utility company Vattenfall AB. HYBRIT aims to develop and commercialize a completely fossil-free H_2 direct reduction (H-DR) steelmaking process based on H_2 production via electrolysis. After a pre-feasibility study in 2016, the three involved companies formed the joint venture company Hybrit Development AB. This company is currently involved in several pilot projects related to various parts of the fossil-free steel supply chain. The main part of the research presented in this thesis has been conducted as part of HYBRIT Research Project 1 (RP1), funded by SSAB, LKAB, Vattenfall AB, and the Swedish Energy Agency (Energimyndigheten).

A prerequisite for cost-effective fossil-free H_2 production via electrolysis is plentiful access to fossil-free electricity. It is widely expected that a large part of the additional electricity demand needed for H-DR steelmaking will be met by an expansion of wind and solar power in most regions, partly due to recent wind turbine and photovoltaic solar panel cost reductions, but also due to capacity expansion limitations for other types of renewable electricity generation, e.g., based on hydropower or biomass combustion [5, 12, 13]. A challenge is that electricity generation from both wind turbines and photovoltaic solar panels varies over time in an essentially uncontrollable manner. Therefore, more

volatile electricity prices are expected as the share of electricity generated by these variable sources in a given electricity market increases [14]. Such electricity price volatility may render H_2 production via electrolysis and, thus, H-DR steelmaking expensive during certain periods.

The integration of a H_2 storage allows for the electrolysis H_2 production rate to be varied so that more can be produced when electricity prices are low and vice versa. However, current experience with the kind of large-scale H_2 storage required for a full industrial-scale H_2 steelmaking plant is essentially entirely limited to storage in salt caverns and the geological salt formations required for the construction of such caverns are neither ubiquitous nor evenly distributed geographically [15, 16]. For instance, no suitable salt formations exist in Sweden, Finland, or large parts of the USA [17-19]. Consequently, other H_2 storage solutions than salt caverns must be sought in several important steelmaking regions.

The value of integrating a H_2 storage into a large-scale H-DR plant was recognized early on in the HYBRIT initiative [20]. As salt caverns are not a feasible option in Sweden, the main route pursued in HYBRIT is H_2 storage in lined rock caverns (LRCs). However, there currently exists only a single commercially operating LRC and it stores natural gas (NG), not H_2. H_2 storage in LRCs is, thus, an unproven concept. It may also be significantly more expensive than in salt cavern storages, particularly for large storage capacities [16, 21]. Moreover, the applicability of the LRC technology is also, like salt caverns, ultimately dependent on local geological conditions and there exist locations where neither storage technology is implementable. However, there exists exceedingly little literature related to large-scale non-geological H_2 storage and no known detailed techno-economic analysis of the integration of such storages in an H-DR steelmaking process. The research presented in this thesis aims to fill this gap by reviewing H_2 storage technologies and evaluating the most promising options for integration with an H-DR process from the perspectives of technological readiness, investment requirements, and operating costs.

1.1 AIM AND SCOPE

This thesis aims to identify and evaluate H_2 storage technologies that do not depend on special geological conditions for fossil-free H-DR steelmaking processes. The following research questions are pursued:

- What non-geological H_2 storage technologies are most promising for integration with a fossil-free H-DR steelmaking process from a techno-economic perspective?
- Could the identified most promising technologies be competitive with geological H_2 storages, particularly LRCs, from a techno-economic perspective?

As the first full industrial-scale H-DR steelmaking plants are planned to come into operation already during the mid to late 2020s, non-geological H_2 storage technologies that may be developed and deployed at the necessary capacity within a similar timeframe are the primary focus in this work [9]. The comparison with LRC-based H_2 storage is due to it being the only viable geological storage option in Sweden and, thus, the main option pursued in HYBRIT RP1. Other geological H_2 storage options potentially viable in other locations, e.g., salt caverns, are only described briefly.

The overall supply chain of fossil-free H-DR steelmaking consists of many steps. Although this thesis is primarily focused on the section of that supply chain that starts at electricity input and ends at H_2 delivery, design choices made both in the downstream iron and steelmaking processes and the upstream H_2 production electrolysis plant will affect the H_2 storage. Therefore, a basic H-DR process model was developed to determine the heat and mass flows of the process and to evaluate opportunities for H_2 storage process integration with an H-DR plant.

Other parts of the fossil-free H-DR steelmaking supply chain are considered outside of the scope of this thesis. This includes upstream aspects, e.g., iron ore mining, electricity generation, iron ore pelletization, and downstream aspects, e.g., metallurgical details of the steelmaking process, casting and rolling processes, and steel markets. Interactions between the H-DR steelmaking plant and the surrounding electricity system are also not analyzed, i.e., the plant is assumed to be an electricity '*price taker*'.

As this thesis is focused on H_2 storage, other potential sources of process flexibility in H-DR steelmaking are only discussed briefly. Consequently, steady-state iron and steelmaking rates are assumed in all calculations. A further delimitation is that only steelmaking processes based on so-called direct reduced iron (DRI, also called sponge iron) production from iron ore pellets containing predominantly hematite (Fe_2O_3) in shaft furnace reactors are considered, which is the main pathway pursued by most European steelmakers, including within the HYBRIT initiative [9, 22].

1.2 THESIS OUTLINE

This thesis consists of nine chapters, including this introductory chapter. The content covered in the remaining eight chapters is described below.

Chapter 2 provides background on current steelmaking practices and possible pathways towards the decarbonization of primary steelmaking. Some potential reasons for the strong current momentum behind H-DR steelmaking compared to other decarbonization pathways are discussed.

Chapter 3 describes the methodology applied in the later chapters of the thesis.

In Chapter 4, the basic principles of the H-DR process are introduced and various process design alternatives are discussed, including different electrolysis technologies. A developed H-DR process model used to determine mass and energy balances is described. Based on this process model, the fundamental economic prospects of H-DR and H_2 supply to such a process are presented and briefly discussed. The option to produce a carburized DRI intermediate, e.g., via H_2O and CO_2 co-electrolysis, is also discussed.

Chapter 5 first motivates and explains the basic function of H_2 storage in a large-scale H-DR steelmaking process. Thereafter, an overview of ways in which large amounts of H_2 have been and potentially can be stored is provided. The feasibility of the large-scale application of these alternative H_2 storage technologies in the context of an H-DR steelmaking process is evaluated based on basic thermodynamic and economic principles.

Chapter 6 considers technical and economic aspects of the integration of different liquid H_2 carriers for H_2 storage in an H-DR steelmaking plant. The prospective investment costs of such H_2 storage systems are compared to those of geological storage options.

Based on conclusions drawn in the previous chapter, chapter 7 compares the potential of LRC and CH_3OH-based H_2 storages to reduce the total H_2 production cost in a full industrial-scale H-DR plant. The analysis is based on a non-linear programming (NLP) storage operation optimization method and historical electricity prices.

Chapter 8 expands upon the analysis of methanol (CH_3OH)-based H_2 storage in the previous chapter to consider the economic impact of various CH_3OH-based H_2 storage process alternatives and also the possibility of selling off excess CH_3OH to external customers to potentially improve the overall economic performance of CH_3OH-based H_2 storage in an H-DR plant.

Chapter 9 Summarizes the main conclusions of the thesis and suggests some potential avenues for further research.

1.3 Relation to the United Nations Sustainable Development Goals

Steel is an important part of nearly all aspects of modern civilization. As the research presented in this thesis is fundamentally about lowering the overall cost of sustainable steelmaking, it, thus, relates to most of the 17 United Nations Sustainable Development Goals (SDG) in some way. Most notably, replacing the current BF-BOF process with fossil-free H-DR also enables reductions in steelmaking-related CO_2 emissions, which connects with SDG 13: climate action and SDG 9: industry, innovation, and infrastructure. However, while steelmaking, particularly from iron ore, is currently associated with significant climate impact, steel is also a material that is critical in achieving several of the SDGs as many fundamental necessities depend on access to it. Low-cost sustainably produced steel is, e.g., critical for sustainable food production (SDG 2: zero hunger); healthcare systems (SDG 3: good health and well-being); construction and transportation (SDG 11: sustainable cities and communities); and water supply systems (SDG 6: clean water and sanitation for all), to name just a few examples.

Looking more specifically at the part of H-DR steelmaking under investigation in this thesis, the role of H_2 storage in fossil-free H-DR steelmaking is to allow for a flexible electricity demand. This enables the H-DR steelmaking plant to adjust production according to variations in electricity supply and to provide various grid services, which can help the integration of increasing shares of wind and solar power in the electricity generation mix. This relates to SDG 7: affordable and clean energy.

2 BACKGROUND

2.1 STEELMAKING TODAY

Steel is an alloy of a greater part of iron (Fe) and up to around 2% (most often <0.5%) by weight carbon (C), often along with other elements, e.g., molybdenum (Mo), boron (B), niobium (Nb), nickel (Ni), vanadium (V), tungsten (W), manganese (Mn), titanium (Ti), or chromium (Cr). Thousands of steel variants exist with a wide array of different properties (e.g., strength, hardness, flexibility, corrosion resistance, hardenability) depending on elemental composition and treatment. However, the most common kind of steel is carbon steel, which consists of predominantly Fe and C [1].

Around 1.9 billion t of steel were produced during 2020 [1, 23]. China is the dominating producer (57% during 2020), followed by the EU countries (7%). Other major steel-producing countries include India (5%), Japan (4%), the USA (4%), Russia (4%), and South Korea (4%). Sweden produces approximately 3% of the total steel production in the EU and is, thus, globally a relatively minor player. The main uses for steel are currently in construction (52%), transport (17%), and mechanical equipment (16%) [23].

Two kinds of steel production exist: 1) '*primary*' production from iron ore via the BF-BOF or, far less commonly today, direct reduction-electric arc furnace (DR-EAF) processes; 2) '*secondary*' production from recycled steel scrap, most often using an EAF[1]. Around 68% of global steel production is based on iron ore and 32% is based on scrap [1]. However, the relative shares of primary and secondary steelmaking vary significantly around the world depending on, e.g., scrap availability, scrap purity, access to natural resources, labor cost, and steel industry structure [24-29]. For instance, 67–68% of steel production in the USA takes place in EAFs, compared to less than 10% in China [27, 30]. Primary steelmaking is mostly concentrated to a few countries while EAF-based secondary steelmaking is more widely geographically distributed due to the lower associated investment costs [28, 30]. BF-BOF-based plants are also typically much larger than EAF-based plants due to different economies of scale. As an example, in Europe, the average steel production capacities of BF-BOF sites (24 in total) and EAF sites (126 in total) are 4.3 and 0.7 Mt steel/y, respectively [31, 32].

Secondary steelmaking is much less energy and CO_2-intensive than primary steelmaking as the iron in the recycled steel scrap has already been reduced. Increased steel scrap recycling would, thus, be beneficial for reducing the climate impact of steelmaking. However, due to projected increases in steel demand and known limitations to recycling, e.g., due to copper contamination, secondary steelmaking in EAFs is only expected to reach 46–70% of total steel production by 2050, leaving significant continued demand for primary steelmaking [5, 26, 33-36].

This thesis deals predominantly with primary steelmaking as this is where most of the industry's CO_2 emissions currently originate and also where H_2 and its large-scale storage could play a major role. Primary steelmaking can be divided into three main processes: 1) raw material preparation, in which mined iron ore is refined, agglomerated, and compacted, predominantly to pellets or sinter; 2) ironmaking, which mainly involves the reduction of iron oxides contained in the iron ore, generally hematite (Fe_2O_3), to metallic iron (Fe); and 3) steelmaking, which involves refining and purification of the products from the ironmaking step to yield crude steel [1, 37]. This crude steel can be refined further via, e.g., vacuum degassing or ladle metallurgy, and then continuously cast into semi-finished steel products, i.e., slabs, billets, or blooms [38].

[1] The distinction is between primary and secondary is somewhat blurred by the fact that smaller amounts of steel scrap and iron ore can be added to BOFs and EAFs, respectively.

The majority of CO_2 emissions related to steel production stem from ironmaking processes. The most common ironmaking processes today are the BF and DR. The fundamental difference between these processes is the state of aggregation of their iron-rich products: BFs yield a liquid product known as pig iron, while DR processes produce solid DRI. The BF also outputs a slag byproduct that contains a large share of the nonferrous material of the fed iron ore. In contrast, no slag is formed in DR processes and, thus, impurities in the iron ore pellets remain in the DRI. Worldwide production of pig iron (1 281 Mt in 2019) currently far outmatches that of DRI (108 Mt in 2019), although DRI production growth has been significant in recent years (up 40% between 2012 and 2019) [23]. DRI production capacity is mainly situated in regions with access to low-cost NG or where access to high-quality bituminous coal is limited. India (32% in 2020) and Iran (29%) dominate current DRI production, followed by Russia (8%), Saudi Arabia (5%), and Mexico (5%) [39].

The BF and various DR ironmaking processes are described in the coming sections. While the BF is the currently dominating ironmaking process, H-DR shares far more similarities with current DR processes. As this thesis is mainly concerned with H-DR, most of the focus is, thus, on the DR processes.

2.1.1 Blast furnace ironmaking

The BF is, in essence, a vertical counter-current flow reactor for the reduction of iron ore to yield pig iron (see Figure 1). The origins of the modern BF lie in the bloomery furnace, from which it evolved during the 14th century [40]. The largest operating BFs have annual production capacities of around 5.5 Mt pig iron [41].

The main BF reduction agent sources are coke and pulverized coal. Coke is usually produced onsite in coke ovens via the pyrolysis of high-quality bituminous coals. In modern BFs, around 290–320 kg of coke, fed along with iron ore pellets or sinter from the top of the furnace, and 150–220 kg of pulverized coal, injected together with hot blast air through tuyéres located towards the bottom of the BF, are consumed per t of pig iron [22, 42, 43]. The amounts of coke and pulverized coal fed to state-of-the-art BFs are very close to theoretical minimum values [44]. Other fuels can also be injected with the blast air, e.g., NG, waste plastics, coke oven gas, H_2, or bio-carbon, but pulverized coal is most commonly used [8, 29, 31, 40, 45].

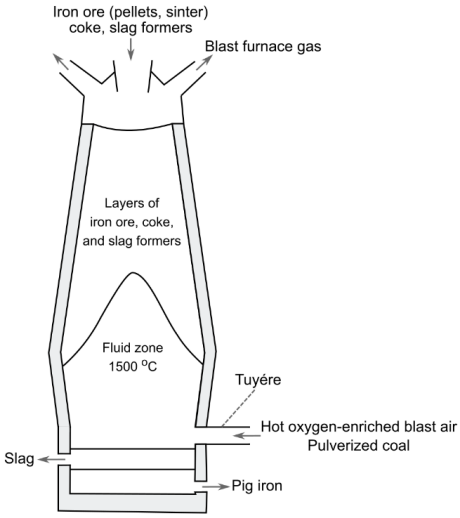

Figure 1: Basic operation of the blast furnace.

Coke and pulverized coal react with O_2 in the air fed through tuyéres. This leads to the formation of carbon monoxide (CO) in an exothermic reaction[2] [46, 47]:

$$C + 0.5\ O_2 \rightarrow CO \qquad \text{(R1)}$$

The CO formed via reaction (R1) rises and meets the descending iron ore, reducing Fe_2O_3 to Fe in an exothermic net reaction. CO_2 is formed as a byproduct:

$$Fe_2O_3 + 3\ CO \rightarrow 2\ Fe + 3\ CO_2\ (\Delta h_R^0 = -24.8 \frac{kJ}{mol}) \qquad \text{(R2)}$$

The conversion of CO to CO_2 via (R2) is never complete and some CO always leaves with the BF (top) gas, which typically contains 20–28% CO, 17–25% CO_2, 45–55% nitrogen (N_2, from blast air) and 1–5% H_2 by volume [29, 48, 49]. Small amounts of H_2 are always present in the BF gas due to the small hydrogen content of coke, moisture in the blast air, and moisture in the pulverized coal [29, 45, 50]. The BF gas is combusted to preheat the blast air and often to generate heat and electricity in an onsite power plant [29, 48]. The overall CO_2 intensity of BF-BOF steelmaking is 1.9–2.0 t/t steel for state-of-the-art plants, including coke production and the combustion of process off-gases [1, 35].

The iron ore pellets and sinter fed to the BF do not consist of pure Fe_2O_3 [51]. The non-iron part, which consists mainly of various oxides, is referred to as gangue [52, 53]. The majority of this gangue is removed in the BF via the formation of a slag [40]. Appropriate BF slag formation is promoted via the addition of slag formers, e.g., burnt lime and dolomitic lime, to the charge [42]. The slag has a lower density than pig iron and is, thus, readily separated out at the bottom of the BF [41].

2.1.2 Direct reduction ironmaking

DR processes are defined by the reduction of iron ore to metallic iron in the solid phase, i.e., the reduction is '*direct*' without melting. This reduction is achieved via reaction with a reducing gas rich in H_2 or CO or a combination thereof, typically generated via NG reforming, although coal gasification is also used in locations where NG is not available or where it is costly [53, 54]. Here only DR processes based on NG are covered as these are both more common and more similar to H-DR.

DRI is generally a more flexible product than pig iron. While pig iron is nearly always immediately brought to an adjacent BOF, standalone DRI production is relatively common [39]. DRI can either be the primary iron source for EAF steelmaking, which is common in a few regions, e.g., in the middle east, or it can be mixed with recycled steel scrap to reduce the concentration of nonferrous metals, most notably copper and tin, in the total EAF charge [29, 55-57]. While most DRI is ultimately fed to EAFs, smaller amounts are also used in BFs or BOFs as supplementary ferrous material [29, 53].

Most DRI production takes place in vertical shaft furnace reactors, in which the gas enters from the bottom and iron ore pellets enter from the top [58]. DR processes based on fluidized bed reactors are much less common and are not considered further here [39]. Reduction of Fe_2O_3 with CO is exothermic and produces CO_2 as a byproduct per (R2); reduction with H_2 instead yields H_2O via an endothermic reaction:

$$Fe_2O_3 + 3\ CO \rightarrow 2\ Fe + 3\ CO_2\ (\Delta h_R^0 = -24.8 \frac{kJ}{mol}) \qquad \text{(R2)}$$

$$Fe_2O_3 + 3\ H_2 \rightarrow 2\ Fe + 3\ H_2O\ (\Delta h_R^0 = 99.5 \frac{kJ}{mol}) \qquad \text{(R3)}$$

[2] Reaction (R1) can also be represented as a two-step process: $C + O_2 \rightarrow CO_2$; $CO_2 + C \rightarrow 2\ CO$.

Due to the larger share of iron ore reduction via reaction with H_2, DR ironmaking is inherently less CO_2-intensive than BF processes [53, 59, 60]. The overall CO_2 intensity of steelmaking via the DR-EAF route depends to a large part on how the electricity supplied to the EAF is generated [45].

It is not economically viable to achieve a complete reduction of all Fe_2O_3 in fed pellets to Fe in DR processes [53, 61, 62]. The DRI metallization describes the share of total Fe in the DRI that is fully reduced. The remaining iron oxide in DRI is in the form of wüstite (FeO) [54]. The DRI metallization is defined as:

$$Metallization_{DRI} = \frac{n_{Fe}}{n_{Fe} + n_{FeO}} \quad (1)$$

In conventional DR plants, typical DRI metallization is 90–96% [53]. The remaining FeO in the DRI can be reduced to Fe in the downstream EAF via reaction with carbon, which is either fed externally or is part of the DRI product due to carburization [51, 63]. However, part of the DRI FeO content is also lost with the EAF slag [51, 64].

DRI produced in modern DR plants typically contains 0.5–5.0% carbon by weight [65, 66]. Most of this carbon (65–90%) is incorporated into the DRI in the form of cementite (Fe_3C) but some is also present as graphite (sometimes referred to as "free" carbon) [67]. DRI carburization reactions can be summarized as [54, 61, 67]:

$$3\,Fe + 2\,CO \rightarrow Fe_3C + CO_2\ (\Delta h_R^0 = -148.7\,\frac{kJ}{mol}) \quad (R4)$$

$$3\,Fe + CO + H_2 \rightarrow Fe_3C + H_2O\ (\Delta h_R^0 = -105.0\,\frac{kJ}{mol}) \quad (R5)$$

$$Fe + CO + H_2 \rightarrow Fe(C_{free}) + H_2O\ (\Delta h_R^0 = -135.6\,\frac{kJ}{mol}) \quad (R6)$$

$$3\,Fe + CH_4 \rightarrow Fe_3C + 2\,H_2\ (\Delta h_R^0 = 98.3\,\frac{kJ}{mol}) \quad (R7)$$

Carburization plays an important role in the downstream processing of the DRI in several ways. Firstly, carbon in the DRI helps reduce remaining FeO in the EAF; utilizing the carbon in carburized DRI for this remaining reduction is far more efficient than via the addition of external carbon as a large part of injected carbon tends to combust rather than reduce FeO [45, 63, 68, 69]. Secondly, carburization makes the DRI less reactive towards air and H_2O, reducing its tendency towards re-oxidation during storage and transportation [70]. Thirdly, any excess carbon in the DRI beyond that needed for FeO reduction can be oxidized inside the furnace to provide heat for the melting process, thereby reducing the EAF electricity demand [63, 71]. Fourthly, oxidation of the carbon in the DRI forms CO, which leads to so-called slag foaming [72, 73]. Slag foaming improves the efficiency of the EAF, helps remove impurities from the steel, stabilizes the electric arcs, reduces furnace noise, and protects the furnace lining and graphite electrodes [72, 74, 75]. However, DRI carburization should also not be too high as the rate at which excess carbon can be burned off in an EAF via O_2 injection is generally limited [63]. An overly high DRI carburization may, thus, decrease the EAF productivity [63, 71]. More O_2 must also be provided to the EAF to burn off more excess carbon, increasing operational costs and increasing the risk of FeO losses with EAF slag [63, 64].

The DRI product emerging from the bottom of the shaft furnace can be directly fed to an EAF. This is advantageous from an energy perspective as the significant sensible heat of the DRI helps reduce the electricity demand and time required for melting in the EAF [53, 55]. Feasible DRI feed temperatures are 600–700 °C for state-of-the-art hot delivery systems [65, 76]. The reduction in EAF electricity demand with increasing DRI feed temperature is approximately 20 kWh/t liquid steel for every 100 °C [29, 77, 78]. However, as mentioned, a significant share of DRI produced today is not intended for

immediate feed to an EAF, and standalone DR plants are rather common [39]. Systems for the direct transferal of hot DRI to EAFs are also relatively new [78].

An important aspect of standalone DRI production is the prevention of DRI re-oxidation during storage or transportation. Such re-oxidation would not only constitute an economic loss, but it could also pose a safety risk due to the strongly exothermic nature of the oxidation process [53, 78, 79]. There are two main ways in which re-oxidation is prevented: 1) rapid DRI cooling to approximately 50–60 °C, typically by injection of cold NG in the bottom section of the shaft furnace; 2) compaction of still hot DRI to produce hot briquetted iron (HBI) [53, 55, 67, 71]. HBI production is particularly suitable if the product is to be shipped long distances as the compaction process also leads to a higher solid density [55, 78]. The vast majority of DRI is currently produced as cold DRI (CDRI, around 80% in 2020), but the share of hot DRI (for direct feed to an EAF) is increasing [39]. DR plants can often produce different kinds of DRI (hot DRI, CDRI, or HBI) in various combinations depending on current downstream requirements [80].

As in the BF, iron ore pellets used in DR processes do not consist solely of Fe_2O_3 [53, 81-83]. Gangue in fed iron ore pellets can later be separated out as slag in a downstream EAF. However, as the capacity for efficient slag separation is more limited in an EAF compared to in the BF-BOF process, iron ore pellets applied for DR processes generally must have lower gangue content and are, thus, more expensive than those intended for BFs [41, 52, 53, 83]. The addition of slag formers, typically 30–60 kg/t liquid steel for DRI feeds, to the EAF facilitates the slag separation process [52, 84, 85].

The current DR market is highly concentrated to just a few equipment suppliers, out of which processes from Midrex Technologies and Tenova HyL currently dominate [39, 53, 86]. As these DR processes differ quite substantially in several regards, despite both being based on shaft furnaces, they are described separately in the upcoming sections.

2.1.2.1 Midrex process

The Midrex process, first developed by the Midland Ross Corporation of Cleveland during the late 1960s, was the first commercialized shaft furnace DR process [54, 86]. Midrex Technologies was acquired by Japanese Kobe Steel (Kobelco) in 1983 [87]. The Midrex process is currently the world's most prominent DR process—in 2020 it was responsible for around 60% of all DRI production (80% of all shaft furnace DRI production) [39]. The largest currently operating Midrex process plants have production capacities of 2.5 Mt DRI/y [88, 89]. A basic process scheme is seen in Figure 2.

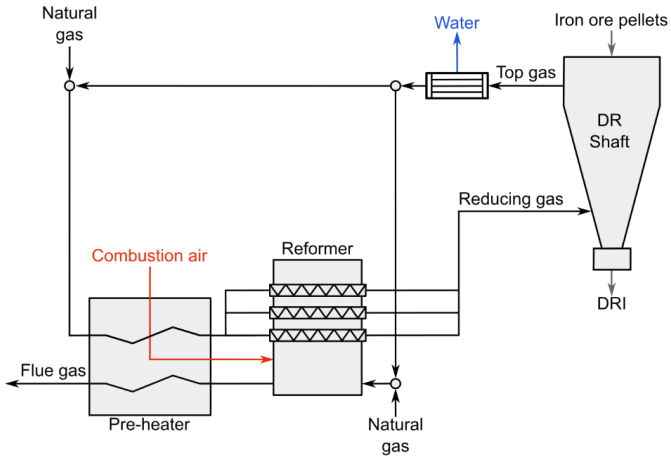

Figure 2: Midrex direct reduction process.

The reducing gas, produced via reforming NG with recycled top gas, enters the shaft reactor at 900–1 000 °C [53, 86]. O_2 produced via an air separation process can be also added to the reducing gas before it enters the shaft furnace to further increase its temperature via partial oxidation [53]. Full conversion of CO and H_2 in the reducing gas is not achieved in a single pass through the shaft furnace; the top gas typically still contains 60–70% H_2 and CO by volume [53]. The temperature of the top gas is commonly around 400 °C [29, 90]. Part of the H_2O in the top gas is removed via a scrubber. This scrubber also removes any dust carried with the top gas from the shaft, which could otherwise damage the reformer catalyst [29, 59]. Typically around a third of the top gas is combusted to provide heat for the reforming process, and the rest is recycled to the reformer along with make-up NG [91]. The shaft furnace pressure is relatively low, typically 1.2 to 2.5 bar [68, 90, 92].

A distinguishing feature of the Midrex process is its reformer. This reformer is different from an ordinary steam methane reformer (SMR) in that NG, which mostly consists of methane (CH_4), reacts with both H_2O (as in SMR) and CO_2 to form H_2 and CO [59].

$$CH_4 + H_2O \rightarrow 3\,H_2 + CO \ (\Delta h_R^0 = 206.0\,\frac{kJ}{mol}) \quad \text{(R8)}$$

$$CH_4 + CO_2 \rightarrow 2\,H_2 + 2\,CO \ (\Delta h_R^0 = 247.0\,\frac{kJ}{mol}) \quad \text{(R9)}$$

Due to the partially CO_2-based reforming process, the resulting reducing gas is quite CO-rich compared to other NG-based DR processes. The reactions take place on a nickel-based catalyst in the reformer. The sulfur content in the recycled top gas must be kept low to prevent the gradual poisoning of this catalyst [93]. The main source of this sulfur is the iron ore pellets fed to the process which generally should contain less than 0.01% sulfur by weight to be suitable for use in the Midrex process [53, 94].

2.1.2.2 HyL Energiron III and ZR processes

Hoyalata y Lamina S.A. (HyL) of Mexico started developing DR processes already in the 1950s [86]. The earliest HyL DR processes (HyL I and HyL II), the first commercialized DR processes of any kind, were fixed bed batch reduction processes, which were made obsolete upon the development of shaft furnace DR technology during the late 1960s and 1970s, first by Midrex and later by HyL themselves (the HyL III process, first introduced in 1979) [54, 61, 67, 95]. The technology developed by HyL is currently owned by the Italian company Tenova [53]. Tenova joined a partnership with Danieli (also Italian) in 2006 to offer two DR processes: HyL Energiron III and ZR [86, 96, 97]. The largest HyL Energiron III and ZR plants currently in operation have production capacities of 2.5 Mt DRI/y [97, 98]. In total, around 12% of global DRI is produced via these processes [39].

The HyL Energiron III process is based on the generation of reducing gas via an external conventional SMR process, i.e., via reaction (R8), which results in a much H_2-richer reducing gas than in the Midrex process [87]. Unlike in the Midrex process, no top gas is recirculated to the reformer. Consequently, CO_2 must be removed from the gas loop in a different way to prevent its accumulation. In the first HyL III plants, this was achieved by purging a large part of the top gas. This strategy is not optimal as the top gas contains large amounts of H_2 and CO that can potentially be recycled to the shaft furnace. To solve this issue, a top gas CO_2 absorption system was introduced to the HyL III process in 1986 [99-101].

Another difference of HyL Energiron III to the Midrex process is the higher shaft furnace pressure (4–6 bar) [102, 103]. This allows for a smaller shaft furnace for the same DRI production capacity and reduces the reducing gas flow velocity, which results in lower dust (and, thus, iron) losses with the top gas [70, 100, 104]. The high pressure also benefits the top gas CO_2 capture process [104, 105]. As no top gas is recycled to the reformer, more sulfur-rich iron ore pellets can be utilized than in the Midrex process.

The HyL Energiron ZR (‘*zero reformer*’) process, first introduced in 1998, does not feature a separate reformer reactor [86]. Instead, NG reforming takes place inside the shaft furnace where the hot DRI acts as a catalyst [68]. A process scheme for the HyL Energiron ZR process is seen in Figure 3.

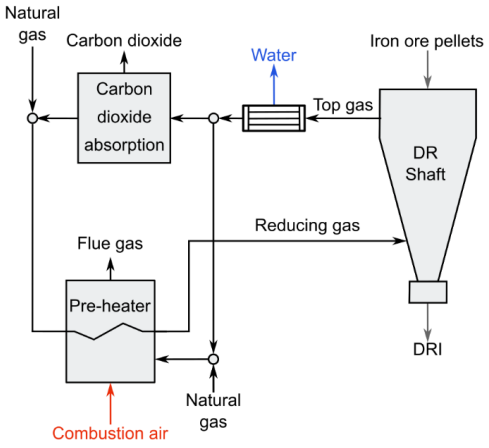

Figure 3: Process scheme for HyL Energiron ZR direct reduction process.

As in HyL Energiron III, both H_2O and CO_2 are removed from the top gas before it is recycled. The reducing gas, rich in CH_4, is preheated and sent directly to the shaft furnace without prior reforming. Typically, additional O_2 is added to the reducing gas before it enters the shaft furnace. The temperature and pressure in the shaft furnace are both high: >1 000 °C and 6–8 bar, respectively [105]. One advantage of internal NG reforming is that higher DRI carburization (up to above 5% by weight) can be achieved compared to when an external reformer is used [68, 105].

2.2 Pathways towards the decarbonization of primary steelmaking

As briefly mentioned in the introduction of this thesis, four pathways for primary steelmaking decarbonization have been suggested: 1) CCS-based approaches, 2) biomass-based approaches, 3) direct electrification, 4) H_2-based approaches [11, 32]. In recent years, steelmakers around the world and particularly in Europe have increasingly focused on the last option in this list and this thesis also primarily deals with this route. Nevertheless, the basic merits and drawbacks of the other primary steelmaking decarbonization routes are briefly discussed in the coming sections to provide some context for H_2-based steelmaking and its potential relative advantages and weaknesses.

2.2.1 Carbon capture and storage

CCS is the process of capturing, compressing, transporting, and then storing CO_2 emitted from power plants or industrial processes. This prevents the CO_2 from reaching the atmosphere where it would affect the earth’s climate. Several CO_2 capture technologies are available, e.g., absorption, adsorption, membranes, and cryogenic separation [106]. The optimal choice of capture technology depends on the partial pressure of CO_2, the presence and concentration of impurities in the stream from which CO_2 is to be captured, costs of electricity and heat, and the possibilities for heat integration with the existing process. The idea of CCS is far from new, having first been suggested by Cesare Marchetti at the Austrian International Institute for Applied Systems Analysis (IIASA) during the 1970s [107-109]. CCS is the only retrofit solution that can significantly reduce direct CO_2 emissions from BF or DR facilities [110]. However, although the continued utilization of assets appears attractive, the actual uptake of CCS in the steel industry is yet negligible.

No major steelmaking company is currently actively pursuing BF CCS [10, 111, 112]. However, at the same time, the need for BF CCS is widely recognized in many prominent industry and energy system roadmaps; CCS-based plants (most BF-based) provide around 50% of primary steel production by 2050 in the IEAs recently published Net Zero Emissions scenario and integrated assessment models used by the Intergovernmental Panel on Climate Change also typically show significant uptake of BF CCS steelmaking by mid-century in Paris Agreement-compliant scenarios [5, 34, 113, 114]. However, the actual role that BF CCS will play in decarbonizing the steel industry is uncertain at present, since these projections say nothing about the actual development and current commercial interest is low.

One prominent technology in the context of BF CCS is top gas recycling (TGR) [47]. TGR allows for a larger share of CO produced in the BF to reduce iron ore instead of being combusted for heat and electricity generation. This increased CO utilization reduces the specific coke and pulverized coal demand and can improve the overall BF productivity [49, 115]. To allow for TGR, pure O_2 is fed through the tuyéres (instead of air) and CO_2 is separated out from the BF gas before recycling. TGR based on vacuum pressure swing adsorption (VPSA) was investigated by LKAB at their Luleå experimental BF as part of the Ultra-low CO_2 Steelmaking (ULCOS) project from 2007 to 2010 [115, 116]. A 76% reduction of the specific CO_2 emissions of the BF could be achieved along with a reduction in specific BF coal and coke demand by 20–25% [117, 118]. Although these initial LKAB trials were successful, no TGR demonstration plant has yet been built.

An inherent problem with CCS in BF-BOF plants is that direct CO_2 emissions occur at multiple points—even if all CO_2 in the BF gas is captured, 30–40% of the plant emissions will remain and also capturing these may be associated with high costs [35, 116, 118-120]. It has been recognized in recent years that this reduction may not be sufficient to meet emissions reduction targets [121]. For instance, the European Steel Association (EUROFER) targets a reduction of specific steelmaking CO_2 emissions by 80–95% by 2050 (compared to 1990 levels) and most major steelmakers have established 2050 carbon or climate-neutrality targets in recent years [9, 36, 113].

As mentioned in section 2.1.2.2, CO_2 capture is an inherent part of the HyL Energiron III and ZR DR processes. However, most CO_2 captured in operating plants is vented, although some is also sold to, e.g., food or beverage industries [122]. To date, there exists a single HyL Energiron plant, located in Abu Dhabi, where the captured CO_2 (around 800 kt/y) is stored underground via so-called enhanced oil recovery, a method to increase the share of extractable crude oil from an oil field [1, 123-125]. This gives a financial incentive to capture and store the CO_2, but since the method is performed to increase the extraction of fossil hydrocarbons, it is controversial to argue that enhanced oil recovery is a measure to mitigate climate change [126]. Nevertheless, the integration of CO_2 transport and storage in existing HyL Energiron plants appears a low-hanging fruit in terms of reducing CO_2 emissions from primary steel production [29]. It should be noted that this would not eliminate CO_2 emissions from such HyL Energiron plants as the reducing gas preheating process still generates CO_2 that is not captured (around 40% of the total CO_2 produced in the process) [85, 122].

2.2.2 Increased use of biomass

Biomass has played a critical role in steelmaking historically as bio-carbon (also known as charcoal), produced via the pyrolysis of biomass, was the original and for a long time the only source of heat and carbon for iron ore reduction [127]. In the early 18th century, the transition from bio-carbon to coke for iron ore reduction commenced, first in England, where access to wood resources was limiting further expansion of domestic ironmaking [128]. However, the transition from bio-carbon to coke was slow, particularly in areas that were less limited by access to biomass. For instance, in forest-rich Sweden, bio-carbon remained dominant well into the 20th century. Eventually, concerns regarding deforestation and process advantages related to coke use, particularly its higher compressive strength compared to bio-carbon, which allowed for larger and more efficient BFs to be constructed, prevailed [29, 129, 130].

Today, only very small BFs (<0.3 Mt/y pig iron) in Brazil operate fully on bio-carbon and replacement of coke with bio-carbon is very limited in modern BFs (generally <10%) [45, 118, 127, 131-133]. Replacing injected pulverized coal with biomass-based alternatives is easier as the mechanical properties are then less critical [28, 43, 44, 127, 131]. Nevertheless, the feasible total reduction in specific net CO_2 emissions via the use of biomass-based reductants in modern BFs has been estimated to be limited to 30–40% [44, 131, 134, 135].

There is no similarly strict limitation to biomass use in DR processes. In theory, it is perfectly possible to operate a DR process with a reducing gas that has been generated via biomass gasification or pyrolysis [134, 136]. That said, there are technical and economic challenges that would have to be overcome for such a DR process to be commercially viable [136].

Beyond physical and chemical properties, another barrier towards increased biomass use in any kind of primary steelmaking is feedstock cost, particularly if the biomass must be upgraded, e.g., to syngas (a mixture of mostly H_2 and CO) via gasification or pyrolysis, synthetic NG, or bio-carbon, before use [43, 131]. An rising competition for available biomass resources is also expected as fossil fuels are gradually phased out from the energy system, particularly due to an increased use of biomass for the production of chemicals and fuels for heavy-duty transportation [35, 137]. Nevertheless, if steelmaking is to become entirely fossil-free, biomass will most likely have to be the source for the carbon contained in all steel at the very least [13, 74].

As previously mentioned, a problem with BF-BOF CCS is that it is difficult to eliminate plant net CO_2 emissions. Therefore, combinations of biomass use and CCS in BFs have been suggested in recent years to get around this issue [28, 134]. However, even combinations of biomass-based injectants and CCS struggle to reduce BF net CO_2 emissions to (below) zero [134]. In contrast, as there are no fundamental limitations to biomass use in DR, combinations of biomass use and CCS may yield negative emissions steelmaking in such processes [28, 91, 134].

2.2.3 Direct electrification

Instead of using an intermediate reducing agent, e.g., coke, coal, bio-carbon, or H_2, it is theoretically possible to directly electrolyze Fe_2O_3 to metallic Fe with O_2 as the sole byproduct:

$$Fe_2O_3 \rightarrow 2\,Fe + 1.5\,O_2 \qquad \text{(R10)}$$

Although iron ore electrolysis appears attractive as inefficiencies related to the production of an intermediate reductant can be avoided, the actual implementation of a process of this kind is challenging for several reasons and has not yet occurred beyond the laboratory scale [1]. Due to this immaturity, it is difficult to assess the role that these technologies will play in decarbonizing primary steelmaking [31]. Two kinds of iron ore electrolysis processes have been suggested: 1) electrowinning, which is based on an alkaline sodium hydroxide electrolyte and an operating temperature of approximately 110 °C, and 2) molten oxide electrolysis, which is based on a molten mixed silicon or calcium oxide electrolyte operating at over 1 500 °C [1, 138-141].

Electrowinning requires that part of the iron ore gangue material is first removed via a leaching process [31, 117]. The subsequent electrolysis process produces nearly entirely pure Fe plates. These plates can then be processed in an EAF to produce steel, similar to DRI-based steelmaking. The total electricity demand of steel production via electrowinning and EAF has been estimated at 3.6 MWh/t liquid steel (76% of this is for the electrolysis process) [31].

Molten oxide electrolysis is similar to the common Hall-Héroult aluminum production process, although that process operates at lower temperatures (around 960 °C vs. >1 500 °C). In contrast to electrowinning, molten oxide electrolysis does not require significant iron ore pretreatment. Instead, this process is more akin to the BF in that iron ore gangue is separated out via a slag [31]. This

potentially allows for direct liquid steel production from iron ore within a single furnace. The electricity demand of scaled-up molten oxide electrolysis has been estimated at 4.1–4.8 MWh/t liquid steel, although what efficiency can be achieved in a full-scale process is still uncertain [31, 142]. If one considers the same efficiency as in principally similar aluminum production plants, the electricity demand of molten oxide electrolysis would be 5.5 MWh/t Fe [143]. One challenge of molten oxide electrolysis is the identification of cost-effective electrode materials that can withstand the highly corrosive conditions in the furnace [140].

2.2.4 Summary of pathways and comparison with hydrogen direct reduction steelmaking

All pathways towards the decarbonization of primary steelmaking are associated with challenges. As mentioned previously, there is currently significant momentum behind H-DR steelmaking, particularly in Europe. Compared to the other primary steelmaking decarbonization pathways, H-DR steelmaking appears to offer an attractive combination of scalability, a relatively high technological readiness level (given the significant similarities to conventional DR processes), and CO_2 emissions mitigation potential. A critical enabling factor of H-DR steelmaking mentioned by most authors is the falling costs of renewable electricity generation. Electrowinning and molten oxide electrolysis also benefit from lower electricity prices but are currently considered much further away from commercialization [1]. Another potential advantage of the H-DR steelmaking route is the flexibility of its product: fossil-free DRI produced vid H-DR may potentially be used in already existing EAFs, BFs, and BOFs, reducing the CO_2 intensity of already existing assets.

Biomass-based approaches are essentially limited by the access to sufficiently large amounts of sustainably sourced biomass and are, therefore, only viable in a limited number of regions. The need for various biomass upgrading processes before use in BFs or DR processes also increases costs. In the case of biomass use in BFs, entirely replacing coke with a biomass-based alternative has proved challenging.

The case for CCS in steelmaking appears strong at first glance given both the relatively high concentrations of CO_2 in process gases and the, by all accounts, successful trials of the TGR concept in the ULCOS project. Despite this, interest from major steelmakers has been low in recent years [10]. One possible reason is the difficulty of completely eliminating CO_2 emissions from a BF-BOF site via CCS. Another possible barrier towards primary steelmaking CCS is its marketability and public perception, particularly regarding CO_2 storage, in certain regions [10, 13, 120, 144]. Nevertheless, it appears that some degree of CCS deployment in the steel industry may be necessary to meet various CO_2 emissions reduction targets. CCS-based steelmaking is also substantially less dependent on electricity generation expansion than H-DR or direct electrification options, which may well end up a limiting factor in regions with low potential for low-cost wind or solar power [34, 114]. In regions where the additional demand for low-CO_2 electricity for H-DR steelmaking has to be met by fossil fuel power plants equipped with CCS, integrating CCS at already existing BF-BOF plants is likely a more sensible approach given the generally higher concentration of CO_2 in steelmaking off-gases than in power plant flue gases and, in the case of the BF, the potential operational advantages of TGR. There has also been recent interest in the combined use of biomass-based reductants and CCS to achieve negative-emissions steelmaking, which may catalyze developments in steelmaking CCS [134].

3 METHODOLOGY

The overall aim of this thesis is to identify and evaluate non-geological H_2 storage technologies for future large-scale H-DR processes from a techno-economic perspective. To achieve this, it was necessary to apply a multi-pronged approach. The first step was to conduct a wide review of existing literature on technologies for H_2 storage. However, very few large-scale H_2 storages exist today. Consequently, most H_2 storage technologies remain unproven in the kind of industrial applications considered in this thesis. The evaluation of these H_2 storage technologies must, thus, necessarily be conceptual as detailed information on investment and operational costs from operational facilities is not available. To overcome this, H_2 storage technologies were compared based on fundamental thermodynamic (prospective heat and electricity demands of the overall storage processes), engineering (e.g., technological maturity and challenges related to dynamic storage operation or heat transfer), and economic aspects (e.g., material costs). All potential H_2 storage technologies were not evaluated for H-DR integration in detail as most could be excluded from consideration based on a single or a few inherent shortcomings that render such integration economically or technically infeasible. Chapter 5 of this thesis provides an overview of this literature review.

After the most promising H_2 storage options had been identified, it was necessary to establish an H-DR process model to enable a techno-economic comparison of the integration of different H_2 storages. The developed H-DR process model is based on literature data for prospective H-DR and operational conventional DR processes and mass and energy balance calculations. As the pressures in H-DR processes are likely to be relatively low (as in conventional DR processes), the specific enthalpy of the process gas streams is assumed to only depend on their temperature, i.e., they are assumed to behave as ideal gases. The enthalpies of gas streams were calculated by the Shomate equation using data from the National Institute of Standards (NIST) Webbook [145, 146].

Due to various process integration options, it was found sensible to consider the H-DR process and its H_2 storage within the same system boundary, particularly for the non-geological H_2 storage technologies as they are associated with significant heat flows. Possibilities for process integration between the most promising non-geological H_2 storage options and H-DR plants are discussed in chapter 6. This includes considerations for heat supply to the dehydrogenation process, utilization of heat generated in hydrogenation processes, and material integration options. Part of the discussion on heat integration utilizes concepts related to pinch technology [147].

The specific H-DR steel production cost was also estimated to establish the effect that H_2 storage may have on the overall process economics. Here the annuity method was utilized to calculate the share of the steel production cost that is related to investment costs of the plant. The annuity method takes the time value of money into account by converting the total investment cost (*IC*) of a plant into an annualized cost via the calculation of an annuity factor (*AF*), which is a function of the weighted average cost of capital (WACC) and the economic lifetime of the plant. If this annualized cost is divided by the yearly production capacity of the product ($\dot{m}$ in, e.g., t liquid steel per year), a specific annualized investment cost ($CAPEX_a$) results:

$$CAPEX_a = \frac{(IC)}{\dot{m}} \cdot AF = \frac{(IC)}{\dot{m}} \cdot \frac{WACC}{1-(1+WACC)^{-lifetime}} \quad (2)$$

The annuity method was also utilized to assess the impact of the investment cost of a H_2 storage on its ability to reduce the cost of H_2 delivery to an H-DR process.

An optimization method based on historical electricity prices was developed to determine the maximum potential reductions in H_2 production cost that can be achieved via the integration of different H_2 storage technologies in an H-DR process. The optimization method identifies the electrolyzer and storage operational profiles that minimize the operational cost of H_2 delivery to an

H-DR process given the operational characteristics and limitations of the H_2 storage for a specified electricity price series. The method is deterministic in that it assumes perfect foresight and that the presence of the H_2 storage does not affect electricity prices, partly because estimating such feedback effects with any degree of certainty is exceedingly challenging considering the complexity of the electricity system. The electrolyzer and storage operation optimization problem was defined and implemented in MATLAB® R2019a using the built-in NLP solver '*fmincon*' set to the default '*interior-point*' algorithm. Historical electricity prices from Sweden and Denmark gathered from the public Nord Pool electricity market database were used in the analysis [148]. The storage operation optimization method and related assumptions are described in detail and discussed in section 7.1.

A crucial process design issue for any liquid H_2 carrier-based storage is how to supply heat to the endothermic dehydrogenation processes. A hybrid heat supply process for CH_3OH dehydrogenation, in which part of the heat is supplied via biomass combustion and part via combustion of released H_2, was developed and its performance was simulated using ASPEN Plus® V10, a well-known chemical process simulation software package, to determine its mass and energy balances. Ideal conditions are assumed in these simulations and reactions are assumed to reach their chemical equilibria. The economic prospect of this heat supply process compared to either combustion of part of released H_2 or reactor electrification as part of a CH_3OH-based H_2 storage for an H-DR process was also evaluated, see section 8.4.

In the case that a liquid H_2 carrier-based storage is implemented in an H-DR process, the storage medium can potentially be sold off to provide the plant operator with additional revenue. This may, e.g., be attractive if prolonged periods of relatively low and stable electricity prices are relatively commonly encountered, and may, thus, improve the overall chances of storage investment profitability. A linear calculation method based on historical electricity price duration curves was developed to estimate the potential economic impact of allowing such sales in the case of CH_3OH-based H_2 storage. A problem with implementing this kind of hybrid CH_3OH production and storage approach is how to prioritize the use of CH_3OH for H_2 storage vs. for selling it off to an external customer. Here, a prioritization method based on the contribution margin concept, i.e., the difference between the potential selling price and the associated variable operational costs per unit of a product, was developed. This calculation method is described and discussed in detail in section 8.1.

4 HYDROGEN DIRECT REDUCTION STEELMAKING (PAPERS II-VI)

The purpose of this chapter is to introduce the principles of the H-DR process with an integrated EAF (henceforth referred to as H-DR-EAF) and to discuss various process design alternatives, including different electrolysis technologies. A basic H-DR-EAF process model is developed. This process model is used to calculate the electricity, heat, and H_2 demand of the H-DR-EAF plant and is also utilized throughout the thesis for evaluating various H_2 storage process integration options. An economic analysis is also included to estimate what impact a H_2 storage can potentially have on the overall H-DR-EAF steel production cost. In section 4.5, an alternative H-DR process based on steam electrolysis or steam and CO_2 co-electrolysis is described and the potential impact this may have on the economics of H-DR-EAF steelmaking is considered.

H-DR is a variant of the conventional shaft furnace DR process in which H_2 is the only reductant. Although the basic process layout is similar, this change in reductant has significant consequences for the energy balance and economic performance of a DR plant. First and foremost, as the sole byproduct of the reduction process is H_2O, the CO_2-intensity of H-DR processes depends nearly entirely on how the H_2 is produced. There are several commercialized H_2 production technologies [149-151]. However, the most mature H_2 production technology with the potential for zero direct CO_2 emissions is (H_2O) electrolysis [9, 10]. If the electricity fed to the electrolysis process is generated from fossil-free sources, it is possible to generate H_2 without any associated direct CO_2 emissions.

The only H-DR plant based on H_2 production via electrolysis in operation at the time of writing is the Hybrit Development AB 1 t DRI/h pilot plant in Luleå, Sweden [22]. This plant utilizes a Tenova HyL shaft furnace and a 4.5 MW_{el} electrolyzer supplied by Norwegian Nel ASA [98, 152]. However, a 0.5 Mt/y HBI plant based on H_2 reduction was operated in Point Lisas, Trinidad already between 1999 and 2016, originally by Cliffs and Associates Ltd. [11, 22, 153]. This plant utilized a set of fluidized bed reactors for the reduction of iron ore fines with H_2 produced from NG reforming [154]. Unfortunately, this plant was plagued by a multitude of technical and economic problems [45, 154]. The use of fluidized bed reactors and the production of H_2 from NG renders the Point Lisas plant very different from the kind of fossil-free shaft furnace-based H-DR process pursued in, e.g., the HYBRIT initiative. Nevertheless, some lessons can be learned from this first H_2-based DR plant, e.g., considerations for EAF operation with carbon-free DRI [153].

As no full industrial-scale shaft furnace H-DR plant has yet been built and no detailed information about the Hybrit Development AB pilot plant is publicly available, the optimal H-DR process conditions and plant layout are currently uncertain. I assess the main process uncertainties to be (in no particular order): 1) if, and if so how, carbon will be introduced into the steel; 2) the optimal shaft furnace conditions (temperature and pressure) and the H_2 conversion per pass through shaft furnace at those conditions; 3) the reducing gas preheating process; 4) if, and if so how much, H_2 must be purged to prevent the accumulation of inerts in the gas loop [155]. There are also, as is discussed later in this chapter, different electrolysis technologies with different H-DR process integration possibilities. Consequently, many different kinds of H-DR plants are conceivable. A simplified flowsheet of one kind of H-DR-EAF plant based on H_2 production via electrolysis is shown in Figure 4.

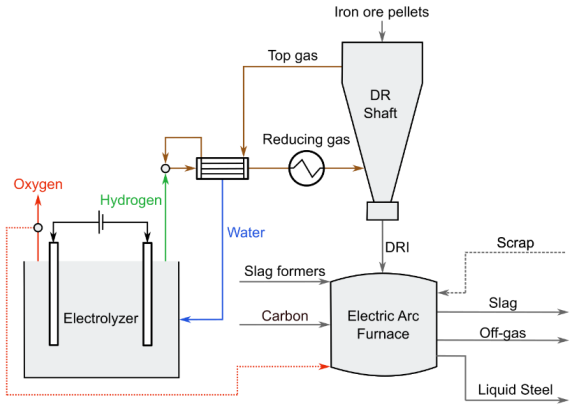

Figure 4: Hydrogen direct reduction-electric arc furnace process.

The H-DR and EAF processes are shown as co-located and integrated in Figure 4. This has certain process advantages, most notably the possibility to directly feed hot DRI and utilize the O_2 byproduct from electrolyzers in the EAF. However, as mentioned previously, it is also perfectly possible to produce DRI in one location and steel in another. In such cases, an external DRI cooling circuit or a briquetting machine would be used to produce CDRI or HBI, which are more suitable for transportation [70].

The main material inputs to an H-DR-EAF plant are iron ore pellets, slag formers, and some carbon source [74, 84, 156]. In a fossil-free process, the carbon fed to the EAF must be biogenic in origin [13, 22]. It should preferably also be low in sulfur and ash to avoid negative effects on the melting process and product quality [70, 157]. Bio-carbon appears to be the most likely candidate at present [29, 45, 74, 157, 158]. Additional fuel can also be injected into EAFs but this is not considered here [64, 84, 159, 160]. The overall H-DR process based on H_2 production via electrolysis is theoretically H_2O neutral—all H_2O consumed for H_2 production is eventually regenerated via the shaft furnace reduction reactions. In practice, some H_2O losses will inevitably occur and, thus, make-up H_2O must be fed to the plant; H_2O recycled and fed to electrolyzers must also be purified. These effects on the plant mass and energy balances as well as the steel production cost are neglected herein as they should be relatively small.

In the shaft furnace, preheated H_2-rich reducing gas meets counterflowing iron ore pellets as in the conventional DR processes. Complete H_2 conversion in a single pass through the shaft furnace is not expected and it is, thus, necessary to recirculate the unconverted H_2. The top gas is first used to exchange heat to the incoming reducing gas and then the H_2O formed as a byproduct of the reduction process is separated out via condensation. Depending on the process pressure and per pass H_2 conversion this may require cooling water. The H_2 purity required for H-DR processes is not as high as in, e.g., fuel cell applications, considering the relatively large concentration of non-reducing species in the reducing gases of conventional shaft furnace processes [161, 162].

In conventional NG-based shaft furnace DR processes, part of the top gas is combusted to preheat the reducing gas. This combustion also prevents the accumulation of inerts, e.g., N_2, in the process gas loop. It is possible that a small part of the top gas must also be purged in H-DR processes [64, 155]. However, it is of economic interest that this purge stream is kept as small as possible considering the high value of the H_2 that would be combusted rather than used for reduction [155]. As it is presently unknown how much top gas must be purged in an H-DR process, I have assumed that the associated H_2 losses are sufficiently small to not signficantly affect the overall energy balances of the H-DR process. The only exception is paper III, in which a top gas purge of 10% (by volume) was assumed.

In the EAF, the DRI is melted and refined to liquid steel. This liquid steel may be processed further via conventional means, e.g., ladle metallurgy or vacuum degassing, and then continuously cast into semi-finished steel slabs, billets, or blooms [1, 38, 49]. The EAF melting process is mainly powered by electricity, which is fed to the furnace via graphite electrodes. This causes an electric arc to form between the electrodes and the charged materials, which generates significant amounts of heat, eventually leading to melt temperatures of above 1 600 °C [73]. The EAF graphite electrodes degrade over time due to the harsh conditions in the furnace and must be replaced regularly [163]. The EAF is essentially a batch reactor, with typical batch times of 40–100 minutes, depending on the charge material (share of DRI vs. scrap, charge temperature, the chemical composition of charge, etc.) and the targeted liquid steel properties [20, 164]. For EAF operation with high shares of DRI, the DRI is typically fed continuously via an opening in the EAF roof (called the EAF fifth hole) during batches [65, 84, 159]. In such scenarios, the EAF is not fully emptied during the end of a batch, leaving a certain amount of liquid melt in the bottom of the furnace (a '*liquid heel*'). At the start of the next batch, DRI is continuously fed into this melt to ensure an even and efficient melting process [165]. The main outputs from an EAF are liquid steel, slag, and an off-gas, which typically mostly consists of CO_2, CO, and O_2 [64, 73, 166-168].

4.1 Mass balances of hydrogen direct reduction steelmaking

The H_2 demand of a H-DR process is determined by the DRI production rate and metallization. The remaining iron oxide in the DRI is in FeO form, formed via partial reduction of Fe_2O_3 [54]:

$$Fe_2O_3 + H_2 \rightarrow 2\,FeO + H_2O\ (\Delta h_R^0 = 18.6 \frac{kJ}{mol}) \quad \text{(R11)}$$

In the absence of DRI carbon content, most of this remaining FeO in the DRI must be reduced to Fe in the EAF via the injection of carbon. This results in the formation of CO [61, 159]:

$$FeO + C \rightarrow Fe + CO\ (\Delta h_R^0 = 155.3 \frac{kJ}{mol}) \quad \text{(R12)}$$

The FeO that is not reduced in the EAF ends up in the slag or, to a generally smaller extent, EAF dust [41, 51, 53]. It is assumed that no other Fe losses, e.g., with dust in the top gas, occur [104]. The CO formed via (R12) is combusted inside the EAF via reaction with a stoichiometric amount of injected O_2 to provide heat for the melting process. One-quarter of the FeO in the DRI is assumed to leave with the EAF slag, while the remainder is reduced to Fe and ends up in the liquid steel. The EAF graphite electrode consumption, which leads to additional CO_2 formation, is neglected in the mass balance, partially because it is currently uncertain what level of electrode consumption to expect when processing carbon-free DRI. In conventional EAF operation, 1–2 kg/t liquid steel electrode consumption is typical, leading to the generation of an additional 4–7 kg of CO_2/t liquid steel [74].

Assuming a DRI metallization of 94%, a liquid steel composition of 99.5% Fe and 0.5% C by weight, and an iron ore pellets gangue content of 5% by weight yields an overall H_2 demand of 52.5 kg per t liquid steel. The assumed liquid steel carbon content is relatively high, but this is offset by the absence of alloying elements (e.g., Cr or Mn) and does not dramatically affect the overall H_2 demand of the H-DR-EAF process [49, 64, 169]. The production of 1.0 t liquid steel requires the production of 1.1 t DRI from 1.5 t iron ore pellets. The calculated iron ore pellets consumption (1.38 t pellets/t DRI) is similar to that of conventional shaft furnace DR plants [53, 104]. The overall mass balance of the H-DR-EAF process for a basis of 100 t liquid steel is seen in Figure 5.

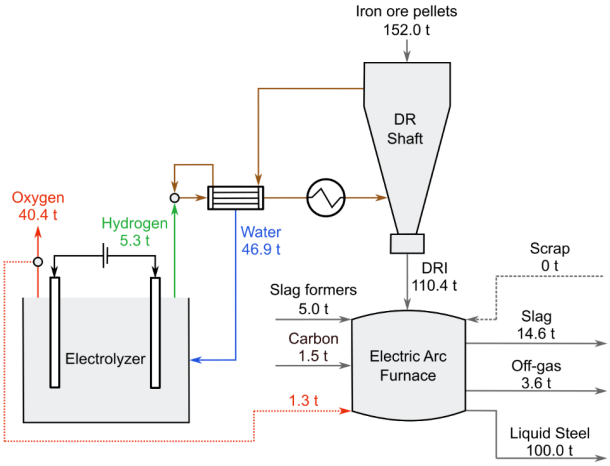

Figure 5: Mass balances of hydrogen direct reduction-electric arc furnace process.

The electrolyzers also generate 417 kg of O_2 per t of liquid steel as a byproduct. Only a very small part of this O_2 is needed in the EAF (approximately 3%). The amount of carbon injected into the EAF (around 15 kg/t liquid steel) is on the high-end of what is typical in EAFs (8–17 kg/t liquid steel for EAF charges rich in conventional DRI (>85% by weight)), which is to be expected given the carbon-free DRI [74, 84, 153]. For a 2 Mt/y H-DR-EAF plant, the calculated EAF bio-carbon demand is 30 000 t/y.

4.2 HYDROGEN PRODUCTION VIA THE ELECTROLYSIS OF WATER

The electricity needed for the production of H_2 via electrolysis will constitute the main energy input to an H-DR-EAF plant. This is also the primary reason why H_2 storage is of interest for H-DR-EAF plants. Therefore, a brief introduction to electrolysis technologies is given in this section.

The concept of H_2O electrolysis is simple: H_2O is electrochemically split (electrolyzed) into O_2 and H_2 via the addition of direct current electricity:

$$H_2O(l) \rightarrow H_2(\mathrm{g}) + 0.5\ O_2(\mathrm{g})\ (\Delta h_R^0 = 285.8\ \frac{kJ}{mol}) \qquad \text{(R13)}$$

The stoichiometry of (R13) gives a co-production of 7.9 kg of O_2 and a H_2O demand of 8.9 kg per kg of H_2. While H_2 is the most valuable product of electrolysis, the value of the O_2 byproduct is not insignificant [170]. At the current market price of approximately 35–70 €/t, O_2 sales may reduce the electrolysis H_2 production cost by up to 0.3–0.6 €/kg H_2 [171, 172]. However, identifying suitable large-scale buyers of O_2 may prove challenging. For most large-scale O_2 consumers it is often more cost-effective to invest in their own O_2 production, e.g., via air VPSA, than purchasing external O_2, especially as high-purity O_2 is rarely required [171, 173-175].

The high chemical stability of H_2O renders its electrolysis inherently demanding. Even at a theoretical 100% efficiency based on the higher heating value (HHV) of H_2 (39.4 kWh/kg; this is the minimum electricity input for liquid H_2O electrolysis [176]), the production of 2 Mt liquid steel/y via the H-DR-EAF process would require an electrolyzer capacity of approximately 520 MW_{el} [177]. Considering that the total global installed electrolyzer capacity was less than 300 MW_{el} in 2020, it is clear that scaling up electrolyzer production will be critical to realize industrial-scale H-DR plants [151].

Fortunately, the H_2O electrolyzer industry is currently in a rapid growth phase—the projected global installed electrolyzer capacity in 2026 is approximately 17 GW_{el} based on announced projects and the European Commission's Fit-for-55 package calls for 40 GW_{el} of installed electrolyzer capacity within the EU alone by 2030 [178].

Three main H_2O electrolysis technologies available on the market today: alkaline electrolysis (AEL), proton exchange membrane (or polymer electrolyte membrane) electrolysis (PEMEL), and solid oxide electrolysis (SOEL) [176, 179, 180]. AEL and PEMEL are low-temperature electrolysis technologies, meaning that they operate on a feed of liquid H_2O, while high-temperature SOEL operates on steam.

Current and projected values for selected performance metrics for AEL, PEMEL, and SOEL are summarized in Table 1. Electrolyzers are associated with certain economies of scale (i.e., larger units have lower specific investment costs), but only up to a certain capacity, beyond which costs scale approximately linearly with production capacity [179, 181-187]. The point at which economy of scale effects start to diminish is not entirely clear but appears to lie before 100 MW_{el}, at least for low-temperature electrolyzers [185, 188].

Table 1: Current and projected future performance metrics for electrolysis technologies [5, 179, 184, 189-194].

	Current (2020–2022)			2050/long-term		
	AEL	PEMEL	SOEL	AEL	PEMEL	SOEL
Operating temperature (°C)	70-90	50-80	600-850	>90	80	<600
Cell pressure (bar)	<30	<70	<25	>70	>70	>20
System efficiency ($kWh_{el}/kg\ H_2$)*	50–78	50–83	40–55	<45	<45	<40
Lifetime (thousands of hours)	60–90	30–90	10–80	100–150	100–120	75–100
System investment cost, $/$kW_{el}$)**	500–1 000	700–1 400	2 800–5 600	<200 (98 [190])	<200	<300–500
Load range (% of nominal load)	10–110	0–160	20–100	5–300	0–300	0–200

*At the nominal electrolyzer H_2 production rate. Higher efficiencies are possible at lower rates.
**For systems larger than 10 MW_{el}. The costs of power electronics (rectifiers and transformers), H_2O and gas purification systems, pumps, cooling and H_2O supply are also included, but not costs of installation (e.g., labor costs and grid connection fees), various owner costs (e.g., owner project management, insurances, grid fees, and operator training), and contingency costs.

All three considered electrolyzer types can be pressurized, which may prove suitable in storage applications as all H_2 storage technologies involve an initial compression step. If part or all of this compression work can be done in the electrolysis cells, the overall compression work can be reduced as electrochemical compression is inherently more efficient than by mechanical means [176, 181, 195, 196]. A potential issue of pressurized SOEL operation is that it increases the H_2O evaporation temperature, which may hamper heat integration with other processes [197].

The specific electricity demand of electrolyzers depends on the applied current density [187, 198]. Consequently, electrolyzers are more efficient when operated at lower loads, in contrast to most thermal and thermochemical processes [183, 193]. This benefits the dynamic operation of H_2O electrolyzers in response to electricity price variations. However, estimating the effect of partial load operation on electrolyzer performance is not trivial and most authors assume a load-independent electrolyzer efficiency in modeling [183, 199]. Although the inclusion of such an effect would favor the general economics of H_2 storage, it would most likely not favor any particular kind of storage over any other. Therefore, this effect has not been considered in this work.

4.2.1 Alkaline electrolysis

AEL is by far the most mature H_2O electrolysis technology and was applied at >100 MW_{el} scale already in the middle of the 20th century, primarily for the manufacture of ammonia (NH_3) before the advent of modern cost-effective NG reforming technologies [151, 200, 201]. In a few outlier cases, e.g., the Egyptian Aswan dam NH_3 production plant, the use of AEL for NH_3 production remained a viable alternative well into the 21st century [202, 203].

The two electrodes of an AEL cell, both often nickel-based, are submerged in a liquid potassium hydroxide (KOH) solution (20–40% by weight) [204]. A porous inorganic separator between the electrodes prevents the mixing of produced gases and short-circuiting. During AEL operation, H_2 and hydroxide ions (OH^-) are produced at the cathode via the reduction of H_2O, while O_2 and H_2O are produced at the anode via the oxidation of OH^-. The relevant electrode and total reaction of AEL are:

Cathode (AEL):	$2\,H_2O(l) + 2\,e^- \rightarrow H_2(g) + 2\,OH^-(aq)$	(R14)
Anode (AEL):	$2\,OH^-(aq) \rightarrow 0.5\,O_2(g) + H_2O(l) + 2\,e^-$	(R15)
Total:	$H_2O(l) \rightarrow H_2(g) + 0.5\,O_2(g)$	(R16)

The purity of the produced gases is high after drying: 99.5-99.9% for H_2 and around 99.3-99.8% for O_2 by volume [176]. As H_2O is consumed on the cathode side and produced on the anode side, it is necessary to at least occasionally mix the anode and cathode electrolyte solutions to stabilize KOH concentrations and maintain the required electrolyte conductivity [204]. This mixing causes some contamination of the product gases as the electrolyte carries with it small amounts of dissolved gases [176]. This is a particularly impactful effect for lower AEL operating loads and can potentially lead to the formation of explosive gas mixtures unless properly controlled [176].

4.2.2 Proton exchange membrane electrolysis

PEMEL was first developed by General Electric (GE) during the 1960s, enabled by the discovery of the Nafion (a solid polyfluorosulfonic acid-based polymer) membrane material by Walther Grot at DuPont, which is still typically the electrolyte of choice [205-208]. The solid Nafion electrolyte, through which protons (H^+) are transported, also acts as a membrane onto which the cathode and anode are directly mounted [206, 207]. This yields a different set of half-cell reactions:

Cathode (PEMEL):	$2\,H^+ + 2\,e^- \rightarrow H_2(g)$	(R17)
Anode (PEMEL):	$H_2O(l) \rightarrow 0.5\,O_2(g) + 2\,H^+ + 2\,e^-$	(R18)
Total:	$H_2O(l) \rightarrow H_2(g) + 0.5\,O_2(g)$	(R19)

The solid electrolyte allows for higher purity H_2 (99.99% by volume) to be produced compared to in AEL [176]. Other advantages of PEMEL over AEL include higher power densities, easier pressurization of cells, improved part-load performance, and faster load ramping capabilities [176]. A downside to PEMEL is that the harsh conditions (acidity, voltages) inside the electrolyzer cells necessitate the use of costly materials to maintain acceptable degradation rates [176]. In particular, electrocatalysts based on platinum group metals (PGMs) are typically used at both the cathode and anode [209, 210]. The prices of these PGMs affect the cost of PEMEL electrolyzers substantially [211].

4.2.3 Solid oxide electrolysis

The SOEL technology was first developed by Westinghouse during the early 1960s, initially for O_2 production in space exploration applications [176, 212, 213]. SOEL must be considered less mature than both AEL and PEMEL [151]. However, both Danish Haldor Topsøe A/S and German Sunfire GmbH are looking to scale up SOEL production capacities in the coming years, indicating that this maturity gap may soon narrow [151, 191, 214, 215].

SOEL, like PEMEL, employs a solid electrolyte [151, 191]. However, the ceramic electrolyte of SOEL, which is essentially always based on yttrium-stabilized zirconia (YSZ), transports oxide ions (O^{2-}) [181] This results in yet another set of half-cell reactions:

Cathode (SOEL):	$H_2O(g) + 2\,e^- \rightarrow H_2(g) + O^{2-}$	(R20)
Anode (SOEL):	$O^{2-} \rightarrow 0.5\,O_2(g) + 2\,e^-$	(R21)
Total:	$H_2O(g) \rightarrow H_2(g) + 0.5\,O_2(g)$	(R22)

The operating temperature of SOEL must be high to allow for sufficient O^{2-} conductivity through the electrolyte. These high operating temperatures, along with the feed of steam, enable favorable kinetics and thermodynamics compared to AEL or PEMEL, which also allows low-cost electrocatalysts to be used [181, 191, 216]. On the other hand, the higher operating temperatures in SOEL are a challenge in terms of material degradation [217].

The thermodynamic motivation for high-temperature steam electrolysis is straightforward: a larger part of the total energy input to split the H_2O can be supplied as heat instead of as electricity [216]. The reaction enthalpy of any reaction (ΔH) consists of two terms, the Gibbs free energy change (ΔG), which describes the electricity demand in the electrolysis case, and the entropic contribution ($T\Delta S$), which in the ideal case describes the heat demand [201]:

$$\Delta H = \Delta G + T\Delta S \tag{3}$$

The reaction enthalpy of electrolysis is lower when starting from steam (this is the difference between the H_2 HHV and its LHV). However, steam superheating has a relatively small effect on ΔH [217]. As ΔS is positive for electrolysis, its electricity demand (ΔG), must, thus, decrease with increasing temperature for the sum $\Delta G+T\Delta S$ to remain relatively constant. At SOEL operating temperatures, electricity demands as low as 35–37 kWh/kg H_2 can be reached if the heat for H_2O evaporation can be supplied from an external source (note that values for SOEL efficiency in Table 1 assume electrical evaporation of H_2O as part of SOEL operation) [218-220].

SOEL has historically been associated with a poor tolerance for dynamic operation [191]. However, recent results have shown that dynamic SOEL operation, on par with low-temperature electrolyzer technologies, is now feasible with little additional degradation [176, 214, 221]. The main challenge of dynamic SOEL operation may now lie with the heat management and steam supply systems [176, 214, 221-224]. However, the cold start-up of SOEL systems is still slow due to the high operating temperatures [176].

A further differentiating aspect of SOEL is its ability to electrolyze other substances than H_2O, most notably CO_2 [225]. The product of the CO_2 electrolysis is CO:

$$CO_2(g) + 2\,e^- \rightarrow CO(g) + O^{2-} \tag{R23}$$

Co-electrolysis of H_2O and CO_2 within the same SOEL unit is possible and yields H_2 and CO mixtures on the cathode side [191, 226, 227]. The electricity demand of CO_2 and H_2O electrolysis are similar at typical SOEL operating temperatures [228]. In the context of H-DR, co-electrolysis using SOEL allows for the provision of a reducing gas that is similar in composition to those in NG-based processes [64]. This allows for DRI carburization as in conventional DR processes with the associated advantages for DRI handling and EAF processing. The integration of steam or steam and CO_2 co-electrolysis in an H-DR-EAF plant is discussed further in section 4.5.

4.3 ENERGY BALANCES OF HYDROGEN DIRECT REDUCTION STEELMAKING

The majority of the electricity demand of an H-DR-EAF plant will go towards H_2 production via electrolysis. With current AEL performance figures, a total of 2.6 MWh_{el}/t liquid steel is needed. With the expected long-term improvements in electrolyzer efficiencies shown in Table 1, this may decrease to below 2.1 MWh_{el}/t liquid steel for SOEL [89]. If electrolyzers are of the AEL or PEMEL kind, they will also generate significant amounts of heat, approximately 85–105 MW for a 2 Mt/y H-DR-EAF plant, that can potentially be utilized for, e.g., district heating if this is an available option [186, 229-232].

The second-largest consumer of electricity in an H-DR-EAF plant will be the EAF. However, estimating its electricity demand is complex as it depends on a host of parameters, e.g., DRI metallization, DRI carburization, DRI temperature, gangue content of iron ore pellets, degree of carbon injection, and the share and quality of scrap [73, 84, 233]. When fed with 100% steel scrap, modern EAFs typically demand 300–400 kWh_{el}/t liquid steel [70, 164, 165]. This increases to 500-700 kWh_{el}/t when the EAF is fed with only CDRI [57, 64, 84]. The use of carbon-free DRI is expected to increase the electricity demand of the EAF, perhaps to 650–760 kWh_{el}/t, as the DRI melting temperature increases with decreasing carbon content and no heat from exothermic oxidation of DRI carbon can be utilized [20, 60, 64, 234]. As mentioned previously, the EAF electricity demand can be reduced by directly feeding hot DRI from the upstream DR process [29, 70, 77].

The electricity demand of the remaining H-DR-EAF plant equipment, such as compressors and pumps, is moderate. Common values for NG-based DR processes are 60–110 kWh_{el}/t liquid steel [85, 104, 155, 235, 236]. Therefore, pressure losses and compression work in the H-DR processes have been neglected here.

The final major energy input to an H-DR-EAF plant is the reducing gas preheating. This heat can be supplied by fuel combustion or by electrical heating. The amount of preheating needed depends primarily on the flow of reducing gas and the energy balance of the shaft furnace. The primary heat flows in an H-DR process are shown in Figure 6.

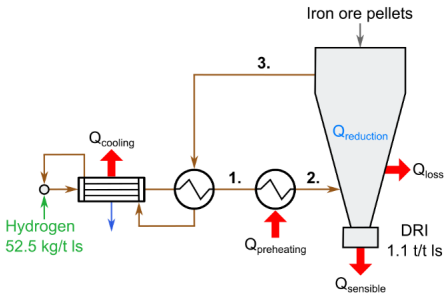

Figure 6: Heat balance of shaft furnace in a hydrogen direct reduction process. The sensible heat of iron ore pellets is assumed to be negligible.

To determine the amount of preheating needed ($Q_{preheating}$), the heat losses from the shaft furnace (Q_{loss}), the endothermicity of the reduction reactions in the shaft furnace ($Q_{reduction}$), and the sensible heat of the DRI ($Q_{sensible}$) must be determined.

The amount of external preheating needed depends on how much heat can be recovered internally in the H-DR process, specifically the heat exchange between the reducing gas and the top gas. The mass flow of the top gas is always larger than that of the reducing gas due to the production of H_2O in the reduction reactions and the incomplete conversion of H_2 per pass through the shaft furnace. Therefore, the heat exchange between the top gas and the reducing gas mainly depends on the achievable temperature difference in the heat exchanger. It is assumed that a minimum temperature difference of 50 °C can be reached, a somewhat conservative value for gas-gas heat exchangers [147]. Due to this temperature difference, there is excess heat left in the top gas after heat exchange with the reducing gas. This excess heat, along with the heat of condensing the H_2O produced in the shaft furnace, is rejected, e.g., using cooling water, before the top gas is recycled. It is assumed that complete condensation and separation of all H_2O in the top gas is not achieved so that the reducing gas contains 10% H_2O by mole.

The flow of reducing gas depends on how much H_2 reacts per pass through the shaft furnace. If the H_2 conversion per pass is low, a larger excess of H_2 in the reducing gas is needed to reach the same DRI production rate. In the absence of any operational data for H_2-based shaft furnace DR processes, I have assumed a H_2 conversion of 30% per pass through the shaft furnace. This is both close to values expected from a chemical equilibrium viewpoint and values reached in NG-based DR plants [45, 92, 146, 155].

The optimal reducing gas temperature in an H-DR process is currently unknown. A higher temperature would be favorable for both thermodynamic and kinetic reasons [161]. However, the potential advantages of a higher reducing gas temperature must be weighed against increasing demands on process equipment and reducing gas preheating. Therefore, an intermediate reducing gas temperature of 900 °C has been assumed here.

Due to the minimum temperature difference achieved in the heat exchange between the top gas and reducing gas, the reducing gas temperature before the preheater (T_1) is determined by the top gas temperature. The top gas temperature is, in turn, determined by the heat balance of the shaft furnace (the sensible heat of the iron ore pellets is assumed to be negligible [90]):

$$\dot{m}_{red.gas} \cdot h_2 = \dot{m}_{top.gas} \cdot h_3 + Q_{sensible} + Q_{loss} + Q_{reduction} \quad (4)$$

Heat losses from the shaft furnace are sufficiently large to significantly affect its energy balance. However, a wide range of heat loss values have been suggested for shaft furnaces in literature (from zero to over 120 kWh/t DRI) [53, 91, 237-241]. I have used the shaft furnace heat loss suggested by LKAB in the ULCORED project here: 37 kWh/t liquid steel, based on communication with Hybrit Development AB [235]. A slightly larger shaft furnace heat loss values than this have been assumed in papers II, III, V, and VI, yielding lower top gas temperatures.

An H-DR top gas temperature of 381 °C is calculated using the shaft furnace energy balance. This is lower than typical top gas temperatures in NG-based processes, which tend to be 400–500 °C [85, 90, 240]. This is to be expected given the absence of the exothermic CO reduction and carburization reactions. More detailed simulations of H-DR shaft furnaces have also reached similar top gas temperatures [155, 161]. The top gas temperature calculation is sensitive to assumptions for the per pass H_2 conversion, reducing gas composition, and heat loss. The H-DR reducing gas preheating demand was determined to be 118 MW or 472 kWh/t liquid steel. If the incoming H_2 from electrolyzers is at 70 °C, typical for AEL or PEMEL electrolyzers, the excess heat in the top gas ($Q_{cooling}$) is approximately 16 MW or 64 kWh/t liquid steel. The temperature of this heat is between 135 °C and 70 °C, indicating that it could be useful for district heating.

The overall electricity demand of the H-DR-EAF plant is approximately 3.7 MWh/t liquid steel assuming electrical reducing gas preheating, an electrolyzer efficiency of 50 MWh_{el}/t H_2, and an EAF electricity demand of 600 kWh_{el}/t liquid steel. This is similar to other recent estimates in the scientific literature [64, 155, 228, 234, 242]. The electrolyzers make up 71% of the overall electricity demand. This increases to 81% if reducing gas preheating is instead achieved via the fuel combustion. The H-DR-EAF plant can also potentially provide 400–480 kWh/t liquid steel of district heating.

4.4 ECONOMICS OF HYDROGEN DIRECT REDUCTION STEELMAKING

As its mass and energy balances have been established in the previous sections, it is now possible to evaluate the cost of producing liquid steel via the H-DR-EAF process. For reference, the crude steel production cost via the BF-BOF route has been estimated to be 240–390 €/t [1, 35, 162, 234, 243, 244]. Presumably, costs towards the lower end of this range are for established BF-BOF plants where assets have already been largely written off [8, 38, 245].

The basis for the calculations is a production capacity of 2 Mt of liquid steel/y at a plant utilization of 8 000 h/y[3] [246]. Low-temperature electrolyzers are assumed. The WACC is 6% and the economic lifetime of all components is assumed to be 20 years. Further assumptions used to estimate the steel production cost are summarized in Table 2. The electrolyzer investment cost is subject to significant uncertainty and lower values may be expected in the future. In contrast, no major cost reductions are expected for the shaft furnace or the EAF as these are relatively mature technologies [111].

Table 2: Assumptions to estimate of steel production cost via the hydrogen direct reduction-electric arc furnace process.

Parameter	Value	Reference
H-DR investment cost ($IC_{H\text{-}DR}$)	606 M€	[111]
EAF investment cost (IC_{EAF})	480 M€	[111]
Electrolyzer investment cost (IC_{EL})	328 M€ (500 €/kW; 656 MW)	See section 4.2
Electrolyzer electricity demand	50 MWh/t H_2	
Slag former demand	50 kg/t liquid steel	[84]
Slag former cost	100 €/t	[234]
EAF electricity demand ($[MWh_{el}/t_{ls}]_{EAF}$)	600 kWh/t liquid steel	[84]
Reducing gas preheating electricity demand ($[MWh_{el}/t_{ls}]_{preheating}$)	472 kWh/t liquid steel	See section 4.3
EAF bio-carbon price	300 €/t	[46]
Labor cost (C_{labor})	52.3 €/t liquid steel	[117]
Iron ore pellets cost	84 €/t	[111]
Scrap charge to EAF	0%	
EAF graphite electrode consumption	2 kg/t liquid steel	[41]
EAF graphite electrode price	4 503 €/t	[111]
Operation and maintenance cost	3% of investment cost per year	[117]

The production cost of liquid steel (*LPC*) is calculated via the following equation based on the annuity method:

$$LPC = \frac{(IC_{H-DR} + IC_{EAF} + IC_{EL}) \cdot AF}{\dot{m}_{liquid\ steel}} + C_{ore} + C_{EAF\ electrodes} + C_{bio-carbon} + C_{labor} + C_{slag\ formers} + \left[\frac{€}{MWh_{el}}\right] \cdot \left(\left[\frac{MWh_{el}}{t_{ls}}\right]_{EAF} + \left[\frac{MWh_{el}}{t_{ls}}\right]_{electrolysis} + \left[\frac{MWh_{el}}{t_{ls}}\right]_{preheating}\right) \quad (5)$$

where C_{ore}, $C_{EAF\ electrodes}$, $C_{bio\text{-}carbon}$, $C_{slag\ formers}$ are the specific costs (in €/t liquid steel) of consumables, $[€/MWh_{el}]$ is the electricity price, and $[MWh_{el}/t_{ls}]_{electrolysis}$ is the specific electricity demand of electrolyzers. The resulting liquid steel production cost as a function of the electricity price is seen in Figure 7. Similar H-DR-EAF steel production costs have been reached by others [35, 162, 234]. The total H-DR-EAF plant investment cost is approximately 1 414 M€ (the annualized specific investment cost is 62 €/t liquid steel), out of which electrolyzers make up 23%. The total specific cost of consumables is 146 €/t liquid steel, out of which the iron ore pellets makes up the vast majority (128 €/t liquid steel).

[3] This H-DR-EAF plant liquid steel production capacity and utilization will be used throughout the rest of this thesis.

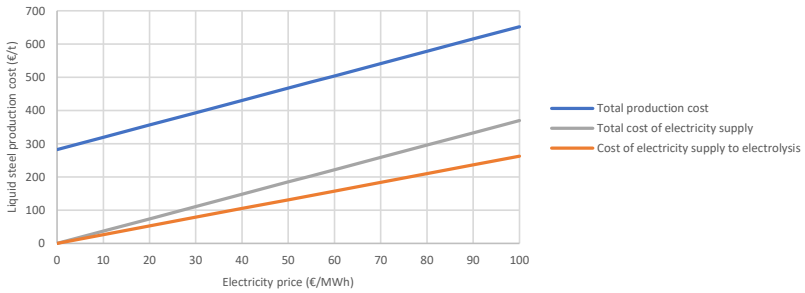

Figure 7: Hydrogen direct reduction-electric arc furnace process liquid steel production cost as a function of the electricity price.

The electricity costs increasingly affect the production cost of liquid steel as the electricity price increases—the production cost is approximately 1.5 times as high at 70 €/MWh compared to at 20 €/MWh, largely driven by an increase in H_2 production cost. At an electricity price of 20 €/MWh, the electricity cost of H_2 production is around 19% of the total plant operational cost. This increases to 40% at 70 €/MWh.

H-DR-EAF is only competitive with the BF-BOF route at relatively low electricity prices (below around 30 €/MWh at least) in the absence of carbon pricing [234]. Assuming a carbon price of 50 €/t CO_2 and a CO_2-intensity of 1.8 t CO_2/t steel for the BF-BOF route would increase the electricity price at which H-DR-EAF may be competitive to around 50 €/MWh. Potential income from sales of district heating and O_2 are not included in the production cost estimates shown in Figure 7. Including such sales could reduce the liquid steel production cost by up to 35–50 €/t liquid steel (considering a district heating price of 50 €/MWh and an O_2 price of 50–70 €/t) [171, 232, 247].

4.5 HIGH-TEMPERATURE ELECTROLYSIS IN HYDROGEN DIRECT REDUCTION STEELMAKING

The use of SOEL instead of low-temperature electrolysis may reduce the electricity demand of an H-DR-EAF plant. Furthermore, the direct utilization of the steam in the H-DR top gas for SOEL would avoid the need for a separate steam generation process, potentially reducing both operating and investment costs. One possible barrier towards such direct top gas utilization is its sulfur content, which may poison the SOEL nickel-based cathode catalyst [217, 248]. This is not an entirely different situation to the Midrex process, which also utilizes a sulfur-sensitive nickel catalyst in the reformer, although it appears that the SOEL cathode catalyst could be even less sulfur-tolerant [53, 93, 94, 249]. If the sulfur content of the top gas is too high for direct feed to an SOEL, various top gas desulphurization technologies could be utilized, some of which may not require condensation of the top gas, e.g., sulfur guard beds based on zinc oxide [250].

Nevertheless, although SOEL integration may allow for more efficient DRI and steel production via H-DR-EAF, these electrolyzers are currently associated with much higher investment costs than AEL or PEMEL. SOEL scale-up and associated cost reductions is, thus, necessary for these kinds of electrolyzers to be attractive for H-DR [184, 191].

4.5.1 Co-electrolysis for the production of carburized direct reduced iron

As mentioned previously, SOEL could also be used to co-electrolyze H_2O and CO_2 to yield a reducing gas similar in composition to those in NG-based DR processes [146, 228]. This allows for a carburized DRI to be produced, with the associated advantages in DRI handling and EAF processing. Different schemes for the integration of SOEL co-electrolysis in H-DR processes have recently been patented [251, 252].

Assuming that no CO_2 generated in the EAF can be recycled (the liquid steel carbon content is in all likelihood significantly smaller than that of the DRI and some CO_2 losses are also inevitable), an H-DR-EAF plant producing carburized DRI requires a CO_2 input. The amount of CO_2 required purely for DRI carburization is in theory rather moderate. The production of 2 Mt/y liquid steel from DRI with a carburization of 1% (by weight) is associated with a carbon flow of approximately 22 000 t C/y with the carburized DRI. For co-electrolysis, all of this carbon must be replenished via the supply of 82 kt CO_2/y to the H-DR-EAF plant. Possible CO_2 sources for an H-DR-EAF plant are discussed in section 6.1.1. The CO_2 generated as a byproduct of the CO-based reduction and carburization shaft furnace reactions can either be directly recycled to the SOEL (again, top gas sulfur content is a potential barrier) or first separated out via, e.g., an absorption process as in conventional HyL Energiron III or ZR processes, and then recycled in purified form [146, 228]. The need for a separate CO_2 separation process is associated with additional operational and investment costs.

The most reasonable alternative way of introducing fossil-free CO into the H-DR shaft furnace would likely be through the reverse water water-gas shift (rWGS) reaction [253, 254]:

$$H_2(g) + CO_2(g) \rightarrow CO(g) + H_2O(g) \; (\Delta h_R^0 = 41.2 \; \frac{kJ}{mol}) \qquad \text{(R24)}$$

The rWGS reaction is studied extensively in the context of liquid hydrocarbon fuel production via the Fisher-Tropsch process from a feed of H_2 and CO_2, where the conversion of CO_2 to CO via the rWGS reaction is the first process step [255]. CH_4 is a possible side product, especially for lower temperatures or higher pressures [254]. However, the rWGS reaction equilibrium can be pushed towards CO production via nickel-based catalysts and by increasing the reactor temperature to 700–900 °C [253, 255, 256].

In the H-DR context, the H_2 consumed in the rWGS reaction for CO production would be produced via low-temperature electrolysis, while the necessary heat can be provided by the combustion of part of the top gas, fuel combustion, or potentially via rWGS reactor electrification [228, 257, 258]. This means that the minimum energy needed to produce CO via this route is the electricity demand of low-temperature electrolysis (around 50 kWh_{el}/kg H_2) plus the heat demand of the rWGS reaction (minimum of 5.7 kWh/kg H_2). This is much less efficient than CO production via SOEL co-electrolysis, particularly if the top gas steam can be directly utilized. In addition, the rWGS reaction results in the formation of H_2O, which is detrimental to the reducing gas reducing power, while co-electrolysis consumes H_2O. The H_2O formed in the rWGS may potentially be removed in an intermediate condensation step before the shaft furnace, but this would be associated with additional investment and operational costs.

The introduction of CO into the H-DR shaft furnace affects its mass and energy balances significantly. Most notably, the CO-based reduction and carburization reactions are exothermic, as opposed to endothermic H_2-based reduction. As more species are present in the shaft furnace, more chemical reactions are possible and the process complexity increases compared to pure H_2 operation.

The simple H-DR-EAF model described in previous sections was expanded to estimate the primary effects of the introduction of CO into the H-DR shaft furnace on the overall heat and mass balances of the process [146]. It is assumed that 30% of CO and H_2 is converted per pass through the shaft furnace via reduction [259]. Consequently, the share of reduction caused by reaction with H_2 or CO depends on the assumed reducing gas composition. In addition, CO is assumed to carburize the DRI via (R4) to form varying amounts of Fe_3C; no other carburization reactions were considered and, thus, all carbon present in the carburized DRI is assumed to be in the form of Fe_3C [67, 68]. The resulting DRI composition as a function of its carburization for a constant DRI metallization is shown in Table 3.

Table 3: Direct reduced iron composition as a function of carburization for metallization of 94%.

DRI carburization		0.0%	1.0%	2.0%
DRI composition (by weight)	Fe	86.0%	71.0%	56.4%
	FeO	7.1%	7.0%	6.9%
	Fe_3C	0.0%	14.9%	29.9%
	Gangue	6.9%	6.8%	6.8%

The CO that is consumed due to carburization is assumed to be in addition to that consumed due to reduction reactions. Consequently, higher degrees of DRI carburization lead to slightly smaller top gas flows (the difference in top gas molar flow is approximately 1.3% between 0% and 1.5% DRI carburization) and slightly higher DRI production rates (due to the added DRI carbon content) in the model. However, as the carbon content of the liquid steel leaving the EAF is assumed to remain constant, the DRI carburization does not affect the H-DR-EAF plant production capacity.

The developed shaft furnace model cannot be used to calculate the achievable DRI carburization for a given reducing gas composition. Instead, the DRI carburization is an input parameter that can be varied to assess its impact on the H-DR-EAF plant mass and energy balances. In practice, a higher reducing gas CO content should be associated with a higher DRI carburization under otherwise similar conditions [260]. For instance, Midrex Technologies recently presented their estimates of the achievable DRI carburization in their process as a function of the share of H_2 co-fed with NG, as seen in Table 4. These values can be used to roughly estimate the realizable DRI carburization for a given reducing gas CO content for a Midrex-type shaft furnace DR process.

Table 4: Effect of reducing gas composition on carburization in the Midrex process [261].

		Conventional Midrex	20% H_2#	50% H_2#	70% H_2#	100% H_2
Reducing gas (mol%)	H_2	55%	62%	72%	77%	90%
	CO	35%	28%	18%	13%	0%
	Others*	10%	10%	10%	10%	10%
DRI carburization (by weight)		2.5%	≈1.5%	≈1.0%	≈0.5%	0.0%

*Mainly CO_2, H_2O, N_2, and CH_4.
#In terms of energy content H2 vs. energy content of conventional NG-based reducing gas.

Although the developed shaft furnace model is simplistic it can capture the most significant effects of CO addition. As the amount of CO in the reducing gas and DRI carburization increases, the overall shaft furnace process becomes less endothermic (under otherwise identical conditions), which results in higher top gas temperatures. If the reducing gas consists of 60% H_2 and 30% CO by volume and a DRI carburization of 1.5% is reached (reasonable given the data in Table 4), the endothermicity of the shaft furnace is reduced from 238 kWh/t liquid steel in the pure H_2 reduction case to approximately 80 kWh/t liquid steel. A major reason for this large drop in endothermicity is the heat generated due to the carburization reaction. This lead to a lowered reducing gas preheating demand [146].

Liquid steel production based on the production of carburized DRI using SOEL co-electrolysis results in significantly lower electricity demand than when a combination of low-temperature electrolysis and a rWGS reactor is utilized, approximately 3.0 vs. 4.0 MWh_{el}/t liquid steel, considering electrical reducing gas preheating [228]. Furthermore, although using SOEL to produce carburized DRI via co-electrolysis rather than un-carburized DRI via steam electrolysis is more electricity-intensive, this may be outweighed by electricity demand savings in the EAF (excluding the additional cost of providing an external carbon source to the EAF to make up for the carbon not contained in the un-carburized DRI) [228]. Consequently, if low-cost CO_2 is available, H-DR reducing gas production via SOEL co-electrolysis may be an attractive route for the production of carburized DRI. However, as with pure steam SOEL, reaching competitive overall steel production costs via the SOEL co-electrolysis route is also largely dependent on reductions in SOEL investment costs and improvements in degradation rates.

5 HYDROGEN STORAGE FOR HYDROGEN DIRECT REDUCTION STEELMAKING (PAPERS I, IV)

This chapter aims to provide an overview of available H_2 storage methods. Based on thermodynamic, engineering, and techno-economic aspects, the suitability of these storage methods for integration with an H-DR-EAF plant is evaluated. As NG is by far the most commonly stored gas today, its storage is considered as a starting point. Today, most NG is stored underground in various geological formations as this offers the lowest storage costs. Therefore, options for the geological storage of gaseous H_2 are then introduced. Thereafter, other potential non-geological options for the large-scale storage of H_2, which are the main focus of this thesis, are discussed. However, first, some general aspects of H-DR-EAF production flexibility, where H_2 storage is just one option, are briefly discussed.

5.1 FLEXIBILITY IN HYDROGEN DIRECT REDUCTION STEELMAKING

The electricity cost will constitute a large share of the overall cost of producing steel via the H-DR-EAF route. A consequence is that the economic viability of the H-DR-EAF process is sensitive towards the price of electricity—when electricity is expensive, H-DR-EAF steelmaking will also be expensive.

Electricity pricing in a liberalized electricity market operates on the same fundamental principles as the pricing of any other commodity: when supply is low and demand high, the price increases and vice versa. Consequently, the electricity price varies over time due to variations in both supply and demand [262]. Variations in electricity supply are expected to increase in many markets due to increasing shares of variable wind and solar power [12]. This may result in increased price volatility and extended periods with relatively high electricity prices when, e.g., there is little wind. Therefore, it is worthwhile to consider and compare some strategies that H-DR-EAF plant operators may apply to manage electricity price variations, out of which H_2 storage is one. The options for H-DR-EAF process flexibility are summarized schematically in Figure 8.

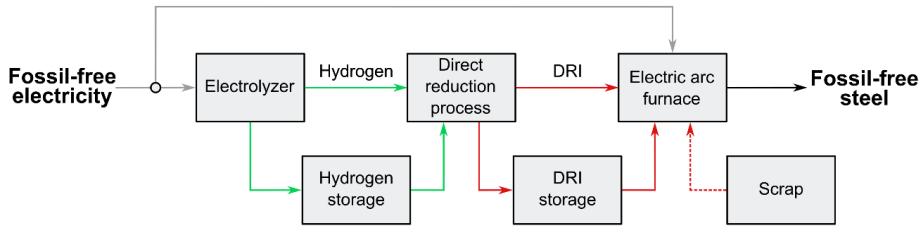

Figure 8: Possibilities for flexibility in hydrogen direct reduction-electric arc furnace steelmaking. Grey arrows: electricity; green arrows: hydrogen; red arrows: electric arc furnace ferrous feedstocks (direct reduced iron and scrap).

The most obvious way for a H-DR-EAF plant operator to manage electricity price peaks is to reduce steel production when the electricity price is high. However, while such an approach could result in lower specific electricity costs of steel production, the accompanying decrease in plant utilization would affect capital costs negatively [1]. Plant start-up may also be associated with significant costs [263]. Nevertheless, the EAF is essentially a batch-wise process, and some degree of optimization of its operation according to electricity price fluctuations is both technically feasible and most likely economically beneficial, particularly in an electricity system featuring relatively large shares of variable renewable power generation. Operating the EAF dynamically but not the upstream H-DR process would, in principle, only require DRI storage, e.g., as CDRI or HBI [53, 65]. A potential downside that the advantage of directly feeding hot DRI to the EAF is lost.

A way to maintain a relatively constant rate of steel production while still allowing for the plant electricity demand to be varied is to dynamically change the feedstock to the EAF depending on the electricity price. When the electricity price is high, less H_2 and DRI would be produced and the EAF would instead be operated on a larger share of either stored DRI or scrap or some combination thereof [234, 264]. While this approach would allow for a constant steel production rate, other challenges may arise. If stored DRI is to be used, there must exist both H-DR and electrolyzer overcapacity (EOC) that allows for DRI in excess of the EAF demand to be produced during low electricity prices, which increases investment costs. If the share of scrap charged to the EAF is to be varied, maintaining a constant steel product quality could be challenging. Nevertheless, any combination of these approaches also necessitates variations in DRI production rate, the feasibility of which is currently unknown [1, 155]. Midrex Technologies claim that their NG-based process can operate down to a minimum load of 30% of its nominal capacity without major efficiency losses [80]. Considering the similarities between H-DR and NG-based DR processes, a comparable load flexibility should be achievable in H-DR. Nevertheless, a reduction of the H-DR plant utilization would be a necessary compromise.

This leaves the storage of H_2 as the final available H-DR-EAF production flexibility strategy. The integration of a H_2 storage allows for a constant production of both DRI and liquid steel while still allowing for a significant reduction in plant electricity demand (70–80%) during electricity price peaks. The utilization of both the H-DR plant and EAF can, thus, both be maximized, while only the electrolyzers are operated dynamically. This is sensible as the electrolyzers will make up a relatively small part of the overall investment costs of an H-DR-EAF plant, as shown in section 4.4, especially considering the expected electrolyzer cost reductions, but a large part of its electricity demand. The rapid achievable ramping rates and higher efficiencies of electrolyzers at lower loads also benefit this scheme.

5.2 Economics of hydrogen storage in hydrogen direct reduction steelmaking

The economic principle of H_2 storage in the context of an H-DR-EAF process is simple: when the electricity price is high, the H-DR process is operated on stored H_2, which means that H_2 production via electrolysis can then be reduced. This requires EOC so that H_2 in excess of the H-DR demand can be produced and stored when the electricity price is low. It also necessitates a H_2 storage, which has both investment and operational costs. For H_2 storage to be worthwhile, the associated reduction in electricity cost of H_2 production must outweigh these additional investment and operational costs, as illustrated in Figure 9.

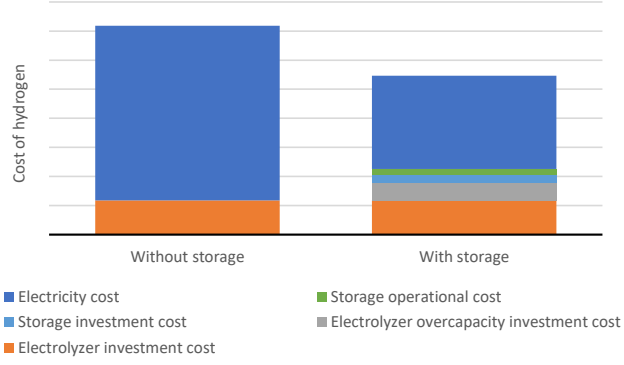

Figure 9: How a hydrogen storage can reduce the overall hydrogen production cost.

The profitability of investment into a H_2 storage depends largely on electricity price variations and the ability of the storage to adjust to them—if electricity prices are relatively stable, the H_2 storage serves no purpose other than increasing the investment cost, and potentially also operational costs, of the H-DR-EAF plant. From the perspective of investment into a H_2 storage, electricity price variations should preferably be both frequent and large in magnitude. If variations are large, the economic benefit of overproduction of H_2 at the lower electricity price to avoid production at the higher price increases. If electricity price variations are frequent, the storage volume can be smaller, resulting in lower investment costs [265].

All H_2 storages have operational limitations. These limitations prevent the optimal distribution of H_2 production to periods of low electricity prices. Some of these limitations can be chosen as storage design parameters and some are inherent to the storage technology. For instance, a storage has a certain maximum capacity that cannot be exceeded. The optimal choice of storage H_2 capacity is a compromise between operational flexibility and investment cost—a larger storage is also costlier. Identifying the optimal storage capacity is, thus, an optimization problem. The situation is similar for the EOC. Too little EOC means that too little excess H_2 can be produced to cover all electricity price peaks. Too much EOC increases investment costs and risks underutilization. An issue here is that the optimal combination of storage H_2 capacity and EOC depends on the electricity prices that the storage operator will encounter, which are not known in advance, at least not over the full intended economic lifetime of the storage.

As mentioned, some storage operational limitations are also inherent to the storage technology and are, thus, fixed. For instance, as shall be seen later in this chapter, H_2 storage based on reversible chemical reactions is often associated with a minimum hydrogenation process load, i.e., some minimum H_2 rate must always be supplied to the storage system. For geological H_2 storages, there are certain maximum allowable H_2 withdrawal and injection rates that cannot be exceeded without concern for the structural integrity of the storage.

The operational costs of H_2 storage depend on the storage technology and can come in different forms. For gaseous H_2 storage, the main operational cost is the cost of compressing the H_2 produced by the process electrolyzers to the storage pressure. Other kinds of storages may have an external heat demand. A consequence of the operational costs of all H_2 storages is that a certain minimum electricity price difference between filling and emptying the storage is needed, i.e., when storage operational costs are higher, the storage cannot be operated with a positive contribution margin as often and its utilization, thus, is lower, ceteris paribus [266].

As the H_2 demand of an industrial-scale H-DR-EAF plant is high, large storage capacities will be necessary for the storage to have a significant effect on the steel production costs. The appropriate H_2 storage volume will primarily be determined by the dynamics of the electricity market in which the H-DR-EAF plant operates. In HYBRIT RP1, analysis by Vattenfall AB has indicated that storage volumes equivalent to 7–14 days of H-DR plant H_2 consumption are optimal for projected north European conditions in 2035–2055 [267]. For the production of 2 Mt liquid steel/y, 7–14 days of H_2 consumption is then equivalent to storage capacities of 2 200–4 400 t H_2.

5.3 COMPARISON WITH LARGE-SCALE STORAGE OF NATURAL GAS

Although helium, propane, ethylene, propylene, and compressed air are all stored in relatively major amounts, NG is by far the most widely stored gas today [15, 268]. Therefore, it is sensible to consider how this gas is stored and handled when discussing the prospects of large-scale H_2 storage.

However, although there certainly exist similarities between the large-scale storage of NG and H_2, the comparison does falter somewhat in that the purposes of storing large amounts of NG or H_2 produced via electrolysis will be different. For NG, storage is needed to match a varying demand, most often across seasons[4], with a relatively steady supply [269, 270]. NG storages also operate in conjunction with other parts of the NG infrastructure in which significant amounts of gas can also be stored via pipeline pressure regulation (so-called '*linepack*') and in liquid NG (LNG) terminals to ensure sufficient supply security and flexibility [271]. For the storage of H_2 produced via electrolysis in the context of a fossil-free H-DR-EAF plant, an essentially standalone storage is needed to match a varying supply of fossil-free electricity with a relatively constant downstream H_2 demand, at least before a wider H_2 infrastructure is established. These different dynamics and purposes of storing NG and H_2 will lead to different operational demands and optimal storage solutions. Therefore, operational experience with NG storage cannot be translated directly to H_2 storage [272]. The consequences of the physical and chemical differences between NG and H_2 on optimal storage solutions should also not be underestimated [273, 274]. The generally higher economic value of H_2 compared to NG also means that partial gas losses or contamination are of more concern for its storage.

The need for large-scale storage of NG to ensure reliable supply was realized at an early stage. Due to the vast volumes required, the aboveground storage of larger amounts of NG is not economical. Therefore, underground storage utilizing various geological formations is utilized to minimize material costs and land use. The first commercial geological storage of NG was initiated already in 1915 in Ontario, Canada in a depleted NG field [268]. However, widespread use of geological NG storage emerged only after the second world war, up until 1950 nearly exclusively in depleted NG fields, then, although to a smaller extent, in aquifers and finally in solution-mined salt caverns [268, 270]. By and large, these remain the three options for large-scale storage of NG today and the choice of storage type is nearly always determined by the local geology [16, 275, 276].

The total NG storage working gas capacity in the EU and the UK is currently approximately 1 200 TWh [271]. During the winter, this storage capacity contributes on average to roughly 20% of the NG demand [271]. In the EU and UK, depleted NG field storage is by far the most common at 67.8% of the total working gas capacity, followed by salt caverns at 17.6% and aquifers at 14.6% [271]. In the US, depleted NG fields also make up most of the overall working NG storage capacity (total working capacity is 1 400 TWh) at 82%, followed by salt caverns at 10% and aquifers at 8% [277].

Salt cavern gas storage is fundamentally different from storage in depleted NG fields or aquifers in that the gas is not stored in the void space of a permeable matrix material. Instead, the gas is stored in a large cavity in a salt formation [278, 279]. The construction of such cavities is achieved via so-called solution mining: H_2O is pumped into an underground salt formation via a borehole, dissolving part of the salt to form brine. This process is continued until the desired salt cavity volume is reached. At this point, most of the brine in the storage is removed via gas pressurization. It is not viable to completely remove all brine and, thus, a small amount of brine sump remains in the bottom of the cavern throughout its operation. Therefore, gas withdrawn from salt caverns is saturated with H_2O and salt and must be generally be cleaned and dried before use [16, 21, 280-282]. Although solution

[4] Natural gas demand is typically higher in winter due to varying outside temperatures and, thus, heating demands.

mining is a simple procedure that can be performed entirely from aboveground, it is still considerably more complex than the construction of a depleted NG field or aquifer storage, which results in smaller gas storage capacities and higher investment costs [276]. It is also time-consuming: cavern construction can take up to five years [16]. The transportation and disposal of brine may also add significant costs [21, 271, 283].

The main advantages of salt cavern storage over depleted NG fields and aquifers are the higher achievable injection and withdrawal rates and the lower need for cushion gas [270]. Salt cavern storages can also reach higher annual turnover frequencies[5] of up to 10–12, while depleted NG field and aquifer storages are perhaps only cycled once or twice per year [21, 270, 278, 283]. A typical maximum storage pressure change rate of 10 bar per day is applied in salt cavern NG storages to maintain the structural stability of the cavern and prevent excessive wellhead erosion [280, 281, 284-286]. One factor limiting the maximum allowable salt cavern withdrawal rate exclusive to NG storage is the formation of CH_4 hydrates at low temperatures, which may cause clogging of wellhead equipment [281, 287]. Higher injection and withdrawal rates may be allowable when other gases than NG are stored. For instance, in the compressed air salt cavern storage in Huntorf, Germany, the maximum pressure reduction rate is reported to be 15 bar per hour [288].

The geological requirements for constructing depleted NG field, aquifer, or salt cavern storages cannot be met in all locations where large-scale NG storage is of interest. This has prompted the development of alternative storage technologies. The most prominent example of this is the lined rock cavern (LRC) concept, first developed in Sweden starting in the early 1980s to be a viable NG storage alternative for the prevailing regional geological conditions, i.e., predominantly crystalline bedrock [18, 289]. Unlined rock caverns, constructed via conventional drill-and-blast rock mining techniques, have been used for underground storage of fluids with low vapor pressures, most prominently crude oil, but also gasoline and liquefied petroleum gas for several decades [16, 18]. For more volatile fluids, e.g., NG, containment of the fluid inside the unlined rock cavern becomes problematic [17]. The innovation of the LRC concept is the introduction of a cavern liner, made from steel or plastic, that prevents gas permeation [275]. The liner is attached to the surrounding rock mass via an intermediate concrete layer, whose purpose is to transfer forces from the liner to the surrounding rock mass and to simplify the installation of the liner [18]. There currently exists only a single operational LRC, located in Skallen, Sweden [289]. This storage, which went into commercial operation in 2004, has a relatively small working gas capacity of 9.5 kt NG [16, 18]. The achievable operational profile of LRCs is claimed to be similar to that of salt caverns, i.e., annual turnover frequencies of 10–12. However, the Skallen storage has so far been operated far less intensively (1–2 annual turnovers) for various reasons [289]. The maximum withdrawal and injection rates as well as the number of storage cycles per year are mainly limited by the mechanical properties or the surrounding rock mass [16].

[5] This is defined as the total integrated injection and withdrawal flows during a full year; storages are generally not completely filled after each injection or emptied after each withdrawal (in terms of working gas).

5.4 GEOLOGICAL STORAGE OF HYDROGEN

For similar reasons as for NG, large amounts of H_2 are preferably stored in geological formations, although such storages are very uncommon today. Out of the main geological NG storage options discussed in the previous section, only salt caverns have been utilized for the storage of H_2 at a total of four sites, seen in Table 5 [19, 271]. The Teesside caverns are unusual in their shallow depth and their constant pressure operation—the pressure inside the salt caverns is kept constant via displacing withdrawn gas with brine, which is stored in surface pools [270].

Table 5: Currently operating salt cavern hydrogen storages [19, 270, 284].

Location	Teesside, UK (3 caverns)	Clemens Dome, Texas, USA	Moss Bluff, Texas, USA	Spindletop, Texas, USA
Operator	Sabic	Conoco Phillips	Praxair	Air Liquide
Start of operation	1972	1983	2007	2014
Storage volume [m³]	70 000·3 = 210 000	580 000	566 000	906 000
Mean depth [m]	365	1 000	1 200	1 340
Pressure [bar]	45	70–135	55–152	68–202
Stored H_2 [t]	810	2 400	3 690	8 230

Salt caverns turn out to be a better fit for large-scale H_2 storage than other geological options for several reasons: they are essentially gas-tight, the salt is inert towards H_2, the cushion gas demand is relatively low, and high storage pressures are achievable [16, 273, 290-292]. The ability to operate salt cavern storages more dynamically than depleted NG fields or aquifer storages is also an important advantage. For these reasons, there exists a growing consensus that salt cavern storage will be the most economical way to store large amounts of H_2 [271, 279, 290, 293-295]. The technical potential for the construction of salt caverns in Europe is also vast although it is far from evenly distributed across the continent [16, 290].

However, there is still uncertainty as to what maximum injection and withdrawal rates and the maximum cycling frequency can be achieved in H_2 salt caverns [272]. Another uncertain aspect is how and to what extent H_2 stored in salt caverns will interact with microorganisms present in the brine sump at the bottom of the cavern [291, 295]. Such interactions could potentially lead to H_2 loss, contamination, and various operational problems, e.g., equipment corrosion or clogging [15, 296, 297].

Given the similar operational characteristics as salt cavern storages, LRCs could be attractive for H_2 storage. Nevertheless, the use of LRCs for H_2 storage is yet entirely unproven, although the general principles of storing H_2 instead of NG in such facilities should not differ considerably [16]. The most notable difference between an LRC storing NG and one storing H_2 should be the choice of liner and aboveground equipment material [271]. Long-term exposure to H_2, especially at elevated pressures, tends to degrade common steel types in a process known as H_2 embrittlement [298, 299]. Therefore, costlier liner materials, e.g., austenitic steels, may be needed in a H_2 LRC [299-301]. A Skallen-sized LRC could theoretically store 640 t of H_2 [16]. A much smaller 100 m³ pilot H_2 LRC is currently under construction in Luleå, Sweden, as part of the HYBRIT initiative [271, 302]. Insights gained from this pilot LRC, e.g., regarding material choices and achievable operational dynamics, will be very important for the further development of H_2 LRCs.

Geological H_2 storage options other than salt caverns and LRCs appear far less appealing. H_2 storage in aquifers or depleted NG fields faces several challenges: the low allowable injection and withdrawal rates, the large demand for cushion gas, and the risks of H_2 losses and contamination during storage [16, 283]. That said, these kinds of H_2 storages may still find use considering the large achievable storage capacities and the potential for low specific cost storage, particularly if a widespread H_2 infrastructure emerges [273, 283]. In such a scenario, it is feasible that depleted NG field and aquifer H_2 storages could fulfill similar roles as they do in the current NG infrastructure: primarily seasonal storage with only a few injection and withdrawal cycles per year [271].

Some performance characteristics of geological H_2 storage options are seen in Table 6. It should be noted that the investment costs estimates are rather uncertain at present due to the limited experience with geological H_2 storage [16, 284, 297]. A prospective reason for the large spread in salt cavern investment costs is the wide range of storage volumes considered; the upper end of the range of investment costs is for a storage capacity of only 500 t H_2 [21]. In addition, it must be emphasized that investment costs of any geological storage also depend on local conditions, e.g., pre-existing knowledge of geology, labor costs, and brine disposal costs (for salt caverns) [16].

Table 6: Selected performance data for geological hydrogen storages [16, 18, 21, 271, 280, 297, 303, 304]. Costs of cushion gas, compressors, and other auxiliary equipment, e.g., for gas purification and drying post-storage, are excluded.

	Salt caverns	Lined rock cavern	Depleted natural gas fields	Aquifers
Storage maximum pressure (bar)	270–180	230	280	315
Working gas capacity (t H_2)	8 000–500*	1 920–640	>300 000	>6 000
Cushion gas requirement (% of total H_2)	54–30	18–4	40	80–50
Maximum injection rate (% of working gas capacity per day)	6–5	8–5	1	4–3
Maximum withdrawal rate (% of working gas capacity per day)	6–5	15–10	3–1	3–1
Specific investment cost (€/kg H_2)	23*–7	56–42	1	1

*Investment costs are generally lower for larger storages.

The salt cavern and LRC volumes in Table 6 are for single caverns; if larger storage volumes are needed and the geology allows it, it is possible to construct multiple caverns in the same geological formation [16, 18, 21]. However, the need for multiple caverns means that the economy of scale diminishes beyond a certain storage volume [16, 21]. For instance, in the HyUnder project (project partners included Shell, ludwig bölkow systemtechnik and E.ON), the specific investment cost per unit of working gas of LRCs was found to vary little between storage capacities of 640 t H_2 and 4 300 t H_2 due to the need for four separate caverns in the latter case [16].

5.4.1 Geological hydrogen storage for hydrogen direct reduction steelmaking

The first large-scale H-DR-EAF plants will likely have to operate without access to a widespread H_2 infrastructure of interconnected pipelines and storages. A consequence is that the onsite H_2 storage facility must be able to meet all electricity price fluctuations on a daily or potentially even hourly basis. Geological NG storages, and the few existing geological H_2 storages, have historically generally not been operated in this way. Depending on the electricity market in which the H-DR-EAF plant operates, managing these fluctuations via geological H_2 storage may prove challenging considering the typical allowable withdrawal and injection rates and annual turnover frequencies.

Nevertheless, the application of any kind of geological storage is naturally restricted by the surrounding geology [21, 305]. This may complicate the conversion of existing BF-BOF steelmaking facilities to the H-DR-EAF process as these were most certainly not located with such geological conditions in mind. At the same time, continued use of existing industrial steelmaking sites for H-DR-EAF steelmaking may be beneficial for several reasons. Some existing equipment and infrastructure, such as downstream steel processing equipment, e.g., for steel refining, casting, and rolling, certain auxiliary equipment, and at least parts of utility systems can continue to be used post-conversion, reducing conversion investment costs [245]. In addition, environmental permitting is likely more straightforward, and the existing skilled steelmaking workforce can be utilized [36, 89, 120, 245]. Furthermore, in certain places, e.g., continental Europe, the high population and building density may make finding a suitable new site, especially with suitable geological conditions for the construction of salt cavern or, potentially LRC, H_2 storages difficult [120]. This may lead to a demand for alternative H_2 storage technologies that are geologically independent, i.e., that can be placed anywhere, including close to existing steelmaking sites [306].

5.5 ALTERNATIVE HYDROGEN STORAGE TECHNOLOGIES

As with NG, larger amounts of H_2 will most likely be stored in geological formations for cost reasons [16, 271]. However, as discussed in the previous section, geological access to geological formations suitable for the construction of these kinds of storages is not ubiquitous, and this may come to be especially important for the conversion of existing BF-BOF sites to H-DR-EAF. Therefore, it is useful to identify geologically independent, economically viable large-scale H_2 storage options.

There are many ways in which large amounts of H_2 can potentially be stored without requiring special geological conditions. Due to the diversity of H_2 storage technologies, it is sensible to attempt to organize these into categories. The categorization that I have apply here, seen in Figure 10, is based on the strength of the interaction between the stored H_2 and the storage [307].

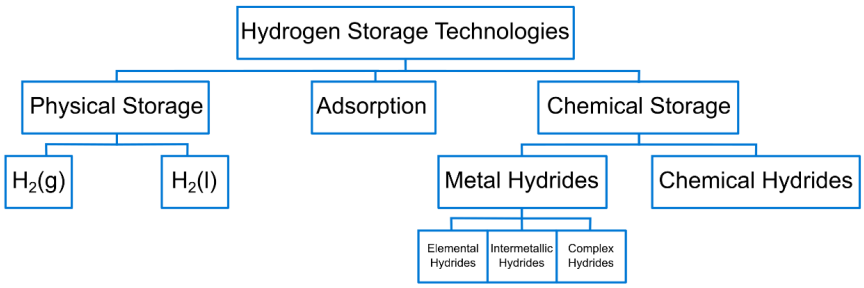

Figure 10: Categorization scheme for hydrogen storage technologies.

In physical H_2 storage, there is no significant physical or chemical interaction between the storage and the stored H_2, and the H_2 storage density is, thus, solely determined by the storage temperature and pressure. In adsorption-based storage, Van der Waals forces between an adsorbent and the stored H_2 are exploited to increase the H_2 density. In chemical storage, the H_2 undergoes a reversible chemical reaction and is then stored in atomic form as part of another molecule, known as a hydride.

5.5.1 Aboveground or near-surface storage of gaseous hydrogen

The use of aboveground tanks is in all likelihood not financially viable for the storage of the kinds of volumes of H_2 needed to significantly shift the electricity demand of an industrial-scale H-DR-EAF plant. Low storage pressures lead to tremendous storage volumes, while higher storage pressures lead to excessive single tank costs. Either way, the investment costs of aboveground H_2 storage tanks are high and are not expected to decrease to below 400–500 €/kg H_2 [170, 308, 309]. Even with optimistic cost developments, this is approximately ten times costlier than any geological H_2 storage option.

An alternative is to store H_2 in a series of shallowly buried pipelines. These kinds of pipe storage facilities are relatively common for NG storage in Germany, Austria, and Switzerland, where they are primarily used for demand peak shaving [16]. The construction of pipe storage facilities involves the excavation of soil to make room for the pipeline strings, and then the construction of the actual storage via welding of pipe segments [21]. The pipes are then buried, generally not more than a few meters below ground level [16]. To prevent corrosion, the exterior of the pipes is coated with, e.g., polyethylene [21]. Existing NG pipe storage facilities are rather small, equivalent H_2 storage capacities for identical maximum and minimum operating pressures are <45 t, although there are no technical limitations to the construction of larger storages [16].

Pipe storage has some advantages compared to the use of aboveground storage tanks. Firstly, the use of only a few pipes instead of many tanks reduces the material cost of the storage. Secondly, as they are buried underground, the land area above the storage can be used for other purposes, e.g., agriculture [310]. Nevertheless, investment costs, dominated by the pipe material costs, will still be much higher than for geological H_2 storage (300–450 €/kg H_2) [16, 21].

5.5.2 Liquid hydrogen

A major limitation of the geologically independent large-scale storage of gaseous H_2 is its low density, which leads to high storage container material costs. Therefore, it appears sensible to consider the liquefaction of H_2. Unfortunately, H_2 is a particularly difficult gas to both liquefy and store as a liquid.

The boiling point of H_2 is extremely low at around -253 °C (20 K) and, furthermore, H_2 does not cool upon isenthalpic expansion (also known as throttling) for temperatures above around -70 °C, which further complicates the liquefaction process [311]. Consequently, achieving large-scale H_2 liquefaction at lower electricity demands than 6 MWh_{el}/t H_2 (or 18% of H_2 LHV) is unlikely, even with process development (current plants require around 10–12 MWh_{el}/t H_2) [312, 313]. H_2 liquefaction plants are also associated with significant investment costs [314, 315]. The recent IDEALHY project (partners included Shell, Linde, SINTEF, and Kawasaki Heavy Industries) investigated opportunities for H_2 liquefaction cost reductions and reached investment costs of approximately 105 M€ for a next-generation 50 t H_2/d liquefaction plant [313]. Recently commissioned liquefaction plants in the USA have had significantly higher investment costs [316]. The viability of the dynamic operation of H_2 liquefaction plants, necessary in a H_2 storage application for an H-DR-EAF plant, is also currently unknown.

Storing liquid H_2 is challenging due to the combination of its low boiling temperature and low evaporation enthalpy [317, 318]. Consequently, liquid H_2 storage tanks are preferably vacuum-insulated, spherical, and large. The investment costs of these are around 25 €/kg H_2, which is significantly lower than for aboveground containers for compressed H_2 storage, but close to or higher than capacity costs of geological H_2 storage [308, 315, 319, 320]. Consequently, both overall liquid H_2 storage system investment and operational costs will be significantly higher than those of geological storages.

5.5.3 Adsorption-based hydrogen storage

Adsorption-based H_2 storages exploit physical Van der Waals bonding between H_2 and adsorbents with a large specific surface area to increase the H_2 storage density in a tank. The basic principle is that the additional volume and mass of the adsorbent is outweighed by the increase in H_2 density near the surface of the adsorbent [321]. Consequently, the H_2 storage density is primarily determined by the choice of adsorbent and the operating temperature and pressure [322]. Ideally, the increase in H_2 storage density caused by the adsorbent leads to a reduced storage pressure, which in turn leads to lower operational (compression) and investment (tank material) costs compared to gaseous H_2 storage [323].

A challenge is that H_2 tends to adsorb weakly and low temperatures and elevated pressures (typically limited to below 100 bar so that low-cost all-metal tanks can be utilized [324]) are, thus, necessary to reach high storage densities [324-327]. Adsorption-based H_2 storages are generally suggested to be operated at the boiling point of N_2 (-196 °C) as this is a relatively low-cost refrigerant capable of reaching low temperatures [325]. The operational costs of providing the necessary liquid N_2 refrigerant could well be in the vicinity of 6 kWh_{el}/kg stored H_2, i.e., close to the projected electricity demand of next-generation H_2 liquefaction plants [307, 312, 328-333]. The highest achieved H_2 storage density using adsorbents at -196 °C and 100 bar is around 40–45 kg/m^3; the density of gaseous H_2 at identical conditions is 31 kg/m^3 [321].

Beyond these potentially significant operational costs, investment costs of adsorption-based H_2 storage will also not be lower than for geological options. Storage vessels must be insulated to prevent desorption of H_2 during storage and also incorporate a liquid N_2 heat exchanger system [334]. Investment into a large-scale ASU for liquid N_2 production would also be needed. Finally, the cost of the adsorbent itself should not be underestimated. Activated carbons, considered one of the lowest-cost adsorbents, are priced at 2–4 €/kg and can achieve gravimetric H_2 storage densities of 5–6% by weight [335, 336]. The resulting adsorbent cost per kg of H_2 stored is, thus, 30–80 €/kg H_2. Total storage investment costs including all necessary auxiliary equipment, e.g., tanks, refrigeration system, and compressors, will be substantially higher. More advanced adsorbents, e.g., metal-organic frameworks, could reach somewhat higher storage densities but are also costlier than activated carbons [337-339]. In summary, the economic prospects of large-scale H_2 storage using adsorbents appear dubious as both operational and investment costs will most likely be high [324].

5.5.4 Solid hydrides

The idea of storing H_2 in solid hydrides has been around since at least the 1950s, with the principal advantage that high volumetric density H_2 storage can occur at atmospheric pressure and ambient temperature [340-342]. This is made possible by the strong chemical bonds formed between stored H_2 and the hydride. The downside to this strong chemical bonding is that H_2 release generally requires a significant amount of heat [343]. The solid hydrides can be divided into three broad categories: elemental hydrides, intermetallic hydrides, and complex hydrides.

Most of the elemental hydrides bind H_2 either too forcefully or loosely for reversible H_2 storage in them to be sensible. Magnesium hydride (MgH_2) is arguably considered the leading candidate due to its both relatively low cost (2–5 €/kg) and high gravimetric H_2 storage density (around 6% H_2 by weight is achievable in practice) [344-348]. The most significant downsides to MgH_2 are its high enthalpy of dehydrogenation and the slow kinetics of both its formation from Mg and its dehydrogenation [349, 350]. Although the kinetics issues can be at least partially managed via the use of catalysts and additives, the thermodynamic hurdle remains. The use of additives and catalysts also increases the investment cost of H_2 storage in MgH_2—finished material costs above 20 €/kg are possible, resulting in specific H_2 storage costs of over 300 €/kg H_2 [351]. Total storage costs, including, e.g., storage tanks and heat exchangers, will be substantially higher.

The discovery of multiple families of so-called intermetallic hydrides during the 1970s at Phillips in the Netherlands and Brookhaven National Laboratory in the USA widened the scope of metal hydrides potentially viable for H_2 storage significantly [352-354]. However, the gravimetric H_2 storage density of the intermetallic hydrides is always rather low (<3% by weight) and many metals in intermetallic hydrides also have relatively high market prices. Taken together, just the specific raw material cost of H_2 storage in intermetallic hydrides will most likely exceed 300 €/kg H_2 [354-356].

The complex hydrides are characterized by the covalent bonding of H_2 to a complex anion [357]. The anions most commonly applied for H_2 storage materials are alanates ($[AlH_4]^-$), amides ($[NH_2]^-$), and borohydrides ($[BH_4]^-$) [358, 359]. A commonly touted advantage of these hydrides is their high H_2 storage density, up to 18.5% by weight for $LiBH_4$. [360, 361]. Nevertheless, actual complex hydride pilot H_2 storages have been very rare [355, 360, 362]. The manufacturing costs of these materials are also currently high; the minimum cost of Ti-doped $NaAlH_4$, considered one of the more promising complex hydrides, has been estimated at around 10 €/kg, which yields a specific H_2 storage cost of 250 €/kg at a reversible H_2 capacity of 4% by weight [339, 355].

In summary, large-scale H_2 storage in the form of solid hydrides is most likely not economically competitive due to the high material costs. This fact has been pointed out previously by several authors [340, 363-365]. Additional barriers include material degradation, the heat demand of dehydrogenation, and the design of large-scale storage vessels that allow for efficient heat transfer to and from the solid material.

5.5.5 Liquid hydrogen carriers

A major barrier towards the large-scale storage of H_2 via adsorption or in the form of solid hydrides is the cost of the necessary materials. It is clear that for large-scale chemical H_2 storage to be economically viable, the material with which the H_2 interacts must be very inexpensive. This can be achieved by certain liquid hydrides (henceforth referred to as liquid H_2 carriers). The hydrogenated form of these carriers is always stored as a liquid, which reduces the investment cost of storage tanks, although it may require refrigeration or pressurization for certain carriers. Both the synthesis of the carriers and their dehydrogenation are similar to various conventional thermochemical processes. This allows for a lot of already existing know-how and equipment to be utilized in the design of liquid carrier H_2 storage systems. The idea of storing hydrogen (H_2) in a more manageable liquid form via reversible chemical reactions is far from a novel idea, having first been suggested in the 1970s [366-368].

The dehydrogenated form of liquid H_2 carriers can be either a gas or a liquid. Carriers that are stored in liquid form in their dehydrogenated state are usually referred to as liquid organic hydrogen carriers (LOHCs) [369, 370]. Although many liquid H_2 carriers have been suggested for H_2 storage in the scientific literature, most are not suitable for integration with H-DR-EAF plants for various reasons, most prominently due to a low technological readiness or a low thermodynamic efficiency of H_2 storage [266, 369, 371-373]. Therefore, two carriers that are gaseous in their dehydrogenated state, ammonia (NH_3) and methanol (CH_3OH), and two LOHCs (toluene and dibenzyltoluene) are considered in this thesis as these are the most technologically mature options [307]. The dehydrogenated forms of NH_3 and CH_3OH are N_2 and CO_2, respectively.

Both the hydrogenation and dehydrogenation processes would have to be operated dynamically without sacrificing too much in terms of process efficiency, catalyst or equipment degradation, maintenance costs, and process safety for liquid carrier-based H_2 storage to be sensible [374, 375]. The incentive for exploring such dynamic operation of thermochemical processes has historically been limited as these have generally operated on steady feeds of, e.g., NG or coal [376-378]. However, this is currently changing as the chemical and petrochemical sectors are increasingly decarbonized, most prominently via various so-called '*power-to-x*' technologies, to meet CO_2 emissions reduction targets and must adapt to the associated process flexibility challenges [379-381]. These developments in dynamic thermochemical process design can be leveraged in the design of liquid carrier-based H_2 storage systems.

5.5.5.1 Ammonia

Ammonia (NH_3) is one of the world's most widely produced chemicals, with around 70% used for fertilizer production [189, 382]. Although NH_3 is gaseous at normal conditions, its liquefaction is easily achieved (the normal boiling point of NH_3 is -33.3 °C), and it is commonly stored in liquid form [383-385]. The volumetric H_2 storage density of liquid NH_3 is significantly higher than that of liquid H_2 (121 kg H_2/m³ NH_3(l) vs. 71 kg H_2/m³ H_2(l)) [386]. Today, nearly all NH_3 is produced from N_2 and H_2 via the well-known Haber-Bosch process:

$$3\,H_2(g) + N_2(g) \rightarrow 2\,NH_3(g)\ (\Delta h_R^0 = -91.8\,\frac{kJ}{mol}) \qquad \text{(R25)}$$

The source of H_2 is most often NG reforming (approximately 70%) or coal gasification (30%) in modern NH_3 plants [382]. The source of N_2 is always air. In natural gas-based NH_3 production processes, N_2 is introduced via the partial oxidation of NG with air in a secondary reformer, which simultaneously consumes the O_2 in the air [387-389]. A simplified Haber-Bosch process flow scheme is shown in Figure 11.

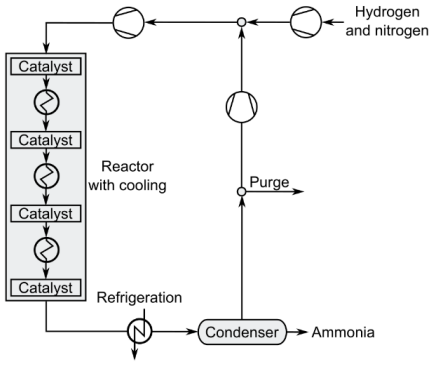

Figure 11: Haber-Bosch process for ammonia production.

The input stream of H_2 and N_2 to a conventional Haber-Bosch process must contain an exceptionally small concentration of impurities to prevent catalyst poisoning [387, 390]. Fe-based NH_3 synthesis catalysts, originally developed by Alvin Mittasch and coworkers at BASF at the start of the 20th century, are used in most modern plants [390, 391].

A high Haber-Bosch reactor temperature (350–600 °C) is necessary for kinetic reasons [387, 389, 390]. The amount of heat generated by the reactor is 0.8–0.9 kWh/kg NH_3; approximately 0.2–0.4 kWh/kg NH_3 may also be recovered from the intercooling of process compressors [392-395]. In modern Haber-Bosch plants, this heat is utilized to produce steam to power process compressors; a part can generally also be exported, e.g., for electricity generation or heat integration with other processes [284, 387, 394].

Typical reactor pressures in the Haber-Bosch process are 150–450 bar [387, 389]. However, complete conversion is still not achieved in a single reactor pass. The produced NH_3 is separated out via condensation and unconverted gases are recompressed and recycled. As the partial pressure of NH_3 at the reactor outlet is generally relatively low, refrigeration is typically needed to reach sufficiently low temperatures to allow for NH_3 condensation (cooling water may be sufficient for high-pressure plants) [394]. A part of the recycled gas is purged to prevent the accumulation of inerts, e.g., CH_4 and argon, in the process.

As the conventional Haber-Bosch process operates on essentially pure N_2 and H_2, converting it to operate on H_2 from electrolysis is not a significant challenge from a technical standpoint and there are several operational electrolysis-based Haber-Bosch pilot plants, e.g., in Minnesota, USA, and Oxfordshire, UK [396, 397]. In such plants, N_2 must be introduced in another way than in the conventional Haber-Bosch process. At large scales, cryogenic air separation via ASU is the most economical process option [333, 386, 398-406]. If H_2 is produced via electrolysis and N_2 is supplied via an ASU, only a very small, if any, purge stream is expected to be necessary, especially as small amounts of inerts are soluble in the NH_3 product [394, 395, 406]. The overall electricity demand of a Haber-Bosch process with H_2 production via electrolysis and N_2 production via an ASU has been estimated to be 0.6–1.8 kWh/kg NH_3, equivalent to 3–10 kWh/kg H_2 stored [320, 332, 386, 395, 401, 406-408].

For NH_3 to be useful as a liquid H_2 carrier it must be possible to operate the synthesis process dynamically. Conventional NH_3 plants typically operate at a minimum load of 50–60% with only rare shutdowns for maintenance and start-up takes multiple days [409, 410]. However, significant developments have occurred in recent years and several equipment suppliers also now claim to provide Haber-Bosch plants capable minimum loads as low as 10% of the nominal capacity [199, 397,

410-416]. The foremost challenge associated with varying the NH_3 production rate in the Haber-Bosch process is maintaining a reactor temperature profile that prevents irreversible catalyst damage [412, 417]. If the Haber-Bosch is to be operated dynamically, the ASU should preferably be able to follow any load changes. Like the Haber-Bosch process, there has existed little demand for the dynamic operation of ASUs historically; conventional ASUs typically have a minimum load of 60% [386, 388, 389]. However, it does appear that more flexible ASU operation is feasible with the development of new process control strategies [418-421].

NH_3 dehydrogenation (also called "cracking") is a far less explored process than NH_3 production [422-424]. Currently operating plants are small (<100 kg H_2/h) and are mainly used for galvanizing and annealing metals [417, 425]. The only exception found in the literature is the Arroyito heavy water production plant in Argentina, where a 3 000 t NH_3/d cracker is used; the plant equipment, similar to that used in a SMR plant, was supplied by Haldor Topsøe A/S [284]. A theoretic minimum of 4.2 kWh/kg of heat is required for the dehydrogenation of NH_3 (13% of the LHV of H_2). This assumes that the heat for NH_3 evaporation is freely available, which is a reasonable assumption if the NH_3 cracker operates at close to atmospheric pressure. However, higher cracker pressures are often suggested as this benefits the downstream gas separation process [284, 306, 424].

Several authors have simulated the prospective performance of NH_3 cracking plants in recent years [284, 306, 424, 426, 427]. These simulated plants utilize an SMR-type fired furnace tube bundle reactor and either a pressure swing adsorption (PSA) or a cryogenic process for gas separation. A 200 t H_2/d NH_3 dehydrogenation plant was simulated in the recent 'Ammonia to Green Hydrogen' study (led by Engie and Siemens among others) [423]. The estimated total plant heat demand was 14.3 kWh/kg H_2 (43% of LHV of H_2). In contrast, the recent 'H21 North of England' study led by Equinor found that only around 20% of released H_2 must be combusted to provide heat for the dehydrogenation process [284]. The viability of the dynamic operation of these SMR-like NH_3 dehydrogenation plants is presently uncertain (conventional SMR plants are not operated dynamically) [428].

A potentially promising pathway towards an NH_3 dehydrogenation process suitable for large-scale H_2 storage is reactor electrification, as was recently suggested for H_2 production via SMR [429, 430]. Haldor Topsøe A/S has patented an NH_3 dehydrogenation process based on an electrified reactor; it is claimed that the electricity demand of such an NH_3 dehydrogenation process can be 6–8 kWh/kg H_2 released, but no detailed description of an electrified NH_3 cracker exists in the open literature [415]. The advantages of reactor electrification could include a higher heat transfer efficiency, improved catalyst utilization, and a more rapid start-up of the process [429, 431].

5.5.5.2 Liquid organic hydrogen carriers

The LOHCs are distinct among the liquid H_2 carriers due to their liquid dehydrogenated form. This provides some noteworthy advantages: 1) the post-dehydrogenation separation of carrier and H_2 is easily achieved; 2) the dehydrogenated carrier can be directly recycled to store additional H_2; 3) H_2 is the only gas that must be compressed to the hydrogenation reactor pressure [432, 433]. Downsides to LOHCs include their relatively high cost, the need for at least two storage tanks, and the generally large heat demand of their dehydrogenation.

The storage of H_2 in LOHCs is based on the reversible saturation of carbon-carbon double bonds. Although the storage mechanism is simple, finding an LOHC that exhibits optimal properties for H_2 storage is not trivial. An ideal LOHC is cheap, has a high H_2 storage density, a low enthalpy of dehydrogenation, a high boiling point, a low freezing point to enable liquid-phase storage at all encountered storage temperatures, and low toxicity [373, 434].

The two most commonly suggested LOHCs, toluene (C_7H_8) and dibenzyltoluene ($C_{21}H_{20}$), are both aromatic in their dehydrogenated state, as seen in Figure 12 [435]. N-ethylcarbazole has previously also been considered a promising LOHC candidate but its high price, along with its melting point at 68 °C, renders it unviable for large-scale H_2 storage [432, 436]. Both toluene and dibenzyltoluene-based LOHC systems are currently being commercialized, toluene most notably by Chiyoda Corporation in Japan and dibenzyltoluene most notably by Hydrogenious GmbH in Germany [432, 437].

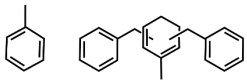

Figure 12: Molecular structures the toluene (left) and dibenzyltoluene (right).

These LOHCs can both theoretically store around 6% H_2 by weight via their hydrogenation; dibenzyltoluene has a higher H_2 storage capacity by volume (57 kg H_2/m^3 vs. 48 kg H_2/m^3 for toluene) [438]. However, full LOHC dehydrogenation is not practical due to reactor kinetics and material degradation, which reduces the usable H_2 storage capacity of LOHCs and increases investment and operational costs [439].

Toluene is already produced in very large capacities today at bulk prices of 0.5–0.7 €/kg [306, 432, 440, 441]. Dibenzyltoluene is inherently more expensive (currently 4–5 €/kg, 2 €/kg is considered achievable upon production scale-up) as it is produced starting from toluene [315, 320, 441, 442]. It is typically assumed that 0.1% of the LOHC must be replaced per storage cycle but as no large-scale LOHC H_2 storage system yet exist, what values to expect in practice must be considered uncertain [320, 435].

LOHC dehydrogenation typically takes place at pressures of 1–5 bar and temperatures of 270–320 °C, often over a platinum (Pt) on alumina (Al_2O_3) catalyst, but catalysts based on ruthenium (Ru) and rhenium (Rh) have also been suggested [373, 437, 443-445]. One of the main challenges of large-scale H_2 storage in LOHCs is the large heat demands of the dehydrogenation processes. This heat demand is mainly determined by the enthalpy of the dehydrogenation reactions, which are 9.7 and 9.0 kWh/kg H_2 for methylcyclohexane and perhydro-dibenzyltoluene, respectively [446]. If this heat is provided by the combustion of part of the released H_2, at least 25–30% of stored H_2 would be lost.

One significant difference between perhydro-dibenzyltoluene and methylcyclohexane relevant for H_2 storage is the much lower vapor pressure of the former. This affects the dehydrogenation process design. The dehydrogenation of methylcyclohexane is, in contrast to that of perhydro-dibenzyltoluene, typically assumed to occur entirely in the gas phase and would, thus, also require heat for evaporation methylcyclohexane. Refrigeration may also be required to achieve satisfactory separation of toluene and H_2 after the dehydrogenation reactor [306, 446].

The hydrogenation of toluene or dibenzyltoluene is typically carried out at pressures of 10–80 bar and temperatures of 150–300 °C [306, 432, 436]. Hydrogenation catalysts are often also based on PGMs on an Al_2O_3 support. For dibenzyltoluene, catalysts based on Ru and Pt are more active below and above 200 °C, respectively [432]. Large amounts of high-temperature heat are generated during the hydrogenation process, which necessitates cooled, e.g., steam raising, reactors [447].

5.5.5.3 Methanol

Methanol (CH_3OH), the simplest alcohol, contains 12.5% H_2 by weight and has long been considered a promising H_2 carrier [448, 449]. Its normal boiling point is 64.7 °C and it is typically stored in conventional floating roof tanks at atmospheric pressure. The global production of CH_3OH is currently nearly 100 Mt per year [450, 451]. It is most often used for the production of formaldehyde or acetic acid, but gasoline blending and other fuel uses are increasingly important applications [451,

452]. CH_3OH is currently near-exclusively produced from NG or, mainly in China, coal [453]. Both routes are associated with significant direct CO_2 emissions, 0.5–1.0 t CO_2/t CH_3OH for the process based on NG and 2.8–3.5 t CO_2/t CH_3OH starting from coal [454, 455]. The first step of both these production processes is the generation of a synthesis gas, which consists mainly of H_2 and CO with small amounts of CO_2, via either NG reforming or coal gasification. This synthesis gas is then compressed and sent to the CH_3OH synthesis reactor loop [452, 455-457]. If CH_3OH is to be utilized as a liquid H_2, it must be possible to reversibly store H_2 produced via electrolysis in it. This can be achieved via reaction (R26) [458]:

$$3\,H_2(g) + CO_2(g) \rightleftharpoons CH_3OH(g) + H_2O(g)\ (\Delta h_R^0 = -49.2\ \frac{kJ}{mol}) \qquad \text{(R26)}$$

The reverse reaction of (R26) is called CH_3OH steam reforming (MSR) [106]. Three moles of H_2 can be released per mole of CH_3OH via MSR and one-third of this H_2 originates from H_2O. Cost-effective H_2 storage in CH_3OH depends on access to a suitable CO_2 source; potential CO_2 sources in the context of an H-DR-EAF plant are discussed in section 6.1.1. The main challenges of CH_3OH production starting from H_2 and CO_2 rather than the conventional synthesis gas are the lower equilibrium conversion and the increased formation of H_2O, which increases the energy demand of the downstream distillation process [459, 460]. The higher concentration of H_2O in the reactor may also reduce the catalyst activity due to the blocking of catalytic sites [459]. An advantage of the CO_2-based route is the less exothermic CH_3OH-forming reaction, which simplifies reactor temperature control and reduces byproduct formation significantly [197, 460-463].

The production of CH_3OH from CO_2 and H_2 is already applied commercially in a 4 000 t/y plant operated by Carbon Recycling International (CRI) in Iceland [453]. Some early CH_3OH plants in the USA also operated on a feed of H_2 and CO_2 already during the 1920s and 1930s [453, 464, 465]. CRI is also planning a 100 000 t/y plant in Finnfjord, Norway and Swedish Liquid Wind has announced plans to build a 50 000 t/y plant in Örnsköldsvik, Sweden [451]. Multiple equipment suppliers currently provide solutions for CO_2-based CH_3OH [451, 462, 466].

The basic layout of a CO_2-based CH_3OH production plant, seen in Figure 13, is identical to that of conventional plants and reactor conditions are also similar (50–100 bar and around 250 °C). As in the Haber-Bosch process, a purge stream is required to prevent to accumulation of inerts in the reactor loop. The necessary purge gas rate is expected to be 0.1–1.0% of the top gas in a CO_2-based CH_3OH production process, mainly depending on the purity of CO_2 fed to the process as this should be the only major source of inerts if H_2 is produced via electrolysis[455, 467, 468].

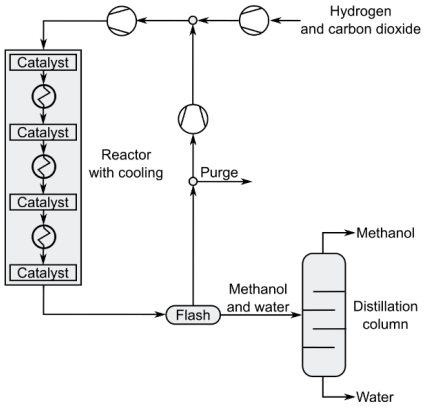

Figure 13: Process for methanol production from hydrogen and carbon dioxide.

The catalyst plays a critical role in CH_3OH synthesis as a wide range of products may potentially be produced from the same gas mixture at similar pressures and temperatures, most notably straight-chain saturated hydrocarbons (the Fischer-Tropsch process) and CH_4 (the Sabatier process). The catalyst applied in modern conventional CH_3OH plants is always based on copper-zinc oxide-alumina ($Cu/ZnO/Al_2O_3$) and these kinds of catalysts are both very active and selective for CH_3OH synthesis [452]. An identical catalyst can be utilized for CO_2-based CH_3OH production, although new catalyst specially engineered for CO_2-based production are also being developed [453, 455, 464].

The majority of the electricity demand of CH_3OH production is due to gas compression [469, 470]. Typical values in the literature are 0.1–0.3 kWh/kg CH_3OH for H_2 supply via pressurized electrolysis at 20–30 bar, equivalent to 0.5–1.6 kWh/kg H_2 stored [320, 462, 467, 468, 470-473]. This does not include the energy needed to provide CO_2 to the CH_3OH production process, which may be significant, e.g., if CO_2 is separated out from a relatively dilute gas stream [106]. The basic overall mass and energy balances of a CO_2-based CH_3OH production process are shown in Figure 14 [470].

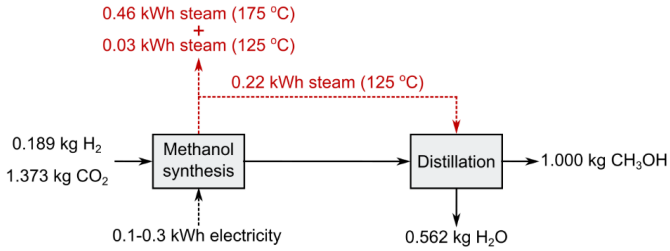

Figure 14: Mass and energy balances of carbon dioxide-based methanol production [462, 463].

The heat required for the distillation process can be completely covered by the heat generated by the CH_3OH synthesis reaction and the overall process, thus, requires no external heating [456, 462]. However, if CH_3OH is to be used as a liquid H_2 carrier, it is not strictly necessary to separate the produced CH_3OH and H_2O as these must be mixed before MSR anyway. Avoiding distillation would reduce plant investment costs and free up low-pressure steam for other uses. However, the technical viability of such a setup is yet uncertain and not separating CH_3OH and H_2O would decrease the effective H_2 storage density [449, 462, 463]. Nevertheless, if distillation is used, H_2O supply for MSR is not a major issue in the context of an H-DR-EAF process as MSR then replaces H_2 production via electrolysis, which requires three times as much H_2O per unit H_2.

The dynamic operation of CH_3OH production processes, necessary for its use as a H_2 storage medium, appears feasible [455, 469, 474-478]. Minimum loads of around 10–20% of the nominal production rate have been reported with maximum load change rates of from 20% per hour to 90% within a few minutes [474, 475, 479]. That said, such dynamic operation is not common and the long-term effects of such operation, e.g., on the CH_3OH synthesis catalyst, requires further investigation.

H_2 production from CH_3OH via MSR is a fully commercialized technology, but only for relatively small-scale applications (up to around 300 kg H_2/h) [480-484]. However, there are no fundamental upscaling limitations to MSR plants as only standard chemical equipment is used in the process [482]. A simplified process scheme of an MSR plant is seen in Figure 15.

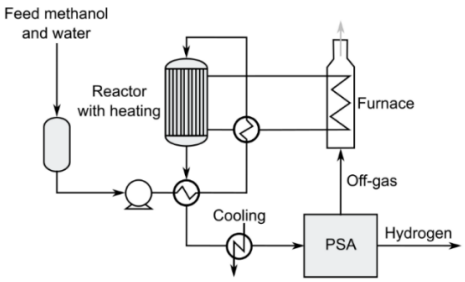

Figure 15: Methanol steam reforming process.

Liquid CH_3OH and H_2O are first pumped to the reactor pressure, which is typically 3–30 bar [306, 483, 485, 486]. The mixture is then heated up via heat exchange with the reactor outlet stream, vaporized via heat exchange with a heat transfer oil, and sent to the catalyst-filled MSR reactor. The reactor temperature is typically 200–300 °C, also maintained via the circulating heat transfer oil [487]. Most commonly, a Cu-based catalyst very similar in composition to that utilized in the CH_3OH production process is utilized [458]. The product mixture is then cooled (typically with cooling water) and sent to a PSA unit for separation [481, 487]. The PSA separation process results in one stream of near-pure H_2 (usually 99.9–99.999% by volume) and a tail gas that is combusted to provide heat for the process. Typical PSA H_2 recovery is 70–95%, mainly depending on the target H_2 purity [488-490]. For instance, an recovery of 80% has been considered reasonable for the production of PEM fuel cell grade H_2 via MSR [306]. Lower H_2 purities are necessary for an H-DR process, rendering higher H_2 PSA recoveries attainable [161, 335].

The majority of the MSR heat demand is for the evaporation of CH_3OH and H_2O, not the MSR reaction itself [483]. As the boiling temperature of the CH_3OH and H_2O mixture depends on the pressure, it may be advantageous to conduct the evaporation at a lower pressure in certain cases to allow for heat integration with other processes [306]. A lower reactor pressure is also favorable in terms of the chemical equilibrium of the MSR reaction. The downside to the low-pressure evaporation strategy is that the MSR reactor product mixture must then be compressed prior to the PSA separation process, which requires more work compared to the pumping of liquid CH_3OH and H_2O [306]. As with NH_3 dehydrogenation, an electrified MSR reactor is also feasible and Haldor Topsøe A/S has recently patented an MSR process based on such a reactor [428, 431, 491]. However, no electrified MSR plants exist today and the achievable performance of such plants is, thus, yet uncertain.

6 LIQUID HYDROGEN CARRIERS IN HYDROGEN DIRECT REDUCTION STEELMAKING (PAPERS II, IV–VI)

Among all options considered in the previous chapter, storage of H_2 in liquid carriers appears the most sensible alternative to its geological storage. The primary reason for this is that it is in all likelihood only these kinds of H_2 storages that have the potential to be competitive with geological storages on both an investment and operational cost basis. Moreover, as similar large-scale chemical processes already exist, the technological readiness of certain liquid carrier-based H_2 storage systems may be considered high.

The storage of H_2 in liquid carriers involves thermochemical processes to both store and release the H_2. It is of interest in the current context to consider how the heat flows of these thermochemical processes may be integrated with the H-DR-EAF steelmaking process as this could enable savings in storage operational costs. In the case of H_2 storage in CH_3OH, the integration of a suitable CO_2 supply is also necessary. The major opportunities for process integration between the H-DR-EAF process and liquid carrier H_2 storages are shown schematically in Figure 16 and is explored in this chapter. At the end of the chapter, the investment costs of liquid carrier-based H_2 storages are also estimated and compared with those of geological storages.

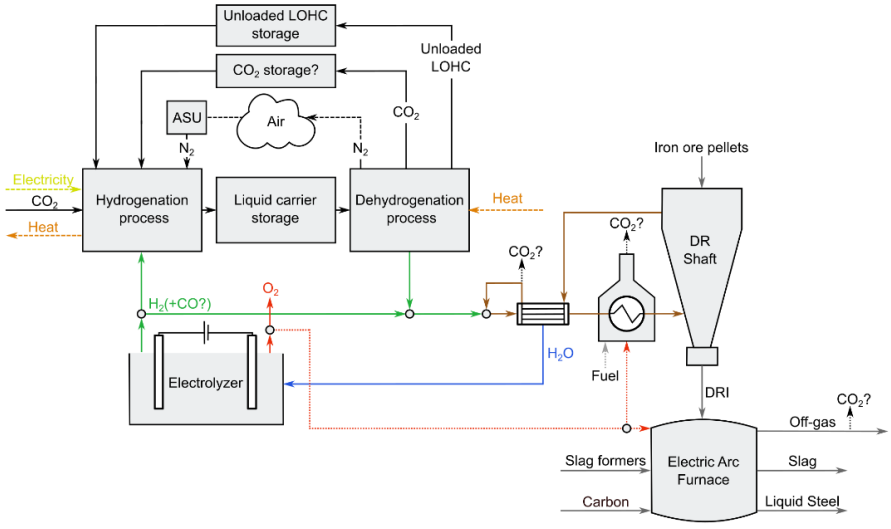

Figure 16: Liquid hydrogen carrier hydrogen direct reduction process integration possibilities.

6.1 POSSIBILITIES FOR LIQUID HYDROGEN CARRIER INTEGRATION

6.1.1 Carbon dioxide sources

As mentioned previously, H_2 storage in CH_3OH requires a suitable source of CO_2. CO_2 sourcing is also of interest for the integration of steam and CO_2 SOEL co-electrolysis in H-DR-EAF plants. As seen in Figure 16, there are in principle three possible CO_2 supply options: internal recycling of CO_2 from the MSR process, an input of external CO_2, and the utilization of CO_2 generated in the H-DR-EAF plant.

6.1.1.1 Internal recycling of carbon dioxide

As the overall CH_3OH-based H_2 storage cycle is theoretically CO_2-neutral (per (R26)) it appears sensible to simply recycle CO_2 released during MSR for the production of new CH_3OH. In such a scenario, CO_2 would essentially be treated as the dehydrogenated form of a LOHC-based H_2 storage system. A theoretical advantage of CH_3OH compared to the LOHCs is the relatively low cost of CO_2; assuming even relatively high CO_2 prices gives to moderate H_2 storage costs (100 €/t CO_2 leads to 0.7 €/kg H_2, at least an order of magnitude below LOHC H_2 storage costs). However, this kind of closed-loop CO_2 recycling for CH_3OH-based H_2 storage is challenging in practice for several reasons.

First and foremost, as the CH_3OH production and MSR processes will not be operated simultaneously, any kind of CO_2 recycling strategy would have to involve CO_2 storage. As CO_2 only exists as a solid or gas at atmospheric pressure, any kind of larger storage must be pressurized and liquefied, which increases both investment and operational costs [492]. Some CO_2 will also inevitably be lost during the storage cycle, predominantly with the combustion of the MSR process PSA off-gas. Consequently, some additional source of CO_2 will in all likelihood both needed and preferable for CH_3OH-based H_2 storage in an H-DR-EAF plant.

Nevertheless, partial internal CO_2 recycling may be sensible in certain cases. For instance, when the MSR process is operated, i.e., predominantly during times of high electricity prices, it may be practical to separate out a relatively small stream of CO_2 from the PSA process that can be directly recycled to the CH_3OH production process operating at minimum load. As the generated CO_2 is immediately recycled in such a scheme, intermediate CO_2 liquefaction and storage is then unnecessary.

6.1.1.2 External carbon dioxide

Biogenic CO_2, which would be necessary for a fossil-free H-DR process, for CH_3OH-based H_2 storage can potentially be sourced at 20 €/t or less from certain processes, e.g., bioethanol or biogas upgrading plants. This would yield a minimum added cost of 0.2 €/kg H_2 stored in CH_3OH [22, 119, 493, 494]. Nevertheless, the viability this approach depends on the presence of such plants within a reasonable distance of the H-DR-EAF plant. In the case that such external sources of CO_2 are utilized for CH_3OH production, it may be advantageous to co-locate the CH_3OH production process with the external CO_2 source considering the relatively low cost of transporting CH_3OH vs. CO_2. However, such schemes are not explored further herein.

6.1.1.3 Internal carbon dioxide generation

There are multiple points at which relatively concentrated streams of CO_2 could arise in an H-DR-EAF plant [266]. Utilizing these sources for H_2 storage in CH_3OH may be more cost-effective than the import of CO_2 to the H-DR site as this CO_2 would essentially be a byproduct and, thus, available at a very low cost. As seen in Figure 16, the potential sources of CO_2 in an H-DR-EAF plant are:

- the EAF off-gas,
- separation of CO_2 from the shaft furnace top gas in case that a carburized DRI is produced,
- the reducing gas preheating process in case an external fuel is combusted.

However, the first two of these sources are unlikely to be suitable for integration with a CH_3OH production process and are associated with few, if any, co-benefits. Only relatively small amounts of relatively diluted CO_2 is generated batch-wise in the EAF and DRI carburization will not generate much excess CO_2 regardless of whether it is based on SOEL co-electrolysis or an externally supplied carburization agent, e.g., biogas (a mixture of mostly CH_4 and CO_2 produced via anaerobic fermentation of biomass), bio-CH_4 (biogas that has been upgraded via selective removal of CO_2), syngas generated via the gasification or pyrolysis of biomass, or CH_4 produced from such gasification or pyrolysis syngas, i.e., synthetic NG (SNG) [495, 496].

The remaining point in the H-DR-EAF process at which significant CO_2 production is conceivable is the reducing gas preheating process. This preheating can be provided in different ways. As mentioned previously, the production and combustion of H_2 purely for the purposes of heat generation is likely not a suitable approach due to the relatively low efficiency of electrolysis [45, 59, 155]. Direct electrical heating of the reducing gas is a more efficient option, but is not used in conventional DR processes and must be developed and tested before application in an H-DR process [497]. Nevertheless, electrical reducing gas preheating would, as seen in section 4.3, increase the overall electricity demand of an H-DR plant by around 10% and may be an expensive solution, particularly during periods of high electricity prices.

The remaining reducing gas preheating option is the combustion of an externally supplied fuel. This is a lower-cost option than electrical heating in most regions and is already utilized in conventional DR plants, in which top gas and NG are combusted for reducing gas preheating [70, 97]. Other, biomass-based, fuels will have to be used in fossil-free H-DR-EAF plants. The biomass-based fuels most similar to those used in conventional DR processes (i.e., mixtures of mostly CH_4, CO, and H_2) are syngas from biomass pyrolysis or gasification, biogas, bio-CH_4, and SNG. However, although the use of these fuels in the preheating process is most likely not associated with any major technical challenges, their production cost may be a barrier [131, 498]. A more cost-effective option may be to directly combust woody biomass in the form of forest residues, waste wood, recovered wood, or, possibly, pellets as this avoids intermediate conversion steps; in forest-rich regions, e.g. Sweden and Finland, solid biomass fuels are generally available at below 25 €/MWh [91, 131, 451, 498-501]. A potential challenge for the application of these kinds of fuels for H-DR reducing gas preheating is achieving sufficiently high reducing gas temperatures [502, 503].

Biomass oxy-fuel combustion utilizing the electrolysis byproduct O_2 is attractive as it may provide both heat and CO_2 to a fossil-free H-DR-EAF plant. By combusting biomass with O_2 instead of air, the resulting flue gas will consist of mainly H_2O and CO_2 [504]. A stream of CO_2 suitable for CH_3OH production can easily be separated out from this flue gas via H_2O condensation and sulfur removal via, e.g., a sulfur guard bed [505]. The remaining heat in the combustion flue gas after heat exchange with the H-DR reducing gas can also be used elsewhere in the plant or for district heating. An additional advantage of oxy-fuel is that the biomass demand can be reduced somewhat compared to if preheating was provided by combustion in air [134, 503].

A basic prerequisite for cost-effective oxy-fuel combustion is that the electrolysis O_2 byproduct is not completely utilized for other purposes. As shown in section 4.1, EAF operation requires only a small fraction of the total O_2 produced in an H-DR-EAF plant. Another conceivable use of the O_2 byproduct is in an upstream iron ore pelletizing plant if this is located reasonably close by [13, 171, 234, 506]. If there is an excess of O_2 after internal utilization that cannot be sold off due to limitations in demand, the opportunity cost of utilizing it for oxy-fuel combustion is close to zero. Consequently, if the oxy-fuel combustion process is sized to supply the reducing gas preheating demand, the resulting CO_2 should also be available at a very low cost.

As the electrolyzers are operated dynamically in response to electricity price variations in an H-DR-EAF plant with integrated H_2 storage, O_2 generation will not be constant. However, the variations in O_2 production will be synchronized with the demand for CO_2 for CH_3OH production. When the electricity price is low, more H_2 and, thus, O_2 is produced via electrolysis and more H_2 can be stored as CH_3OH. When the electricity price is high, less H_2 is stored in CH_3OH and it is, thus, not strictly necessary to apply oxy-fuel combustion and the biomass can be combusted in air instead to provide the necessary reducing gas preheating. As mentioned in section 6.1.1.1, any CO_2 necessary to maintain a minimum CH_3OH production rate can then be sourced from the PSA section of the MSR process instead [488, 489].

The amount of biomass required for supplying the required reducing gas preheating for a 2 Mt H-DR-EAF plant via oxy-fuel combustion is 143 MW (LHV) and this requires 46% of the O_2 produced in the process electrolyzers. Around half of all O_2 produced by electrolyzers is, thus, still left after utilization in the EAF and oxy-fuel biomass combustion for reducing gas preheating. The associated production of CO_2 is 1 361 t/d (454 kt/y) or 227 kg CO_2/t liquid steel. This CO_2 can be used to store a maximum of 187 t H_2/d or 31 kg H_2/t liquid steel as CH_3OH, which is equivalent to 59% of the H_2 demand of the H-DR-EAF plant. In addition, up to 28 MW of additional district heating (112 kWh/t liquid steel) can be generated via flue gas cooling and condensation to 50 °C, increasing the total potential district heating output of the H-DR-EAF plant by 23–28% compared to the case with electrical reducing gas preheating.

6.1.2 Dehydrogenation processes

The majority of the energy demand of H_2 storage in liquid carries is associated with the supply of heat to dehydrogenation processes. Consequently, the economic viability of H_2 storage in these carriers depends to a large extent on the cost of this heat supply. In this section, the main options for sourcing this heat in the context of an H-DR-EAF process and the potential advantages and disadvantages of these are discussed.

The amount and temperature of heat necessary for dehydrogenation depend on the liquid H_2 carrier. For NH_3 and the LOHCs, the majority of the necessary heat is at the reactor temperature (>300 °C). For CH_3OH, a large part of the heat demand of MSR is for the evaporation of CH_3OH and H_2O, which can potentially be supplied at a lower temperature, depending on the evaporation pressure. Nevertheless, the dehydrogenation heat demand is substantial for all considered liquid H_2 carriers. The theoretical minimum heat demand is determined by the enthalpy of the dehydrogenation reactions. For a 2 Mt/y H-DR-EAF plant, the minimum dehydrogenation heat demand to supply the total shaft furnace H_2 demand varies significantly depending on the chosen liquid carrier: 127 MW for methylcyclohexane, 110 MW for perhydro-dibenzyltoluene, 55 MW for NH_3, and 30 MW for CH_3OH (79 MW including heat to evaporate CH_3OH and H_2O) [307].

6.1.2.1 Possibilities for heat integration with hydrogen direct reduction steelmaking

Although the overall H-DR-EAF process is endothermic, there are certain points in the process where surplus heat could potentially be generated. This surplus heat may potentially be utilized to improve the overall efficiency of H_2 storage in liquid carriers via decreasing the demand for external fuel or electricity. Firstly, electrolyzers will always generate a certain amount of surplus heat at their operating temperature. PEMELs and AELs will generate more such surplus heat than SOELs due to their lower electrical efficiencies, but the heat is at a relatively low temperature (50–90 °C), typically too low for it to be directly utilizable in liquid carrier dehydrogenation processes [229, 230, 454]. Moreover, in the context of H_2 storage in an H-DR-EAF plant, the electrolyzers will generally only operate at lower loads when the dehydrogenation process is operated anyway, limiting possibilities for direct integration without heat storage [186, 230, 507].

After the electrolyzers, the EAF is the most electricity-intensive part of an H-DR-EAF plant. Therefore, it may be sensible to halt EAF operation when electricity prices are high. In such a scenario, CDRI could be produced for storage and later EAF processing when electricity prices return to more moderate levels [105, 508]. The heat generated via DRI cooling may potentially be utilized in a liquid H_2 carrier dehydrogenation process, although processes for the recovery of this heat are not described in the open literature [266]. DRI cooling could generate up to 32 MW of heat from 850 °C down to 100 °C in a 2 Mt/y liquid steel H-DR-EAF plant, equivalent to 129 kWh/t liquid steel plant. The heat generated via DRI cooling would also be available in a standalone CDRI H-DR plant. However, other heat integration options may potentially be more beneficial in such plants considering that this heat would then be generated continuously.

If the EAF and the dehydrogenation plant are instead operated concurrently, there may also exist possibilities for heat integration between these units. In particular, the EAF off-gas typically has a significant sensible heat content, up to 140–340 kWh/t liquid steel, equivalent to 35–85 MW in a 2 Mt/y H-DR-EAF plant [29, 509, 510]. Although it is challenging to efficiently utilize this heat due to the harsh conditions in the off-gas fume system, e.g., the high temperatures and large amounts of dust, and the batch-wise nature of EAF operation, EAF off-gas heat recovery systems are commercialized technology and are, e.g., integrated with around 10% of installed EAFs in the USA; the recovered heat is used for scrap preheating or steam generation [29, 511]. The varying heat generation from the EAF can be managed via a heat storage system [510, 512, 513]. This generated heat could also, e.g., be utilized to generate steam for SOEL [64, 514]. It may also be feasible to recover some heat from EAF slag cooling, but such approaches must be explored in more detail [29, 160].

Per the H-DR-EAF plant energy balance in section 4.3, reducing gas preheating is supplied at temperatures between 331 °C and 900 °C in the case that carbon-free DRI is produced[6]. In the case that an external fuel is combusted to supply this heat, there will, thus, still be a significant amount of heat left in the flue gas after heat exchange with the reducing gas. This remaining flue gas heat is available at below 381 °C for an assumed minimum temperature difference of 50 °C in the reducing gas preheater. Only a fraction of this heat is usable in NH_3 or LOHC dehydrogenation processes but could be used to provide 40–50% of the heat necessary to evaporate CH_3OH and H_2O for an MSR process if CH_3OH and H_2O evaporation takes place at close to atmospheric pressure. The heat in the reducing gas preheater flue gas below 381 °C could potentially be utilized for other purposes, e.g., district heating. Consequently, using this heat for evaporation of CH_3OH and H_2O may be associated with an opportunity cost in certain scenarios.

6.1.2.2 External supply of dehydrogenation heat

As seen in the preceding sections, although it is conceivable that part of the necessary heat for liquid H_2 carrier dehydrogenation can be supplied via integration with the H-DR-EAF plant, additional heating will also be needed. This heat can be provided in three ways: 1) combustion of part of the released H_2; 2) dehydrogenation reactor electrification; 3) combustion of an external fuel [266]. Combinations of these approaches are also conceivable.

Combustion of part of released H_2 means that more H_2 must be both stored and released per unit of H_2 delivered to the H-DR process, increasing storage investment and operational costs. Nevertheless, H_2 combustion is often a practical approach, particularly when full recovery of H_2 from the dehydrogenation process is difficult anyway. In MSR or NH_3 dehydrogenation processes, H_2 must always be separated out from a gaseous mixture, e.g., via PSA or a cryogenic process, before being sent to the shaft furnace. This typically results in one stream of near-pure H_2 and an off-gas consisting of small amounts of H_2 diluted in mostly CO_2 or N_2. Combusting this off-gas may be sensible considering its low concentration of H_2, which renders further H_2 recovery challenging. The combusted off-gas H_2 will also, due to the dynamic operation of the hydrogenation process, predominantly have been produced at relatively low electricity prices, which partially makes up for the low efficiency of electrolysis. The share of H_2 that must be combusted to provide the required dehydrogenation reaction enthalpy (X_{H_2}) can be calculated using[7] [307, 515]:

$$X_{H_2} = \frac{\Delta h_{R,H_2}}{LHV_{H_2} \cdot (\eta_{burner} \cdot \eta_{HEX})} \tag{6}$$

[6]DRI carburization will lead to higher top gas temperatures and, thus, higher reducing gas temperatures after internal heat exchange.

[7] This equation was originally misprinted in paper I. A corrigendum was published to correct this.

where $\Delta h_{R,H_2}$ is the reaction enthalpy of the dehydrogenation reaction, and η_{burner} and η_{HEX} are the burner and heat exchanger efficiencies of the combustion process, respectively (including combustion air preheating) [515]. Considering a burner efficiency of 90% and a heat exchanger efficiency of 97.5% yields the values in Table 7 for the considered liquid H_2 carriers [307].

Table 7: Share of released hydrogen that must be combusted to provide the necessary heat for liquid hydrogen carrier dehydrogenation.

Liquid hydrogen carrier	Enthalpy of dehydrogenation (kJ/mol H_2)	Share of released hydrogen that must be combusted
Ammonia	30.6	14%
Methanol	16.4/43.7*	8%/20%*
Perhydro-dibenzyltoluene	65	31%
Methylcyclohexane	68	32%

*For the case of liquid rather than gaseous CH_3OH and H_2O reactants.

Reactor electrification is more efficient than partial H_2 combustion [8], but suffers from the fact that the dehydrogenation process will mainly operate when electricity prices are high. Ultimately, the choice between partial H_2 combustion and reactor electrification will depend on the efficiencies of electrolyzers, the H_2 combustion process, and the electrified reactor as well as the average electricity price difference between hydrogenation and dehydrogenation processes operation. Another factor that may play a role is the possibility to operate electrically heated reactors more dynamically, but more research is needed to quantify such potential effects [428, 430].

The attractiveness of supplying the dehydrogenation heat via the combustion of a fuel depends mostly on the price of this fuel. The same options exist for providing this heat as for providing H-DR reducing gas preheating. In the case that reducing gas preheating is already provided by the combustion of a fuel, e.g., woody biomass or biogas, it may be feasible to increase the load of this combustion process during periods of high electricity prices to also provide heat for the dehydrogenation process. This would require that the combustion process is oversized compared to the reducing gas preheating demand. However, this is most likely more cost-effective than investment into a separate furnace for the generation of dehydrogenation process heat. A process for preheating and evaporation of CH_3OH and H_2O for an MSR process based on this principle was developed and is described in more detail in the next section.

6.1.2.3 Integration of methanol steam reforming and reducing gas preheating

All current MSR plant designs utilize the combustion of the PSA off-gas to provide the necessary process heat [483]. As seen in Table 7, the combustion of less than 10% of released H_2 should be sufficient to supply the heat needed for MSR if evaporated CH_3OH and H_2O are fed to the process. This kind of PSA H_2 recovery ought to be achievable for H-DR H_2 purity requirements [335, 481, 489]. Consequently, providing the heat for the evaporation and preheating of CH_3OH and H_2O via external means may be sensible as this could improve the overall H_2 recovery of the MSR process.

It may be possible to further increase the PSA H_2 recovery in MSR via separating out part of the H_2 in the PSA off-gas stream using, e.g., membrane technology [488, 489, 516]. A challenging aspect is that the H_2 partial pressure in the PSA off-gas is relatively low, which likely necessitates recompression before additional separation steps, adding both investment and operational costs [489]. An alternative is to integrate a membrane separation process directly into the MSR reactor, which would

[8] The production of one kg of H_2 (33.3 kWh in LHV) via low-temperature electrolysis requires around 50 kWh_{el}. Combustion of this kg H_2 may yield around 30 kWh of heat useful for a dehydrogenation process. The overall electricity-to-heat efficiency is, thus, 60%. When heat is supplied via Joule heating in an electrified dehydrogenation reactor, electricity-to-heat efficiencies close to 100% can be expected

allow for the direct production of high-purity H_2 [485]. However, such membrane reactors are currently far away from commercialization [517]. Nevertheless, complete H_2 recovery is difficult to achieve in any separation process, and utilizing the heat content of the resulting off-gas via combustion is then sensible.

In paper VI, a hybrid MSR heat supply process based on the principles above was developed and its heat flows were determined based on simulation in ASPEN Plus® V10. A scheme for this process is seen in Figure 17. The basic idea of this process is to utilize the already existing reducing gas preheating furnace in an H-DR process to also supply heat for the preheating and evaporation of CH_3OH and H_2O when the MSR process is operated. This temporarily increases the overall furnace and H-DR plant biomass demand, but this may be economically advantageous to other dehydrogenation heat supply options if the biomass price is relatively low.

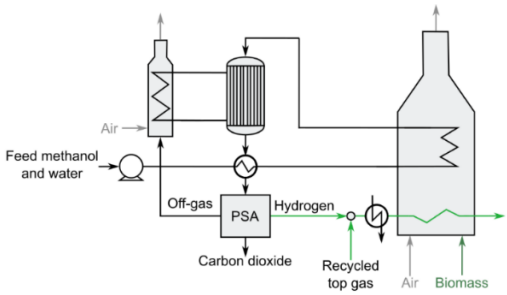

Figure 17: Methanol steam reforming hybrid heat supply process for integration with a hydrogen direct reduction process. Hydrogen from the pressure swing adsorption (PSA) unit is first mixed with recycled dried top gas and is then heated via heat exchange with the top gas before being sent to the preheating furnace where biomass is combusted.

A 40% increase in H-DR-EAF biomass consumption during MSR operation is sufficient to provide the necessary preheating and evaporation. The remaining heat demand of the MSR reactor at 250 °C is covered by the combustion of the PSA off-gas. The maximum achievable H_2 recovery is around 91% using this hybrid heat supply system, considering an overall H_2 burner and heat exchanger efficiency of 90% and 97.5%, respectively [515]. A heat exchange diagram of the process is shown in Figure 18, excluding heat demand of the MSR reactor.

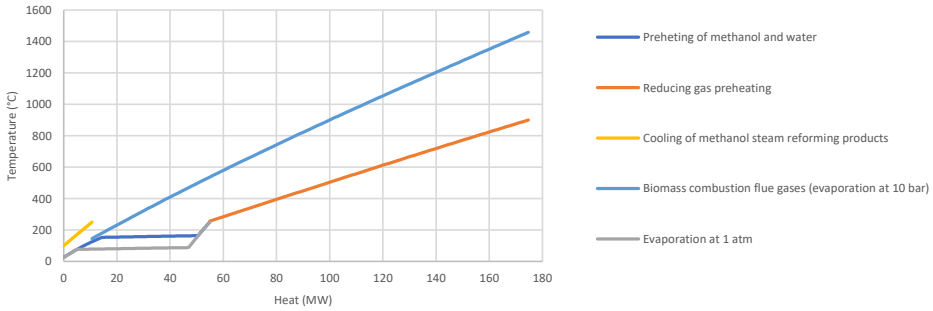

Figure 18: Heat exchange process for integration of methanol steam reforming feed preheating and evaporation with reducing gas preheating process. The minimum temperature difference occurs between the methanol-water mixture and the combustion flue gases at 145 °C/125 °C. Evaporation of the methanol-water mixture at 1 atm is also shown.

The evaporation process takes place at the reactor pressure in the scheme in Figure 17. However, it is, as mentioned previously, also possible to preheat and evaporate the feed at a lower pressure followed by gas compression. As the chemical equilibrium of the MSR reaction itself benefits from lower pressures, it is sensible to perform this vapor compression after the reactor but before the PSA [306]. The advantage is that the evaporation process can then occur at a lower temperature, which means that a larger share of the heat in the biomass combustion flue gases can be utilized, lowering the additional biomass demand during MSR operation. As discussed in section 6.1.2, evaporation at lower pressures may also facilitate heat integration with other parts of the H-DR-EAF process. However, as compression of gases requires significantly more work than the pumping of liquids, low-pressure evaporation would increase the overall electricity demand of the MSR process, which would at least partially offset the heat utilization advantage (depending on the relative costs of electricity and biomass). The economic performance of different MSR heat supply options (the hybrid process described in this section, partial H_2 combustion, and MSR electrification) for H_2 supply to an H-DR-EAF plant are compared using historical electricity prices in section 8.4

6.1.3 Hydrogenation processes

Storing H_2 in liquid carriers generates heat via the exothermic hydrogenation reactions. Cost-effective utilization of this heat may improve the economic viability of H_2 storage in such liquid carriers in an H-DR-EAF process. The viability of heat integration between liquid H_2 carrier hydrogenation processes and other parts of the H-DR-EAF plant depends mainly on the temperature and amount of heat generated, which depends on the liquid H_2 carrier. The timing of the heat generation also plays a role; hydrogenation will predominately occur when the electricity price is low, which may or may not synchronize well with the heat demand of potential heat sinks.

Most of the heat generated in hydrogenation processes is due to the exothermic hydrogenation reactions but some may also be recoverable from the intercooling of compressors. In some hydrogenation processes, part of the generated heat is utilized internally for separation purposes, e.g., in a CH_3OH production plant with integrated distillation. In the NH_3 production and, particularly, LOHC hydrogenation processes, a relatively small part of the generated heat can be utilized internally. The maximum amount of excess heat that can be exported is 2.4–3.6 kWh/kg H_2 for CH_3OH production (higher value excludes distillation), 5.6–7.3 kWh/kg H_2 for NH_3 production, 9.0 kWh/kg H_2 for dibenzyltoluene hydrogenation, and 9.7 kWh/kg H_2 for toluene hydrogenation.

One attractive idea is to utilize this excess heat to generate steam for H_2 production via SOEL. If SOEL EOC is utilized to generate the H_2 for the hydrogenation process, H_2 production and the generation of hydrogenation heat for steam production will be synchronized. The preferred feed to SOEL is typically saturated steam at 3 bar [193]. The majority of the heat needed to generate this steam is the H_2O evaporation heat, which is around 0.6 kWh/kg H_2O at 3 bar (134 °C), equivalent to 5.4 kWh/kg H_2 produced per the electrolysis reaction stoichiometry. Consequently, it is technically possible to generate all steam necessary for SOEL operation via heat integration with NH_3 production or LOHC hydrogenation but not for CH_3OH production, even if distillation is avoided. Similar conclusions have been reached for the integration of SOEL with NH_3 or CH_3OH production by other authors [197, 395, 518, 519]. Heat integration possibilities between CH_3OH production and SOEL may be greater in the case of steam and CO_2 co-electrolysis, partly due to the lower evaporation heat demand and partly due to the more exothermic CH_3OH-forming reaction with CO [519, 520]. However, such routes are not explored here.

6.2 SIZING AND INVESTMENT COSTS OF LIQUID HYDROGEN CARRIER STORAGE SYSTEMS

A liquid H_2 carrier storage system consists of three main components: a hydrogenation plant, one or several storage tanks, and a dehydrogenation plant. Although no full industrial-scale liquid H_2 carrier storage systems exist today, it is possible to provide estimates of the investment costs of such systems by considering costs of their components.

For NH_3 and CH_3OH, the hydrogenation processes are essentially completely mature already today and there exists plenty of literature investment cost data. Investment costs of large-scale NH_3 and CH_3OH dehydrogenation plants are more uncertain as no such plants exist today (except the unique Arroyito plant NH_3 cracker). Nevertheless, small NH_3 and CH_3OH dehydrogenation plants are available, and upscaling would only involve the use of standard process equipment [423, 482]. Estimating the investment costs of a large-scale LOHC-based H_2 storage system is associated with the most uncertainty among the considered liquid H_2 carriers, which is understandable given the relative immaturity of the LOHC concept [435, 521]. Few estimates of the investment cost of both LOHC hydrogenation and dehydrogenation processes exist and those that are available are very scattered [435].

Liquid H_2 carrier hydrogenation and dehydrogenation are thermochemical processes. Such processes are typically associated with economies of scale, i.e., larger plants have lower specific investment costs [184, 522, 523]. This relationship between the investment cost and production capacity can typically be described via a scaling factor:

$$IC = IC_{ref} \cdot \left(\frac{Capacity}{Capacity_{ref}} \right)^{scaling\ factor} \quad (7)$$

where IC is the sought investment cost and IC_{ref} is the known investment cost of a reference process with a known capacity ($Capacity_{ref}$). For thermochemical processes, a scaling factor of 0.6 is most commonly used (the '*six-tenths rule*') and is applied here for the analysis of hydrogenation and dehydrogenation plant investment costs [523-526]. The use of a scaling factor to identify investment costs is most accurate when the capacity of the reference facility is relatively close to that of the investigated facility [317]. Therefore, only cost estimates for large-scale hydrogenation and dehydrogenation facilities (>100 t H_2/d) have been used as cost references in the analysis. Nevertheless, the resulting investment costs based on this extrapolation procedure should just be considered order-of-magnitude estimates [526]. Older literature investment cost estimates were also adjusted for inflation to the reference year 2020 values based on an average 2%/y rate.

Process investment costs can be divided into direct and indirect costs. Direct costs are related to the purchase and installation of plant equipment including, e.g., piping, electrical equipment, utility systems, process control equipment, buildings (including offices and laboratories), site preparation, and land. Indirect costs include, e.g., engineering and supervision costs, contractor costs, insurance, legal costs, freight costs, and working capital. Direct and indirect costs can be calculated from the estimated plant purchased equipment cost by multiplying by one factor representing installation costs and one representing indirect costs. In practice, both of these factors depend on, e.g., plant location and the availability of infrastructure and process utilities [424, 493, 526]. For instance, these factors are generally lower if a process is assumed to be installed at an already active industrial site (so-called brownfield investment) rather than in an entirely new location (so-called greenfield investment) [89, 120]. In the context of an H-DR-EAF plant site, it is reasonable to assume that certain cost synergies may be possible for liquid H_2 carriers, e.g. in terms of land development as well as utility and electrical systems, although it is difficult to quantify these synergies at present and this is not attempted here.

6.2.1 Investment costs of hydrogenation plants

The investment cost of CO_2-based CH_3OH production processes, excluding CO_2 capture, has been estimated to be approximately 300 €/kW on average for a 200 MW production rate (based on CH_3OH LHV) [320, 462, 463, 470, 493]. A 150 MW H_2O-electrolysis NH_3 production plant (based on NH_3 LHV) has an investment cost of around 690 €/kW, including ASU [320, 408, 527]. A recent investment cost estimate for a dibenzyltoluene hydrogenation plant is 60 M€ for a 120 t H_2/d capacity, but significantly lower cost estimates also exist (e.g., 40 M€ for a 300 t H_2/d plant) [315, 320]. For toluene hydrogenation, an estimate of 43 M€ for a capacity of 350 t H_2/ is one of the few existing values in the open literature for a large-scale plant [306]. The considered hydrogenation plant investment cost estimates are plotted in Figure 19 as a function of H_2 rate capacity. Three levels of specific electrolyzer investment costs are also shown for comparison.

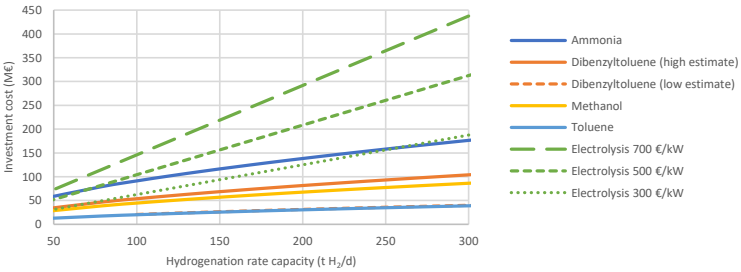

Figure 19: Investment cost of liquid carrier hydrogenation plants as a function of their rate capacity. Electrolyzer investment costs at three levels are also shown. The lower dibenzyltoluene estimate and the estimate for toluene overlap.

NH_3 production is has the highest investment costs out of all considered hydrogenation processes. This is to be expected considering the high temperatures and pressures in the Haber-Bosch process, the need for an ASU to produce the required N_2, and the need for refrigeration to condense NH_3. In comparison, the CH_3OH production process is significantly less complex and costly (approximately 50% less at 100 t H_2/d). Estimated investment costs of dibenzyltoluene hydrogenation plants range from slightly higher to significantly lower than CH_3OH production plants. The low dibenzyltoluene hydrogenation plant investment estimate is similar to that of the toluene hydrogenation plants. This is sensible as these plants ought to be rather similar in terms of equipment and overall layout.

Integration of any kind of H_2 storage in an H-DR process would necessitate investment into EOC. At a specific electrolyzer investment cost of 500 €/kW, the investment cost of this EOC is higher than the investment cost of all hydrogenation plants already at 70 t H_2/d, equivalent to a 22% EOC for a 2 Mt/y H-DR-EAF plant.

6.2.2 Investment costs of dehydrogenation plants

The dehydrogenation plant is meant to deliver H_2 to the H-DR shaft furnace during periods of high electricity prices so that expensive H_2 production via electrolysis can then be ramped down or, preferably, halted entirely. The dehydrogenation plant should, thus, be able to completely fulfill the H_2 demand of the downstream H-DR process.

The recent 'Ammonia to Green Hydrogen' study estimated the purchased equipment cost of a 200 t H_2/d plant to be 89.5 M€ [423, 424]. However, the plant considered in this study delivers fuel cell grade H_2, which is, not required for an H-DR process. As part of the 'H21 North of England' study, Equinor estimated the purchased equipment cost of a 910 H_2/d NH_3 dehydrogenation plant to be 188 M€ [284]. This is similar to the 'Ammonia to Green Hydrogen' estimate if one adjusts for the different scales of production using equation (7) and a scaling factor of 0.6. However, despite the similar purchased equipment costs, the two studies reach considerably different total investment costs for

NH_3 dehydrogenation plants due to different economic assumptions regarding installation and indirect costs. The reasons for these different cost assumptions are not clear. As the plant in the 'H21 North of England' study delivers H_2 at a purity and pressure more similar to expected conditions in an H-DR process, cost data from this study is utilized herein [161].

The investment costs of large-scale perhydro-dibenzyltoluene dehydrogenation plants have been estimated to be between 30 M€ for a 300 t H_2/d capacity to 60 M€ for a capacity of 120 t H_2/d [315, 320]. The latter estimate is utilized here given its recency and because it originates from direct conversations with Hydrogenious GmbH [320]. For methylcyclohexane, the only identified estimate comes from a recent study by the US Argonne National Laboratory, in which investment costs of a 350 t H_2/d plant are estimated to be 88 M€, although this plant produces fuel cell grade H_2; lower purities are allowable in an H-DR process, which may lead to lower investment costs [306].

Investment cost estimates for large-scale MSR plants are scarce in the open literature. A Lurgi GmbH (now part of Air Liquide S.A.) study from 2001 estimated the investment cost of a 216 t H_2/d MSR plant to be approximately 42 M€ (adjusted for inflation). The only other identified large-scale MSR investment cost estimate comes from the aforementioned Argonne National Laboratory study [306]. The investment cost estimate in that study is approximately 122 M€ for a 350 t H_2/d plant, which is nearly twice as high (when adjusted for capacity) as the one from Lurgi. It is not entirely certain why there is such a discrepancy between the Lurgi and Argonne MSR investment cost estimates but one reason could be different targeted H_2 purities, which was fuel cell grade in the Argonne study. Considering that the Lurgi study is from 2001, a lower H_2 product purity than fuel cell grade can be assumed as there existed no demand for fuel cell grade H_2 then. Therefore, the Lurgi estimate is used here.

The considered dehydrogenation plant investment cost estimates are plotted in Figure 20. Also shown are the H_2 demands of 2 Mt/y, 3 Mt/y, and 4 Mt/y H-DR-EAF plants to indicate the sizing of these dehydrogenation plants.

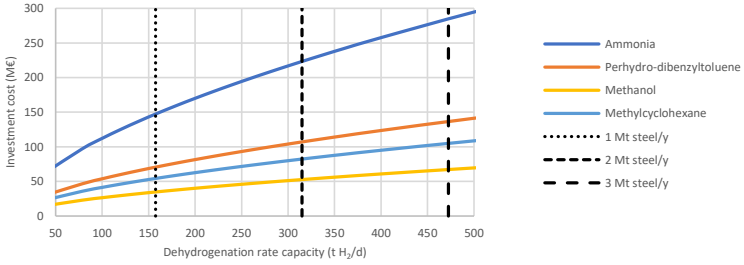

Figure 20: Investment costs of liquid hydrogen carrier dehydrogenation plants as a function of their rate capacity. The hydrogen demand of 2 Mt, 3 Mt, and 4 Mt liquid steel per year hydrogen direct reduction-electric arc furnace plants are also shown.

MSR has the lowest investment costs among the considered dehydrogenation processes and NH_3 dehydrogenation has by far the highest. At the same H_2 rate capacity, an MSR plant is found to be around one-quarter as capital-intensive as a NH_3 dehydrogenation plant. However, as noted, these investment costs are subject to uncertainty. For instance, utilizing other previously mentioned alternative literature estimates would render MSR roughly twice as expensive and perhydro-dibenzyltoluene dehydrogenation 70% lower in investment cost than shown in Figure 20. Nevertheless, it does appear that NH_3 dehydrogenation is the most capital-intensive option, which appears sensible given its much higher operating temperature than other carrier dehydrogenation processes and the demanding fired furnace design [365, 424, 428].

6.2.3 Investment costs of storage capacity

Storage tanks for all considered liquid carriers are commercially available and will make up a relatively small part of the overall liquid H_2 carrier-based storage investment cost. The LOHCs and CH_3OH can be stored in floating roof tanks, identical to those used to store various petroleum products [320]. Cost data for floating roof tanks is widely available and such tanks can have capacities of over 100 000 m^3 [447, 528-531]. Large amounts of NH_3 are preferably stored in liquid form, which necessitates more expensive refrigerated tanks [384, 386]. The necessary storage tank size to store a given amount of H_2 in a liquid carrier is determined by the density of the carrier and its gravimetric H_2 storage capacity, which are seen in Table 8.

Table 8: Density and hydrogen storage capacity of liquid hydrogen carriers [284, 446, 532, 533].

Liquid H_2 carrier	Density (kg/m^3)	kg H_2/t carrier	kg H_2/m^3 liquid carrier storage
Ammonia	682[§]	178	121
Methanol	792[+]/882[+]	126/189[*]	150[*]/107[+]
Perhydro-dibenzyltoluene	913	62[#]	57
Dibenzyltoluene	1044	-	-
Methylcyclohexane	770	62[#]	48
Toluene	867	-	-

[§]Liquid NH_3 at boiling point (-33.3 °C).
[+]Equimolar H_2O-CH_3OH solution for case without distillation.
[*]Per the stoichiometry of (R26) and considering pure CH_3OH storage.
[#]Maximum reversible H_2 storage capacity.

Around two to three times as much H_2 can be stored per volume of NH_3 or CH_3OH compared to the considered LOHCs. The volumetric density of H_2 storage in CH_3OH depends in part on how the H_2O formed during the CO_2 hydrogenation process is managed. If distillation of H_2O and CH_3OH is avoided, the achievable storage density is lower, but, as mentioned previously in section 5.5.5.3, the investment and operational cost of the distillation column(s) can be avoided. Here it is assumed that a distillation column is integrated into the CH_3OH production process and, thus, that pure CH_3OH is stored.

Both the hydrogenated and dehydrogenated forms of LOHCs must be stored. In addition, it is necessary to purchase sufficient amounts of the dehydrogenated LOHC for the intended H_2 storage capacity [266]. The costs of LOHC storage tanks are based on a base cost of 68 €/t perhydro-dibenzyltoluene and the densities of the hydrogenated and dehydrogenated LOHCs [320]. The investment costs of liquid carrier H_2 storage capacity are seen in Table 9. Due to the modular nature of these large storage tanks and that the dehydrogenated LOHCs are purchased in bulk, these liquid H_2 carrier storage capacity costs are assumed to scale linearly with capacity.

Table 9: Hydrogen storage capacity costs for liquid hydrogen carriers [320, 528].

Liquid H_2 carrier	Storage tank cost (€/t liquid carrier)	Storage tank cost (€/kg H_2)	Carrier cost (€/kg)	Total storage capacity cost (€/kg H_2)
Ammonia	350	2.0	-	2.0
Methanol	75	0.6/0.4[*]	-	0.6/0.4[*]
Perhydro-dibenzyltoluene	68	1.1[#]	-	34.0[#]
Dibenzyltoluene	59	0.9[#]	2.0	
Methylcyclohexane	81	1.3[#]	-	10.5[#]
Toluene	72	1.1[#]	0.5	

[*]Per the stoichiometry of (R26).
[#] Maximum reversible H_2 storage capacity.

The H_2 storage capacity investment cost is significantly higher for the LOHCs compared to those of NH_3 and, especially, CH_3OH. Although the specific cost of NH_3 storage is relatively high due to the need for refrigerated storage tanks, its high H_2 storage density partially compensates for this. The cost of H_2 storage capacity in the LOHCs is sensitive to how much of their maximum H_2 storage capacity can be utilized; the values seen in Table 9 assume that the LOHCs can be fully dehydrogenated during every storage cycle, which may not be achievable in practice [439]. Assuming that 95% of the

maximum reversible H_2 storage capacity can be utilized increases H_2 storage capacity costs to 35.7 and 10.9 €/kg H_2 for dibenzyltoluene and toluene-based storage, respectively.

6.2.4 Total liquid hydrogen carrier system investment costs

The total investment costs of the considered liquid H_2 carrier storage systems as a function of their H_2 storage capacity are shown in Figure 21. The dehydrogenation rate capacity is assumed to be equal to the H_2 demand of a 2 Mt/y H-DR-EAF plant. Results are plotted for two hydrogenation rate capacities, equivalent to 25% and 50% of the H-DR-EAF H_2 demand, for all carriers. EOC investment costs are not included.

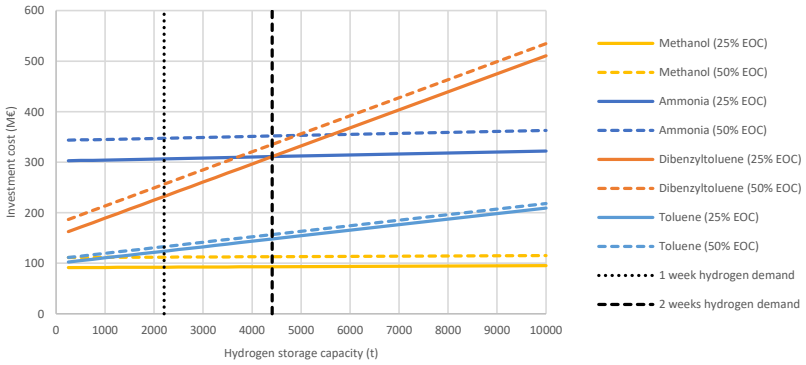

Figure 21: Investment cost of liquid hydrogen carrier storage systems as a function of storage capacity. The dehydrogenation rate capacity is 315 t hydrogen per day in all scenarios.

CH_3OH is the liquid H_2 carrier associated with the lowest investment cost, particularly for larger H_2 storage capacities. In the context of the overall H_2 storage system, the CH_3OH storage tanks make up a small part of the total investment costs even for large storage volumes. H_2 storage in perhydro-dibenzyltoluene is by far the most expensive option for larger H_2 storage capacities, mostly due to the high cost of dibenzyltoluene. A similar trend is seen for toluene but the effect is far less pronounced due to its lower costs.

The investment cost of the EOC is not included in Figure 21. At 500 €/kW, the investment cost of 50% EOC is approximately 164 M€. As this cost is the same irrespective of the choice of storage technology, it evens out the differences in overall storage investment cost between the carriers. At a H_2 storage capacity of 1 000 t H_2, the relative difference in investment cost between all considered liquid H_2 carriers is less than 46% if the EOC costs are included. The impact of liquid H_2 carrier choice has a more significant impact for larger storage capacities due to differences in specific storage costs. Nevertheless, the investment costs of these liquid H_2 carrier systems will make up a relatively small part of the overall investment cost of a large-scale H-DR-EAF steelmaking plant (investment costs are >1 400 M€ for a 2 Mt/y H-DR-EAF plant, per section 4.4).

6.2.5 Comparison with investment costs of geological hydrogen storage options

The aim of this thesis is to identify techno-economically viable alternatives to large-scale geological H_2 storage. Therefore, results in Figure 21 are compared to the estimated investment costs for geological H_2 storage options in this section. Only salt cavern and LRC storage are considered here as the viability of H_2 storage in depleted NG fields or aquifers is presently highly uncertain. Also, as discussed in section 5.4.1, the limited operational flexibility of depleted NG field and aquifer NG storages renders the viability and general attractiveness of their use for H_2 storage for H-DR-EAF plant questionable.

As the salt cavern or LRC storage pressure is typically higher than the output pressure of electrolyzers, H_2 must be compressed before injection into such geological storages. Consequently, the investment cost of the injection compressor should be included when comparing costs of geological H_2 storages with liquid H_2 carrier-based storage. A specific compressor investment cost of 300 €/kW (based on H_2 LHV) is assumed for both salt cavern and LRC storages considering the similar storage pressures [297, 303]. In the case of salt cavern storage, a post-withdrawal H_2 drying process is also necessary. The investment cost of this drying process is assumed to be 6 €/kW (based on H_2 LHV) [297]. Using the storage capacity investment costs ranges in Table 6 yields the results in Figure 22 for an injection compressor rate capacity equivalent to 25% of the H_2 demand of a 2 Mt/y H-DR-EAF plant. The salt cavern and LRC storage capacity costs in Table 6 utilized to generate Figure 22 should be seen as upper and lower boundaries. As discussed in section 5.4, the lower investment cost bounds are more likely for larger storage volumes and vice versa due to economies of scale. This is particularly true for salt cavern storages considering their larger maximum single-cavern storage capacity. The investment cost of EOC is excluded for ease of comparison with results seen in Figure 21. Costs of cushion gas are also not included [9].

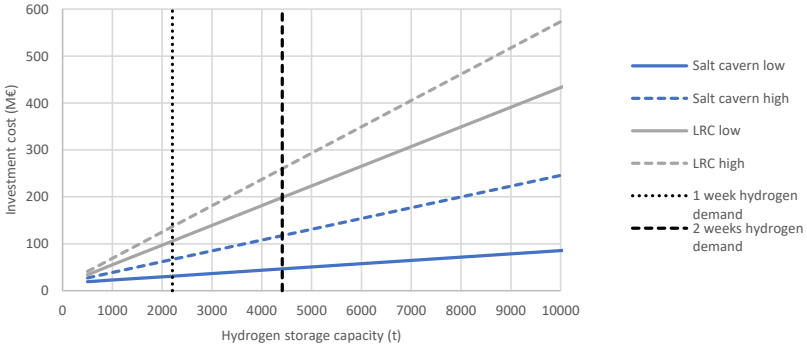

Figure 22: Investment cost of salt cavern and lined rock cavern hydrogen storages as a function of their capacity. Inlet compressor rate capacity is 25% of hydrogen demand of 2 Mt liquid steel/y hydrogen direct reduction-electric arc furnace plant. The post-withdrawal drying equipment is sized for 100% of the hydrogen demand of the hydrogen direct reduction process for salt cavern storages.

The first conclusion one can draw upon a comparison of Figure 21 and Figure 22 is that none of the liquid H_2 carriers are competitive with H_2 storage in salt caverns from an investment cost perspective as long as salt cavern capacity costs are close to the lower bound (7 €/kg H_2); a CH_3OH-based storage has a 30% higher investment cost for two weeks of H-DR H_2 demand storage capacity. However, the liquid H_2 carriers do better when compared with LRC storages, at least the CH_3OH and toluene-based systems, which are both likely less investment cost-intensive for two weeks of H-DR H_2 demand storage capacity. The liquid H_2 carriers, excluding dibenzyltoluene, are increasingly at an advantage over LRCs for larger H_2 storage capacities in terms of investment cost. This is due to the relatively low cost of storing the liquid carriers. Consequently, in the advent that demand for very large H_2 storage capacities arises, e.g., storage of the H_2 demand of an H-DR process on a seasonal basis, a liquid H_2 carrier-based storage may be a promising option.

[9] Costs of cushion gas are not included in Figure 22 but do not affect general results considerably; a cushion gas price of 3 €/kg H_2 leads to a maximum increase in specific investment cost of 1.7 €/kg H_2 for salt cavern storage (considering 0.55 t cushion gas/t working gas).

7 HYDROGEN STORAGE IN METHANOL IN HYDROGEN DIRECT REDUCTION STEELMAKING (PAPER V)

In the previous chapter, H-DR-EAF integration possibilities and the investment costs of liquid carrier-based H_2 storage systems were considered. Investment costs were compared with those of geological H_2 storages. A sensible next step of the techno-economic comparison of geological and liquid carrier-based H_2 storage is to consider differences in operational costs and characteristics, which is the overarching purpose of this chapter. Out of the liquid H_2 carriers, methanol (CH_3OH) appears most promising for integration into an H-DR-EAF plant for several reasons:

- it can be stored in conventional, low-cost floating roof tanks at atmospheric pressure,
- its production from H_2 and CO_2 is a mature process that can be operated dynamically,
- high H_2 recoveries can be achieved in MSR,
- investment costs of both CH_3OH production and MSR plants are relatively low,

The use of biomass oxy-fuel combustion for the provision of both CO_2 and H-DR reducing gas preheating is also potentially attractive if low-cost biomass is available. As this is typically the case in the regions under investigation in HYBRIT RP1, i.e., Sweden and Finland, it was decided to go forward with CH_3OH-based H_2 storage for further analysis of operational costs. However, as seen in the previous chapter, all liquid carrier-based H_2 storages share certain characteristics and, thus, some of the conclusions drawn for the CH_3OH example in this and later chapters may also apply for other liquid H_2 carriers.

In this chapter, the achievable reductions in overall H_2 production cost via the integration of CH_3OH-based storage in an H-DR-EAF plant under fluctuating electricity prices is presented. Results are compared with geological LRC storage as this is the main geological storage pursued in HYBRIT RP1 [17]. As seen previously, salt cavern storages may have certain similar operational characteristics as LRCs but will have lower investment costs [16]. A storage operation NLP optimization method that utilizes historical electricity prices taken from the public Nord Pool database was developed [148]. This optimization method is described in detail in section 7.1.2.

Nord Pool is an electricity market operator, providing day-ahead and intraday electricity prices in, e.g., Sweden, Norway, Finland, and Denmark [534]. Full-year historical electricity market data dating back to the year 2013 are available from the Nord Pool website [148]. Historical day-ahead electricity spot prices are utilized in the storage model as a proxy for the variable industrial electricity costs of a future industrial H-DR-EAF plant in Sweden. This is a reasonable approach as energy-intensive industries are essentially entirely exempted from energy-related taxes in Sweden and typically have fixed electricity transmission and distribution costs established via contracts [535-537].

The H-DR-EAF plant is assumed to be located in the north of Sweden inside of electricity pricing region SE1. However, historical electricity prices from other pricing regions are also be used. Electricity prices from western Denmark (Jylland, DK1) are included in the analysis a as a relatively large part of electricity generation in the region is based on wind power—over 50% in recent years [538, 539]. A consequence of this is that electricity prices in DK1 have been more volatile than in SE1, which should benefit H_2 storage. As an increased share of wind power is expected in northern Sweden, it is, thus, thinkable that more volatile electricity prices could arise [14]. Therefore, historical electricity prices from DK1 can be used as at least an indication of the direction in which prices in SE1 may develop. Electricity prices from SE4 (southern Sweden) are also included as an intermediate between SE1 and DK1.

The developed storage operation optimization method is entirely deterministic, i.e., electricity prices for the full duration of the simulated period are assumed to be known in advance, and assumes that the H-DR plant operator is an electricity '*price taker*', i.e. that the electricity demand of the H-DR does not affect the electricity price.

The price taker assumption is generally only valid if the electricity demand of a process is insignificant relative to the market size, which will generally not apply for H-DR plants—the total annual electricity demand of a 2 Mt/y H-DR-EAF plant is 7–8 TWh, which is equivalent to 4–5% of total Swedish electricity generation during 2021 [267, 540-542]. In theory, the additional electricity demand of an H-DR-EAF plant will cause electricity prices to increase, ceteris paribus. However, this is only true for an otherwise static H-DR H_2 demand and surrounding electricity market, which is not the case in practice if a H_2 storage is part of the process.

The integration of a H_2 storage allows for flexible H_2 production so that a larger share may be produced during low electricity prices. In a liberalized electricity market where a large part of the generation capacity is based on wind or solar power, a low electricity price is generally correlated with a high share of wind or solar power as the incremental electricity generation cost of these technologies is close to zero (as they have no fuel cost) [12, 14]. Consequently, flexible H_2 production may increase the utilization and, thus, the value of these intermittent electricity generators, which would spur investment into additional wind and solar generation capacity [12, 267, 543, 544]. This, in turn, may increase the number of hours and days per year with low electricity prices in a given electricity market, which may result in a lower overall electricity cost for the H-DR-EAF plant operator [267, 543, 545]. As an example, simulations by Vattenfall AB as part of HYBRIT RP1 for the north European electricity market in 2035–2055 have indicated that flexible H_2 production and storage in the context of H-DR-EAF steelmaking may simultaneously increase the local value of wind power and decrease the average H_2 production cost for the steelmaker [267].

As a consequence of the aforementioned assumptions, the method described in this chapter cannot predict whether investment into large-scale H_2 storage as part of a future H-DR-EAF plant will be profitable or not. Such an analysis would have to have a much broader scope to include, e.g., projections for future developments in climate, and electricity generation, demand, and infrastructure. Nevertheless, some general conclusions regarding the conditions needed for H-DR H_2 storage to reach profitability can be drawn and the overall potential of different kinds of H_2 storages to be profitable can be compared under ideal, controllable conditions. This is useful in this conceptual study of potential H_2 storage technologies for H-DR-EAF plants.

7.1 METHOD OVERVIEW

The calculations presented here are based on a 2 Mt liquid steel/y H-DR-EAF plant with a H_2 demand of 315 t/d. Only results with a daily time resolution are discussed herein due to uncertainties regarding the flexible operation of H_2 storages on an hourly basis. Nevertheless, some tentative hourly resolution results are provided in paper V.

The H_2 demand of the H-DR-EAF plant can be fulfilled via H_2 production or via emptying the H_2 storage. The H_2 storage is assumed to be half-filled at the start and end of all simulated periods to enable easier comparison of storages and scenarios. The economic value of the (identical amount of) stored H_2 at the start and end of simulations is assumed to be equal so that it can be ignored in the economic calculations. Reducing gas preheating is assumed to be provided by biomass oxy-fuel combustion in all cases and the opportunity cost of utilizing the generated CO_2 is assumed to be zero, i.e., it is assumed that no more than around 50% of all byproduct O_2 can be sold off. This allows for a maximum EOC of 59% for CH_3OH-based H_2 storage. In the case that an LRC storage is used, it is assumed that any generated CO_2 is vented or, potentially, captured.

It is assumed that the integration of a H_2 storage into an H-DR plant does not affect its H_2 demand or DRI production rate. Therefore, it is sensible to only consider the additional marginal investment cost of the H_2 storage and the accompanying EOC when evaluating its economic impact on the H-DR process, per Figure 23. If this additional marginal investment cost is lower than the associated reduction in the operational cost of H_2 delivery to the H-DR process, the investment into a H_2 storage may be considered worthwhile.

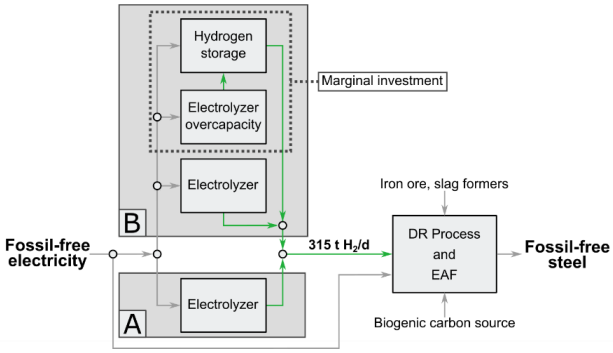

Figure 23: Visualization of the basis for economic comparison of hydrogen delivery to direct reduction process without (A) or with (B) a hydrogen storage. The hydrogen rate is based on the production of 2 Mt/y liquid steel. The marginal investment cost of B compared to A are those of electrolyzer overcapacity and hydrogen storage.

To take the time value of money into account, H_2 storage and EOC investment costs are annualized and converted to a per unit H_2 basis using an AF:

$$CAPEX_a = \frac{(IC_{storage} + IC_{EOC}) \cdot AF}{\dot{m}_{H-DR}} \quad (8)$$

where $IC_{storage}$ and IC_{EOC} are the total investment costs of the H_2 storage and EOC, respectively, $\dot{m}_{H-DR}$ the annual H_2 demand of the H-DR process, and $CAPEX_a$ the annualized specific marginal investment cost of H_2 storage. WACC is taken to be 6% and the economic lifetimes of the both the storage and the EOC are assumed to be 20 years. The change in the specific cost of delivering H_2 to the H-DR process achieved by investment into a H_2 storage with accompanying EOC (in €/kg H_2) can be calculated as:

$$\Delta c_{H_2} = (OPEX_{no\ storage} - OPEX_{storage}) - CAPEX_a \quad (9)$$

$OPEX_{no\ storage}$ is the average electricity cost of H_2 production without a storage and $OPEX_{storage}$ is the electricity cost of H_2 production when the storage is integrated plus any additional operational cost of the H_2 storage itself. When Δc_{H_2} is positive, investment into H_2 storage is profitable. Only changes in operational and investment costs when integrating a H_2 storage in an H-DR process are considered in the analysis. Changes in, e.g., maintenance costs are presently difficult to estimate (especially differences for different H_2 storage technologies) but should be relatively minor in comparison to the changes in operational costs.

The operational cost of H_2 delivery in the absence of a H_2 storage is dominated by the electricity demand of the electrolyzers (E_{elec}). As the H_2 production rate must remain constant in the absence of a storage, the average electricity price during the considered simulation period ($[€/MWh_{el}]_{average}$) can be utilized:

$$OPEX_{no\ storage} = \left[\frac{€}{MWh_{el}}\right]_{average} \cdot E_{elec} \quad (10)$$

It is assumed that low-temperature electrolyzers are utilized, primarily due to their presently lower investment costs, with a constant electricity demand of 50 $MWh_{el}/kg\ H_2$ and an output pressure of 20 bar.

Determining the minimum operational costs of H_2 delivery with a H_2 storage requires optimization. Firstly, as H_2 production will no longer be constant, the electricity price in each time step of the simulation must be considered. Secondly, operational characteristics and limitations of the H_2 storage must be considered.

7.1.1 Operational characteristics and limitations of hydrogen storages

The maximum H_2 withdrawal and injection rates are limited for all geological gas storages. The maximum LRC withdrawal and injection rates used here are based on values calculated for the Skallen LRC as part of the HyUnder project, which is the only known detailed reference in the open literature; the underlaying assumption is that identical pressure change rates are achievable when storing NG and H_2 [16]. Consequently, a 640 t H_2 working gas capacity LRC has maximum withdrawal and injection rates of 86.4 and 31.2 t H_2/d, respectively. This maximum withdrawal rate is equivalent to 27% of the H-DR H_2 demand. The maximum allowable withdrawal and injection rates are then assumed to scale linearly with the LRC working gas capacity. The maximum LRC H_2 injection rate determines the maximum allowable EOC. For the 2 Mt/y H-DR-EAF plant considered here, the maximum EOC is, thus, 10% for a Skallen-sized LRC. For comparison, a case with an LRC-based storage with a five times larger storage working gas capacity (3 200 t H_2), which has an allowable withdrawal rate in excess of the H_2 demand of the H-DR process, is also considered.

Some notable operational characteristics that differentiate CH_3OH-based storage from geological storage include the minimum load of the CH_3OH production process, the H_2 losses in MSR, and the independent sizing of the three main components (production process, storage, MSR process). It is assumed that the minimum load of the CH_3OH production process, taken to be 20% of its nominal rate capacity, is maintained via H_2 production by electrolysis. In theory, the minimum H_2 demand of the CH_3OH production process could be fulfilled via oversizing the MSR process, but such options are not explored here.

The maximum allowable H_2 storage and release rates can be chosen independently of the storage volume for a CH_3OH-based storage. This opens up further optimization opportunities. However, only the case that the MSR process is sized to deliver the entire H_2 demand of the H-DR process (315 t/d) is considered as this minimizes the H-DR electricity demand during electricity price peaks. The heat necessary for the MSR process is assumed to be sourced via the partial combustion of released H_2. One optimistic case where the heat demand for the evaporation CH_3OH and H_2O can be fulfilled via heat integration with the H-DR-EAF process (as discussed in section 6.1.2) and one pessimistic case where the only source of heat for MSR is combustion of part of the released H_2 are considered. In the optimistic case, 10% of released H_2 is lost in the MSR process. In the pessimistic case, the share of released H_2 that must be combusted increases to 20% [307, 515]. The assumed combined burner and heat exchange efficiency is higher in the pessimistic case (90% vs 70%) as a large part of the supplied heat is at a lower temperature for the evaporation process (see Figure 18) [515]. No other H_2 losses are assumed to occur during the CH_3OH-based H_2 storage cycle.

The H_2 storage filling processes are associated with certain electricity demands in addition to that of producing the stored H_2 via electrolysis. In the case of LRC storage, H_2 produced via electrolysis must be compressed to a varying pressure. Maximum and minimum allowable LRC pressures are approximately 230 bar and 10–30 bar, respectively [16]. The necessary minimum compression work for H_2 injection depends on the electrolyzer outlet pressure and the pressure in the LRC when injection occurs. The actual compression work also depends on the compressor efficiency. In practice, large-scale H_2 compression takes place in multiple stages with intercooling to increase the overall efficiency of the process and avoid unsafe gas temperatures inside the compressors [546, 547]. For

multistage compression of H_2 considering a typical isothermal single-stage efficiency of 0.7 and intercooling using cooling water between each stage, the total electricity demand can be approximated via the following logarithmic equation [343, 548]:

$$P_{comp} = 1.2 \cdot \log(\frac{p_2}{p_1}) \tag{11}$$

where p_1 and p_2 are the inlet and outlet pressures of the H_2 compression process, respectively. Assuming that the LRC is half-filled on average (equivalent to a pressure of 125 bar) and an electrolyzer output pressure of 20 bar, the average compressor work is approximately 1.0 kWh/kg H_2, which is the value used in the model. If the storage usually operates at higher pressures than 125 bar, this assumption may be considered optimistic and vice versa.

Literature estimates of the electricity demand of CH_3OH production from H_2 and CO_2 considering an electrolyzer output pressure of 20–30 bar are 0.5–1.6 kWh/kg H_2, as seen in section 5.5.5.3. An intermediate total CH_3OH production electricity demand of 1.0 kWh/kg H_2 is assumed in the model.

7.1.2 Storage operation optimization

The goal of the developed storage operation optimization method is to minimize the specific operational cost of delivering H_2 to the H-DR process for a given series of electricity prices. The specific operational cost of H_2 delivery is the sum of the electricity costs of the electrolyzers and the storage in each time step (i) of the simulated period divided by the total amount of H_2 delivered to the H-DR process during the simulated period:

$$OPEX_{storage} = \sum_i \frac{C_{elec,i} + C_{store,i}}{m_{H-DR,i}} \tag{12}$$

Equation (12) is the objective function of the optimization problem. For a given vector of simulated electricity prices, EOC, and, in the case of CH_3OH-based storage, CH_3OH production process minimum load, $OPEX_{storage}$ depends only on the amount of H_2 produced in each time step of the simulated period, i.e., the electrolyzer operating profile ($\vec{m}_{elec}$):

$$\vec{m}_{elec} = [m_{elec,1}\ m_{elec,2}\ \cdots\ m_{elec,n}] \tag{13}$$

where $m_{elec,i}$ is the mass of H_2 produced via electrolyzers in time step i and n is the number of time steps in the simulated period. The electricity costs of the process electrolyzers ($C_{elec,i}$), including EOC, is calculated in each time step i by multiplying the electricity price by the electrolyzer electricity demand (E_{elec}) and the amount of H_2 produced in the time step:

$$C_{elec,i} = m_{elec,i} \cdot E_{elec} \cdot \left[\frac{€}{MWh_{el}}\right]_i \tag{14}$$

The electricity cost of the storage process is calculated similarly, but considering the electricity demand of the storage process (E_{store}) and the mass of H_2 stored per time step ($m_{store,i}$) instead:

$$C_{store,i} = m_{store,i} \cdot E_{store} \cdot \left[\frac{€}{MWh_{el}}\right]_i \tag{15}$$

The amount of H_2 that is stored ($m_{store,i}$) in each time step depends on how much H_2 is produced. In the LRC case, any H_2 production in excess of the H-DR H_2 demand is stored. In the CH_3OH-based storage case, any H_2 produced in excess of the combined H_2 demand of the H-DR process and that needed to maintain the minimum load of CH_3OH production is stored.

The value that the elements of $\vec{m}_{elec}$ can assume is subject to different upper and lower bounds depending on whether H_2 is stored in an LRC or as CH_3OH. In the LRC case, the lower and upper bounds are determined by the maximum allowable H_2 withdrawal rate from the storage and the EOC. In the CH_3OH case, the upper boundary is also determined by the EOC, while the lower bound is determined by the minimum load of the CH_3OH production process.

The electrolyzer operating profile ($\vec{m}_{elec}$) is also subject to both linear and nonlinear constraints. These constraints are related to the operational limitations of the storages. For LRC storage, no H_2 losses are assumed to occur during the storage procedure. Consequently, the total amount of H_2 produced during a simulated period is identical to the H_2 demand of the H-DR process (as the storage is assumed to be equally filled at the start and end of all simulated periods). This can be formulated as a linear equality constraint:

$$\sum \vec{m}_{elec,LRC} = \sum_i m_{H-DR,i} \tag{16}$$

For the LRC case, the nonlinear constraints relate to the (working gas) filling level of the storage, which cannot exceed the maximum LRC storage capacity ($Fill_{LRC}^{Max}$) or be below zero at any time step. This can be formulated as a set of two inequality constraints:

$$0 < Fill_{LRC,i} + (m_{elec,i} - m_{H-DR,i}) < Fill_{LRC}^{Max} \tag{17}$$

The same storage fill constraints also exist for CH_3OH-based storage. In addition, as some of the stored H_2 is combusted to provide heat for the MSR process, the assumption of equal storage fill level at the start and end of each simulation arises as a nonlinear equality constraint. The storage fill level change of the CH_3OH-based storage as a function of the H_2 produced via electrolyzers in time step i depends on whether the MSR process is operated or not:

$$\begin{gathered}\left(m_{elec,i} - m_{H-DR,i} - m_{CH_3OH}^{Min}\right) > 0\text{:} \\ Fill_{CH_3OH,i+1} = Fill_{CH_3OH,i} + (m_{elec,i} - m_{H-DR,i})\end{gathered} \tag{18}$$

$$\begin{gathered}(m_{elec,i} - m_{H-DR,i} - m_{CH_3OH}^{Min}) < 0\text{:} \\ Fill_{CH_3OH,i+1} = Fill_{CH_3OH,i} + m_{CH_3OH}^{Min} - \left(\frac{1}{1 - loss_{MSR}}\right) \cdot (m_{H-DR,i} - m_{elec,i} + m_{CH_3OH}^{Min})\end{gathered} \tag{19}$$

The MSR process must provide H_2 to the H-DR plant if the electrolysis H_2 production is lower than the sum of the H_2 demand of the H-DR process and the H_2 demand of maintaining the minimum load of the CH_3OH production process ($m_{CH_3OH}^{Min}$). When the MSR process is operated, the H_2 lost to provide heat for the MSR process must be accounted for, which is the purpose of equation (19). The sum of all changes in CH_3OH storage fill per time step is zero if the storage is equally filled at the start and end of the simulated period:

$$\sum_i (Fill_{CH_3OH,i+1} - Fill_{CH_3OH,i}) = 0 \tag{20}$$

Consequently, additional H_2 must be produced when a CH_3OH-based storage is implemented in the H-DR process to compensate for H_2 lost in the MSR process under the assumed conditions.

The objective function, the upper and lower bounds of the mass of H_2 produced via electrolyzers in each time step ($m_{elec,i}$), and all linear and nonlinear constraints are utilized to define the non-linear H_2 storage optimization problem in MATLAB® R2019. Finally, the built-in NLP solver '*fmincon*' is utilized to solve the optimization problem (using the standard settings for the solver and the '*interior-point*' algorithm).

The output of the optimization procedure, values of $OPEX_{storage}$ per equation (12), can be used to evaluate the overall profitability of investment into the simulated storage configuration using equation (9). Note that some of the input parameters of the optimization method, e.g., assumptions regarding EOC and the maximum storage capacity, also affect $CAPEX_a$.

7.2 ILLUSTRATIVE OPTIMIZATION RESULTS

Here some selected results from the optimization method described in the previous section are presented. Further results utilizing this same method can be found in paper V. Results shown here are mainly used to provide material for discussing differences in integrating an LRC or a CH_3OH-based H_2 storage in an H-DR process. Electricity prices from SE1 during 2020 is utilized as an example throughout this section. Results for a 50% EOC CH_3OH-based H_2 storage, assuming a 20% H_2 loss in MSR and a 10 000 t H_2 storage capacity, are seen in Figure 24.

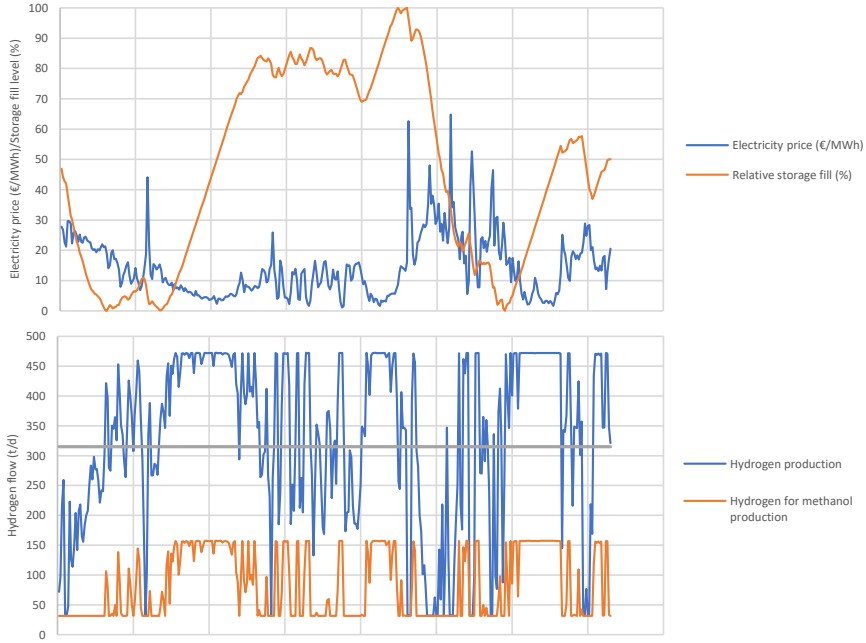

Figure 24: Day-wise optimization for operation of methanol-based hydrogen storage for SE1 2020 scenario with an electrolyzer overcapacity of 50%, a storage capacity of 10 000 t hydrogen, and a 20% methanol steam reforming hydrogen loss.

Clearly, a CH_3OH-based storage has the potential to allow for significant flexibility in H_2 production when integrated into an H-DR process. In the case shown in Figure 24, the operational cost of H_2 delivery could be reduced by approximately 22% compared to the case without a H_2 storage, even though the total H_2 production during the period is around 5% higher than it would have been without a storage due to MSR losses. This is achievable because H_2 is predominantly produced when electricity prices are low. When electricity prices are high, the MSR is operated and the electrolyzers are operated at minimum capacity (decided by the minimum load of the CH_3OH production plant)

The $CAPEX_a$ of the CH_3OH-based storage configuration in Figure 24 is 0.23 €/kg H_2 for a specific EOC investment cost of 500 €/kW. This is higher than the expected savings in operational costs (0.16 €/kg), rendering the investment into storage unprofitable in this case. This is also true if a lower MSR H_2 loss of 10% is assumed, although the savings in H_2 delivery operational costs do decrease (27% vs. case without storage, OPEX reduction of 0.20 €/kg). Assuming a lower specific electrolyzer investment cost of 300 €/kW leads to a storage $CAPEX_a$ of 0.18 €/kg H_2 and, thus, profitability in the case of 10% H_2 MSR loss. Despite the large assumed storage capacity (10 000 H_2), the storage fill level reaches both close to 0% and 100% on multiple occasions during the simulated year of operation. Considering the relatively low cost of H_2 storage capacity for CH_3OH-based storage, investment into a larger storage may, thus, be justified in this case.

Increasing the H_2 storage capacity in CH_3OH allows for an increasingly seasonal pattern of H_2 storage. This can be seen in Figure 25, where a larger storage capacity of 30 000 t H_2 has been assumed for the same electricity price scenario.

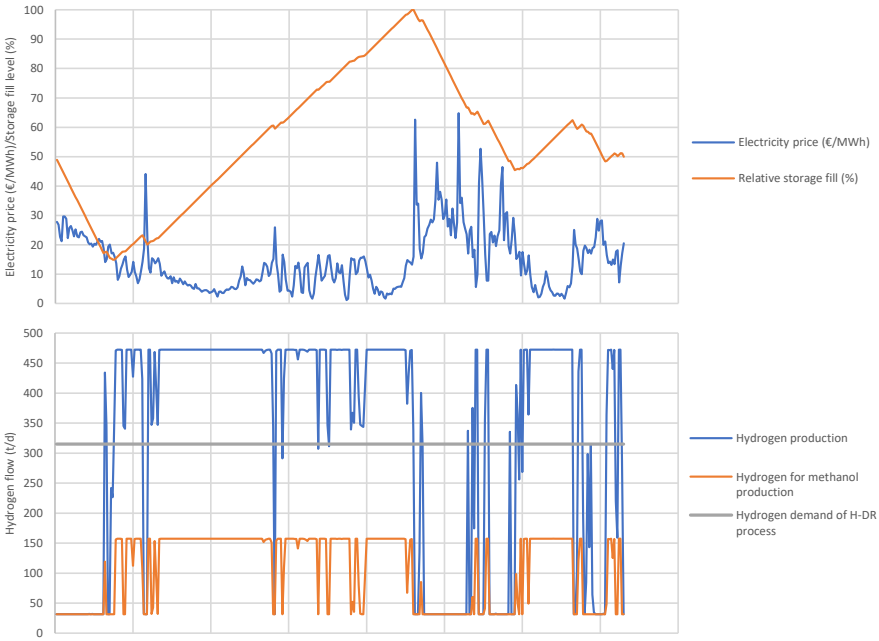

Figure 25: Day-wise optimization for operation of methanol-based hydrogen storage for SE1 2020 scenario with an electrolyzer overcapacity of 50%, a storage capacity of 30 000 t hydrogen, and a 10% methanol steam reforming hydrogen loss

Here, when the storage capacity is larger, the storage can be near-continuously filled from early march until mid-august. This allows for all electricity price peaks during the latter part of the year to be covered by the storage; the average H_2 production via electrolysis is just 223 t/d during the final 135 days of the year (71% of the nominal H-DR H_2 demand). As a result, the year-average reduction in H_2 delivery cost achieved by storage increases to 0.24 €/kg H_2. The increased $CAPEX_a$ of the total storage system due to the larger CH_3OH storage capacity is simultaneously moderate (less than 3%), rendering the storage investment profitable in this case.

Storage operation optimization results for a 640 t H_2 working gas capacity LRC storage are shown in Figure 26.

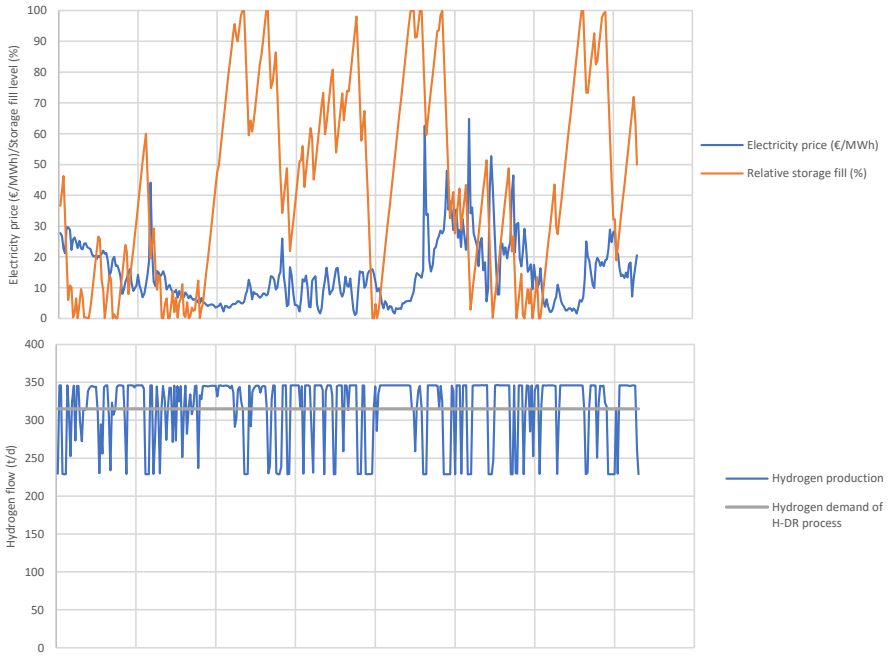

Figure 26: Day-wise optimization for operation of lined rock cavern hydrogen storage for SE1 2020 electricity prices with an electrolyzer overcapacity of 10% and a storage capacity of 640 t hydrogen.

The effects of introducing a 640 t H_2 capacity LRC on the overall economics of H_2 delivery to the H-DR process are relatively minor. The maximum reduction in the operational cost of H_2 delivery caused by LRC integration is around 6% (0.04 €/kg H_2), which is outweighed by the $CAPEX_a$ of the storage (0.06 €/kg H_2 for a specific LRC capacity cost of 42 €/kg H_2 and a specific electrolyzer investment cost of 500 €/kW). This 640 t H_2 LRC is simply too small and limited in terms of withdrawal and injection rates to significantly alter the cost of H_2 delivery to the H-DR process. Even during electricity price peaks, process electrolyzers still must produce a minimum of 229 t H_2/d, approximately 73% of the H-DR demand. For the CH_3OH-based storage considered in Figure 24, the equivalent minimum H_2 production rate is just 10% of the H-DR demand.

Results seen for five times larger (3 200 t H_2) LRC storage are seen in Figure 27. The maximum H_2 injection rate of this LRC allows for an EOC of 50%, identical to the one of the CH_3OH-based storage considered previously, and the maximum withdrawal rate is in excess of the H_2 demand of the H-DR process. If this LRC is completely filled, it can completely supply the H-DR plant with H_2 for around ten straight days before being completely emptied (considering only the working gas).

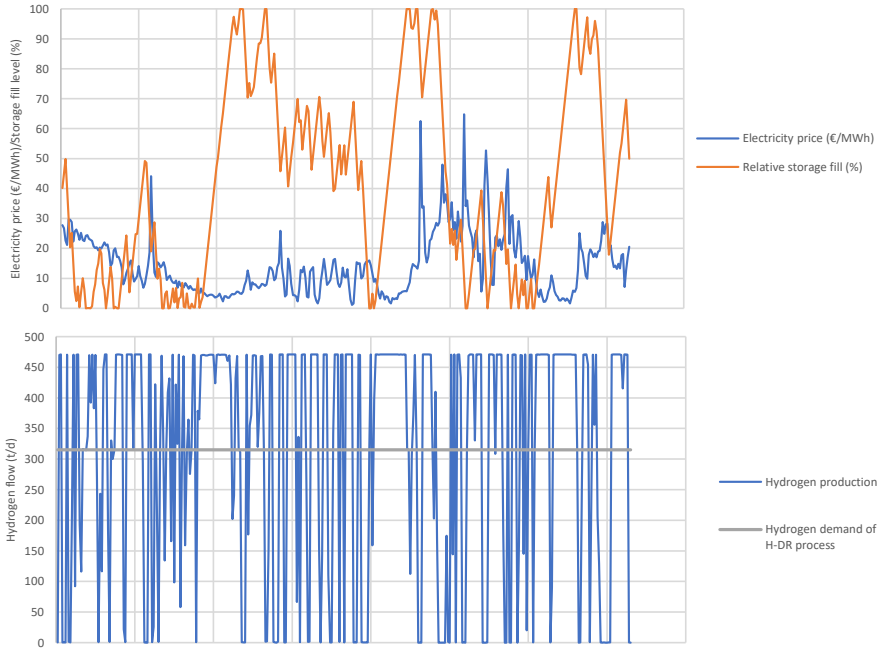

Figure 27: Day-wise optimization of lined rock cavern hydrogen storage operation for SE1 2020 with an electrolyzer overcapacity of 50% and a storage capacity of 3 200 t hydrogen.

This larger LRC has a far greater ability to affect the cost of H-DR H_2 delivery. However, despite the much larger storage capacity, the LRC still reaches often both close to 0% and 100% fill throughout the simulated year, indicating that an even larger storage capacity would be beneficial for storage operation. As a result, the reduction in the operational cost of H_2 delivery compared to the case without a storage is actually less than for the CH_3OH-based storage case in Figure 25 (0.18 €/kg H_2 for LRC vs. 0.24 €/kg H_2 for CH_3OH-based storage with the same EOC). In addition, the $CAPEX_a$ of this larger LRC storage option is also higher, around 0.30 €/kg H_2 vs. 0.23 €/kg H_2 for a specific electrolyzer investment cost of 500 €/kW. Increasing the LRC storage capacity even further has a larger negative effect in terms of increasing $CAPEX_a$ compared to the positive effect of reducing the operational cost of H_2 delivery to the H-DR process; increasing the LRC storage capacity to 4 500 t H2 reduces the operational cost of H_2 deliver by less than 0.02 €/kg H_2.

7.3 Reflections on optimization method results

The storage of H_2 in gaseous form in an LRC or as CH_3OH via reversible CO_2 hydrogenation are two very different approaches to the same problem. Differences in the techno-economic performance of the two approaches stem from their different investment costs and operational characteristics. Even though H_2 storage in an LRC is more efficient and avoids the H_2 losses of MSR, the CH_3OH-based storage achieves larger reductions in H_2 delivery cost in the example considered in section 7.2, particularly when the CH_3OH storage capacity is large. The CH_3OH storage system also has an around 20% lower $CAPEX_a$ than the 3 200 H_2 working gas LRC. The conclusion is that certain losses during H_2 storage may be tolerable as long as the storage allows for H_2 production via electrolysis to be highly concentrated to periods with relatively low electricity prices. The H_2 lost in the MSR process is produced at a relatively low electricity price on average, reducing the negative impact. Likewise, the minimum load production of CH_3OH is also primarily utilized to replace H_2 production at particularly

high electricity prices (as all produced CH_3OH is also reformed during the simulated period due to the optimization method constraints).

No limitation on the allowable LRC annual turnover frequency was assumed when generating the optimization results seen in section 7.2. However, these results indicate that optimal LRC operation for integration with an H-DR-EAF plant may require annual turnover rates far higher than those typically encountered in geological NG storage. The calculated LRC annual turnover frequencies for the cases in Figure 26 Figure 27 are both around 20, which can be compared to the typical maximum of 10–12 achieved for NG salt cavern and LRC storages [16, 289]. It is presently uncertain whether this kind of LRC operation is feasible, particularly for one storing H_2. This highlights part of the challenge of adapting existing geological NG storage technologies to H_2 storages for H-DR-EAF plants.

The ability for any H_2 storage to reduce the costs of H_2 delivery to an H-DR process will, as previously discussed, depend on the encountered electricity prices to a very large extent. For the SE1 2020 case considered in section 7.2, the average electricity price was rather low (14 €/MWh) and there were few high price peaks (prices exceeded 50 €/MWh on only three occasions). Consequently, the electricity cost of H_2 production was relatively low during this period even in the absence of a storage (0.7 €/kg) and there is, thus, little room for reductions in H_2 production electricity costs. Larger reductions in H_2 delivery costs can be achieved in other scenarios. As an example, electricity prices in SE1 during 2021 were both higher (42 €/MWh on average) and considerably more volatile than during the previous year. In this scenario, the 10% H_2 MSR loss, 30 000 t capacity CH_3OH-based storage achieves a reduction of the operational cost of H_2 delivery cost by 0.50 €/kg H_2, while the 3 200 t LRC achieves a reduction of 0.46 €/kg H_2. Consequently, investment into any of these two storages is potentially profitable for this scenario, although the potential is higher for the CH_3OH option (0.26 €/kg H_2 overall cost reduction vs. 0.16 €/kg H_2 for the LRC considering an EOC cost of 500 €/kW).

The results shown in section 7.2 are based on several parameter assumptions. A sensitivity analysis of important storage parameters is included in paper V. For CH_3OH-based storage, the most important parameters are the input EOC (and associated CH_3OH production capacity), the CH_3OH production minimum load, and the MSR H_2 loss. The CH_3OH production storage capacity matters less as long as it is sufficiently large to avoid operational limitations; this effect was, e.g., seen when increasing the storage capacity from 10 000 t H_2 in Figure 24 to 30 000 t H_2 in Figure 25. Determining the minimum CH_3OH storage capacity needed to avoid operational limitations is discussed further in section 8.3. The minimum load of the CH_3OH production process has been assumed to be 20% of the nominal load. Lower minimum loads may be feasible according to certain equipment suppliers and would improve storage economics [474]. The impact of MSR H2 loss on the economics of CH3OH-based H2 storage for H-DR plants is investigated further in section 8.4.

The developed deterministic method is useful in that the maximum achievable reductions in H-DR H_2 delivery cost via storage can be determined, which allows for the techno-economic performance of LRC and CH_3OH-based H_2 storages to be compared under identical conditions. Nevertheless, the developed method does not necessarily model realistic storage operation due to assumptions regarding, e.g., perfect electricity price foresight and the H-DR plant being a price taker.

In practice, electricity prices will not be known to the H-DR plant operator in advance. While reasonably reliable short-term electricity price forecasting methods are available, it is exceedingly difficult to predict, e.g., a full year of prices in advance with any degree of certainty and this will in all likelihood remain the case in the foreseeable future, e.g., due to the inherent unpredictability of solar and wind power [12, 265]. This makes the investment into a H_2 storage inherently associated with a certain amount of risk. If the electricity market should develop such that electricity prices are relatively stable over time, e.g., due to other large investments into electricity storage or dispatchable electricity generation, the H_2 storage risks becoming a stranded asset, i.e., potentially abandoned

before the end of its economic lifetime. One way in which this risk could be at least partially mitigated is to introduce the option to sell accumulated CH_3OH to external customers, which may potentially improve the utilization of the CH_3OH production process. This approach is discussed in the next chapter.

The price taker assumption is more complex to evaluate considering that it involves the dynamics of the entire electricity system in which the H-DR plant operates. As discussed at the start of this chapter, the introduction of a H_2 storage into the H-DR plant may allow for a reduction in overall plant electricity costs not only due to the avoidance of H_2 production via electrolysis during electricity peaks but also due to positive synergies with variable renewable electricity generation. The latter effect is, as previously mentioned, not included in the present analysis but could significantly improve the overall economic prospect of H_2 storage in an H-DR plant. The results presented in this chapter should, therefore, not necessarily be considered wholly optimistic, despite the assumption of perfect foresight, due to the absence of this variable renewable electricity synergy effect. Indeed, if the electricity demand of an H-DR plant is to be mostly met by additional wind or solar power it may even be this synergy effect enabled by large-scale H_2 storage that allows for the plant to be built in the first place.

8 CO-PRODUCTION OF METHANOL IN HYDROGEN DIRECT REDUCTION STEELMAKING (PAPER VI)

The results in the previous chapter indicate that CH_3OH-based H_2 storage for H-DR processes may be techno-economically competitive with storage in LRCs in certain scenarios. The purpose of this chapter is to expand upon results in the previous chapter by evaluating different CH_3OH-based H_2 storage configurations for integration with an H-DR-EAF plant, including the option to also sell CH_3OH to external customers.

The costs of storage capacity have a major influence on the overall cost of an LRC H_2 storage, but not for one based on CH_3OH. Furthermore, should there arise an acute shortage of CH_3OH or CH_3OH storage capacity, this can potentially be momentarily increased via, e.g., the use of a tanker ship or other temporary storage means. Therefore, a calculation method specifically for CH_3OH-based H_2 storage was developed in which the storage capacity is an output parameter instead of an input. The output CH_3OH storage capacity is the minimum capacity needed to prevent any storage operation limitations. As seen in the previous chapter, the CH_3OH storage capacities needed to avoid these limitations must not necessarily be exceedingly large. This ostensibly simple alteration of the calculation approach has significant repercussions for the storage operation optimization calculations. Firstly, the chronological order of data points becomes irrelevant. Secondly, the NLP optimization problem is reduced to a much simpler linear form that can be solved analytically. From a practical standpoint, this simplification results in a dramatic decrease in computational strain, which is beneficial for screening different CH_3OH storage configurations presented in this chapter.

A unique aspect of CH_3OH-based H_2 storage compared to the storage of gaseous H_2 is that the stored CH_3OH has an inherent added value as a chemical or fuel and can also easily be distributed via ship, truck, or rail [456]. Therefore, the possibility to also sell off part of produced CH_3OH to an external actor was integrated into the developed linear calculation method [380]. The hypothesis is that integrating the possibility of selling CH_3OH may allow for increased utilization of the CH_3OH production process and, thus, profitability, particularly in scenarios when a storage-only strategy is largely ineffective, e.g., those featuring long periods of relatively low and stable electricity prices. Therefore, CH_3OH co-production may be a way of hedging investments in CH_3OH-based H_2 storage against uncertain electricity market conditions. Introducing the possibility to sell CH_3OH does not significantly affect the investment cost of the CH_3OH-based H_2 storage as all necessary equipment is already in place. Furthermore, the demand for fossil-free CH_3OH is expected to increase considerably over the coming years due to the decarbonization of different industries, ranging from plastics production (via the methanol-to-olefins process) to marine fuel [35, 451, 549, 550].

8.1 CALCULATION METHOD

The calculation method developed for paper VI is, in contrast to the NLP-based method described in the previous chapter, linear and non-iterative. This is allowed by assuming that no storage operational limitations due to CH_3OH storage capacity arise. Like the NLP-based method, the purpose of this linear model is the identification of the electrolyzer operating profile that minimizes the operational cost of H_2 delivery to an H-DR-EAF plant. This is achieved by concentrating EOC and MSR utilization to periods with low and high electricity prices, respectively.

The starting step of the method is to organize the electricity prices of the period to be simulated in ascending order, i.e., as a duration curve. Only full-year daily resolution electricity price data is used here and in paper VI. The maximum available electricity price gradient between H_2 storage and release can now be identified by considering the first and last data days of the duration curve. The contribution margin of H_2 storage ($CM_{storage}$) between these two days can now be described as the

avoided cost of H_2 production at the high electricity price ($[€/MWh_{el}]_{high}$) subtracted by the cost of overproducing and storing H_2 as CH_3OH at the lower electricity price ($[€/MWh_{el}]_{low}$).

$$CM_{storage} = \left[\frac{€}{MWh_{el}}\right]_{high} \cdot E_{elec} \cdot m_{H_2,avoided} - \left[\frac{€}{MWh_{el}}\right]_{low} \cdot (E_{elec} + E_{store}) \cdot m_{H_2,stored} \quad (21)$$

Due to MSR H_2 losses and the electricity demand of CH_3OH production, a certain minimum electricity price difference between filling and emptying the storage ($[€/MWh_{el}]_{high}$-$[€/MWh_{el}]_{low}$) is necessary to reach a positive CM. This will not always be achievable—as we move from the outside towards the middle of a given electricity price duration curve (around the average electricity price of the considered period), electricity price differences grow smaller. When a positive CM cannot be reached, storage should be avoided. Three CH_3OH storage system operating modes can, thus, be defined:

1. Storage: the electricity price is relatively low and H_2 in excess of the H-DR demand is produced. This excess H_2 is stored as CH_3OH.
2. Reforming: the MSR process is operated and electrolyzers are at minimum load.
3. Neutral: storage has a negative CM. As little H_2 as possible is stored to minimize losses.

Due to the minimum load of the CH_3OH production process, some H_2 must still be produced even if the CM of H_2 storage is negative. However, as it is assumed that no CH_3OH is accumulated in the storage during simulated periods, all CH_3OH that is produced is also reformed. It is assumed that this additional MSR operation occurs at the highest remaining electricity prices during the period not already covered by positive-CM reforming.

When the CM of storage is positive, as much H_2 as possible should be stored. The maximum amount of H_2 stored per day is limited by the EOC:

$$m_{H_2,stored} = m_{H-DR} \cdot EOC \quad (22)$$

$$m_{H_2,avoided} = (1 - loss_{MSR}) \cdot m_{H_2,stored} = (1 - loss_{MSR}) \cdot m_{H-DR} \cdot EOC \quad (23)$$

Due to the high investment cost of EOC and the CH_3OH production process, economically optimal EOCs are typically below unity. Consequently, multiple days in the storage operating mode are required per day in the reforming operating mode. This means that the electricity prices used to calculate the CM of storage generally must be weighted average values across multiple days.

Once the storage operating mode for each day of the considered period has been determined, the operating profiles of electrolyzers, the MSR process, and the CH_3OH production process can be determined and, from there, the specific operational cost of H_2 delivery to the H-DR process. This can then be compared to the electricity cost of H_2 delivery without storage and the specific marginal investment cost of the storage to assess storage profitability per equation (9).

The description of the CM of storage via equation (21) assumes that heat needed for MSR is sourced via partial combustion of released H_2, reflected in the difference between $m_{H_2,stored}$ and $m_{H_2,avoided}$. However, the equation can be easily modified to consider other MSR heat sources. For instance, if part of the MSR heat is provided by the combustion of an external fuel, a term that describes the cost of this fuel as a function of the associated heat demand and the specific fuel cost is added to the right side of the equation. If the heat for MSR is provided by reactor electrification, the first term of the left side of equation (21) may be modified to take this into account:

$$CM_{storage} = \left[\frac{€}{MWh_{el}}\right]_{high} \cdot \left(E_{elec} - E_{ref}\right) \cdot m_{H_2,avoided} - \left[\frac{€}{MWh_{el}}\right]_{low} \cdot (E_{elec} + E_{store}) \cdot m_{H_2,stored} \quad (24)$$

Note that the electricity demand of such reactor electrification (E_{ref}) occurs at the higher electricity price during the reforming operating mode while the additional H_2 production associated with providing the heat for dehydrogenation via partial H_2 combustion occurs at the lower electricity price.

Whether partial H_2 combustion or reactor electrification is optimal depends, thus, on the relative efficiencies of heat supply via the routes and the average change in electricity price between the storage and reforming operating modes. The economic prospects of different MSR heat supply options are investigated in section 8.4.

8.1.1 Integrating methanol sales

Allowing the possibility to sell off CH_3OH is one of the main purposes of the linear calculation method described in this chapter. As the produced CH_3OH can now be used for two different purposes, it is necessary to identify a sensible system that decide of how CH_3OH sales and reforming should be prioritized. Theoretically, the optimal choice between selling and storing CH_3OH for later reforming should be based on which option has the highest CM per unit CH_3OH produced in every considered time step. However, prioritizing H_2 storage whenever $CM_{storage}$ is positive may be beneficial from a wider electricity system perspective as the responsiveness of the electricity load of the H-DR process towards electricity price variations is then maximized. Although these effects cannot be quantified in the present calculation method, this storage-prioritized operation strategy is included for the sake of comparison.

The CM of CH_3OH sales is the difference between the CH_3OH sales price and its variable production cost. The variable production cost of CH_3OH production based on CO_2 and electrolysis is dominated by the costs of electricity and CO_2:

$$CM_{sales,CH_3OH} = (€/t_{CH_3OH})_{price} - (€/t_{CH_3OH})_{var.\ prod} \tag{25}$$

$$(€/t_{CH_3OH})_{var.\ prod} = \left[\frac{€}{MWh_{el}}\right] \cdot \left[\frac{MWh_{el}}{t_{CH_3OH}}\right] + \left[\frac{€}{t_{CO_2}}\right] \cdot \left[\frac{t_{CO_2}}{t_{CH_3OH}}\right] \tag{26}$$

The CH_3OH sales price can be converted into an equivalent electricity price by considering the electricity demand of its production [471, 551, 552]. This is useful in the present context as it determines the highest electricity price at which CH_3OH can be sold with a positive CM. The linear relationship between the CH_3OH price and its equivalent electricity price described is shown in Figure 28. The effect of different CO_2 costs is also shown. As in the previous chapter, CO_2 supply via biomass oxy-fuel combustion is assumed and the cost of CO_2 for CH_3OH production is taken to be zero in calculations, i.e., it is assumed that there exits an excess of electrolyzer O_2 byproduct so that the opportunity cost of utilizing it for oxy-fuel combustion is zero.

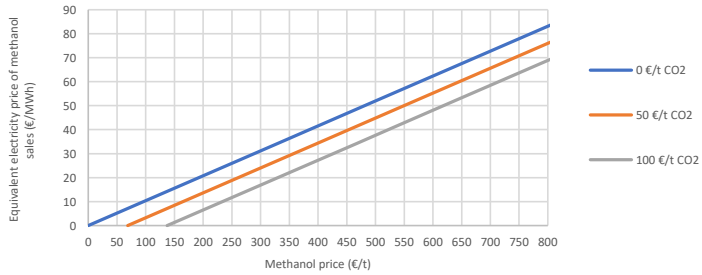

Figure 28: Equivalent electricity price of methanol as a function of the selling price and the carbon dioxide price. When the electricity price is below the equivalent methanol price, methanol can be sold with positive contribution margin.

The equivalent electricity price for a CH_3OH production cost of 500 €/t is approximately 52 €/MWh for a zero CO_2 cost. The CH_3OH production cost increases by approximately 69 €/t for a CO_2 price of 50 €/t. Therefore, for the CM of CH_3OH sales to be positive at an electricity price of, say, 40 €/MWh, a minimum CH_3OH sales price of 385 €/t for a zero CO_2 cost or 454 €/t for a CO_2 cost of 50 €/t is

required. Considering the CM of CH_3OH sales on a per unit H_2 basis to enable comparison with the CM of H_2 storage via equation (21) yields:

$$CM_{sales,H_2} = \left(\left[\frac{€}{MWh_{el}} \right]_{CH_3OH} - \left[\frac{€}{MWh_{el}} \right]_{el} \right) \cdot (E_{elec} + E_{store}) \quad (27)$$

This equation can be compared to the CM of storage to determine whether CH_3OH sales or storage is most economically beneficial for every time step of a simulated period. If H_2 storage is prioritized, storage is chosen whenever it can be achieved with a positive CM. Selling CH_3OH is then only an option during days when the CM of storage is negative but the CM of sales is still positive. Alternatively, the option with the highest CM in each data point of the considered period is chosen. To enable comparison with cases without CH_3OH sales, the CM of any sales of CH_3OH is assumed to be entirely allocated towards decreasing the operational cost of H_2 delivery to the downstream H-DR process.

The attractiveness of introducing the possibility to sell off CH_3OH from the H-DR plant naturally depends on the CH_3OH sales price. As NG is both the main chemical feedstock and fuel in most CH_3OH plants today (at least outside of China), the market price of CH_3OH closely follows that of NG [452, 553]. Methanex Corporation's regularly posted regional contract CH_3OH market prices are the typical benchmark values [554]. Historical month-wise European CH_3OH market prices from Methanex are shown in Figure 29. The average price during the last five years is around 350 €/t, but it can be seen that prices have generally increased over time. The latest posted European market price at the time of writing (March 2022) is 505 €/t CH_3OH, which is particularly high compared to historical values.

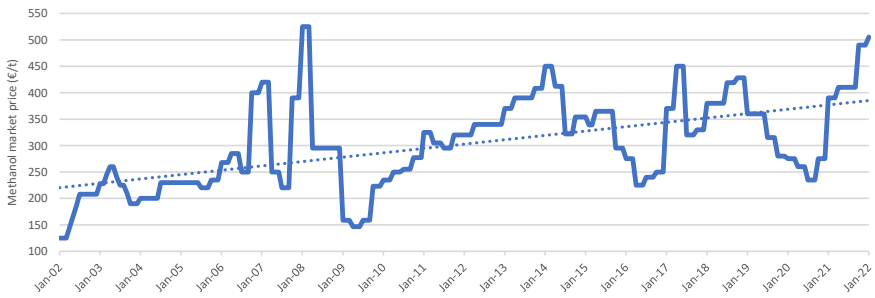

Figure 29: European methanol contract market prices from Methanex with a linear trendline [554].

A certain price premium may be expected if CH_3OH is produced from non-fossil sources [463, 555]. However, as the current market for fossil-free CH_3OH is very small, it is difficult to estimate the magnitude of this premium [197, 451, 455]. According to both CRI, currently the largest producer of electrolysis-based CH_3OH, and Energinet, the Danish national transmission system operator, fossil-free CH_3OH can currently be sold via long-term fixed price agreements at 550–600 €/t [471, 552]. Similar acceptable fossil-free CH_3OH market prices have also been assumed in the scientific literature [463, 555]. Two different CH_3OH market prices are considered in the upcoming analysis to assess its the effect on the economics of allowing CH_3OH sales: 350 €/t (equivalent electricity price 36 €/MWh), similar to the recent average fossil CH_3OH process, and 550 €/t (equivalent electricity price 57 €/MWh), assumed to be a competitive price for fossil-free CH_3OH.

8.2 COMPARISON WITH THE NON-LINEAR PROGRAMMING OPTIMIZATION METHOD

In the absence of the possibility to sell off CH_3OH, the linear calculation method described in this chapter gives, as expected, very similar results as the NLP-based method described in chapter 7 when a sufficiently large CH_3OH storage capacity so that operational limitations can be avoided is assumed. Optimized electrolyzer load profiles for SE1 2020 considering an EOC of 50%, a 10% H_2 loss in MSR, and, for the NLP method, a 30 000 t H_2 storage capacity for the two methods are shown in Figure 30.

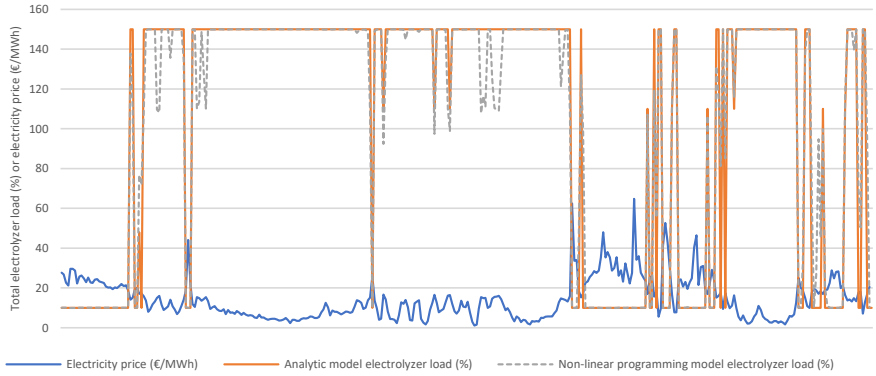

Figure 30: Optimal electrolyzer load profiles calculated using methods described in chapters 7 and 8. Electrolyzer overcapacity: 50%, methanol steam reforming hydrogen loss: 10%. Storage capacity in non-linear programming case: 30 000 t H_2. Electricity prices are from SE1 during 2020.

The difference in the calculated specific operational cost of H_2 delivery between the two methods is around 0.1%. The linear method gives, per definition, a slightly lower optimized H_2 delivery operational cost due to its non-iterative nature. Increasing the number of allowed iterations in the NLP solver algorithm would lead to even more similar results.

8.3 GENERAL TRENDS FOR METHANOL-BASED HYDROGEN STORAGE

The three operating modes of the CH_3OH-based storage can clearly be perceived if results from the linear method are plotted based on the electricity price duration curve. This is seen in Figure 31 for electricity prices from SE1 during 2020, considering EOCs of 50% and 25%.

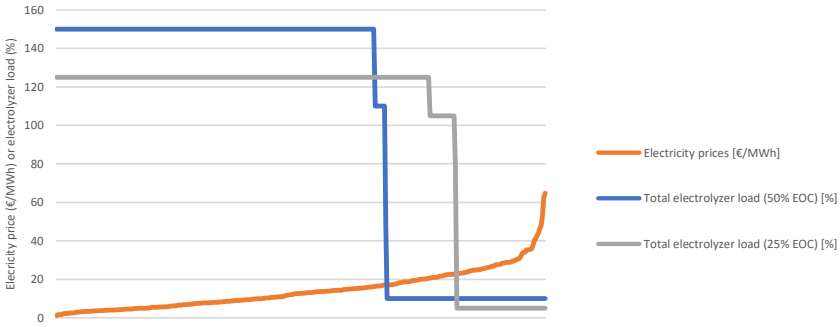

Figure 31: Storage-optimized electrolyzer operating profiles for SE1 2020 with electrolyzer overcapacities of 25% or 50%.

In the case of SE1 2020 the storages are very rarely in the neutral operating mode (8 days for 50% EOC, 19 days for 25% EOC). This indicates that a positive CM of storage can often be achieved, leading to a relatively high storage utilization in both cases. This is partially due to the rather steep incline of the electricity duration curve. Duration curves more commonly have a broad relatively flat middle section with relatively few instances of low or high electricity prices. Such a case can, e.g., be found for SE1 during 2019, which is seen in Figure 32.

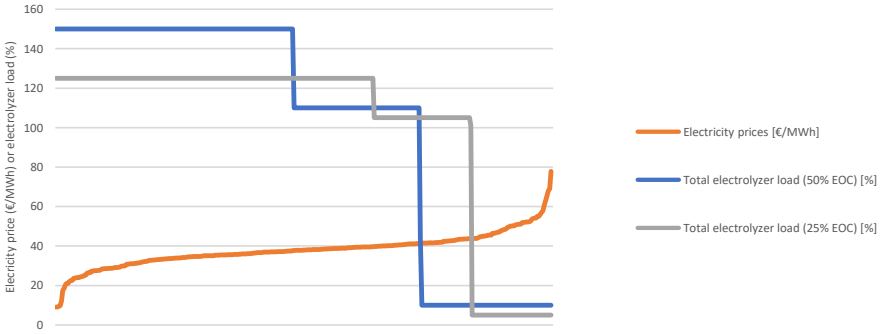

Figure 32: Storage-optimized electrolyzer operating profiles for SE1 2019 with electrolyzer overcapacities of 25% or 50%.

In this case, the storage is relatively often in the neutral operating mode (93 days for 50% EOC, 71 days for 25% EOC). As the electricity price was in the range of 25–45 €/MWh for over 80% of days during 2019 in SE1, a high CM of storage can rarely be reached. Due to this absence of electricity price volatility, the storage becomes an economic burden, increasing the overall H-DR-EAF plant investment cost without significantly reducing the operational cost of H_2 delivery. Of course, this dependency on electricity price volatility applies to all kinds of H_2 storages, not just those based on CH_3OH.

Indeed, in the absence of operational limitations due to storage capacity, the potential to reduce the costs of H_2 delivery via CH_3OH-based storage is well-correlated (R^2>0.9) with the electricity price volatility. This trend can be seen in Figure 33, where the standard deviation of the electricity price in electricity pricing zones SE1, SE4, and DK1 for all years from 2013 to 2020 (a total of 24 electricity price scenarios) are plotted against the calculated achievable reduction via H_2 storage in CH_3OH, considering an EOC of 50% and an MSR H_2 loss of 10%.

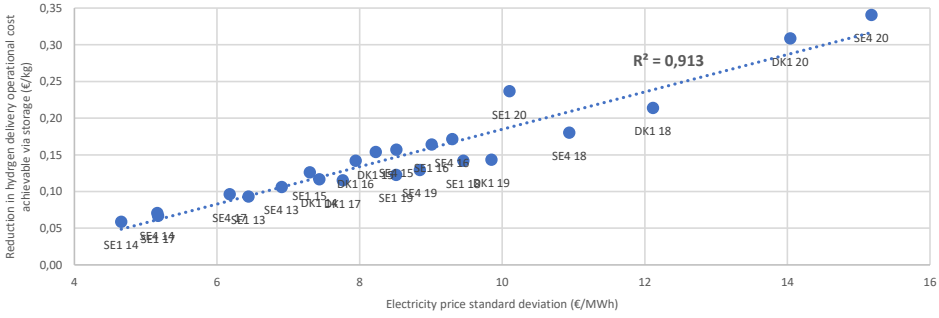

Figure 33: Correlation between electricity price volatility (with standard deviation as a proxy) and the achievable reduction in operational cost of hydrogen delivery to a hydrogen direct reduction process. Each dot represents average values of a year in SE1, SE4 or DK1 during the period 2013–2020.

Based on the trend seen in Figure 33 and the $CAPEX_a$ of CH_3OH-based H_2 storage systems (0.24 €/kg H_2 for an EOC investment cost of 500 €/kW and a 30 000 t H_2 capacity), a minimum electricity price standard deviation of at least 12–14 €/MWh is likely necessary to reach storage profitability. Evidently, this has rarely occurred in any of the considered electricity pricing regions during the period 2013–2020. However, a trend towards increasing electricity price volatility over time can be seen.

As mentioned at the start of this chapter, the minimum CH_3OH storage capacity needed to avoid operational limitations is an output of the linear calculation model. A clear trend between the EOC (and associated CH_3OH production capacity) and this minimum necessary CH_3OH storage capacity to avoid operational limitations is seen, per Figure 34.

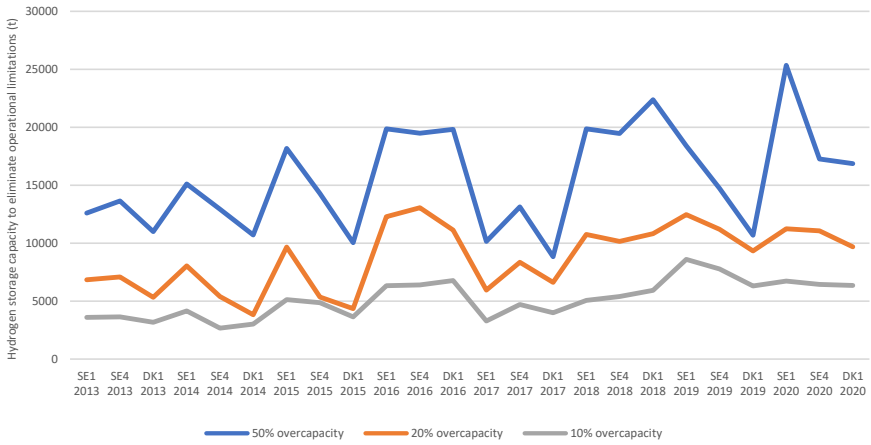

Figure 34: Minimum required hydrogen storage capacity to avoid operational limitations for methanol-based storage as a function of the electrolyzer overcapacity. Methanol steam reforming hydrogen loss: 10%.

For 10% EOC, a storage capacity of 8 000 t is sufficient in all scenarios, with an average of around 5 000 t H_2. This increases to an average of 16 000 t H_2 for a 50% EOC. The low cost of CH_3OH storage renders such large H_2 capacities relatively easily attainable; a single 100 000 m³ floating roof CH_3OH tank can hold 10 000–15 000 t of H_2 [456, 531]. In comparison, the storage of H_2 in an LRC will nearly always be associated with certain operational limitations due to storage capacity—an 8 000 t H_2 working gas capacity LRC (excluding additional costs of EOC) will likely have an investment cost in excess of that of the H-DR electrolyzers.

8.4 Economic impact of methanol steam reforming heat supply options

The heat required for the MSR process can be generated in different ways. In this section, the impact of the MSR heat supply on the overall ability of CH_3OH-based storage to reduce the H-DR H_2 delivery cost is investigated using the linear calculation method described at the start of this chapter. First, the impact of H_2 losses in the MSR process on the ability of the storage to reduce the operational cost of H delivery is analyzed. Results of this analysis in terms of the average reduction in H_2 delivery operational cost over all full years of electricity prices in SE1, SE4, and DK1 during 2013–2020 are seen in Figure 35. Also seen are results for the previously suggested hybrid heat supply process (per Figure 18) at two biomass price levels (20 and 40 €/MWh).

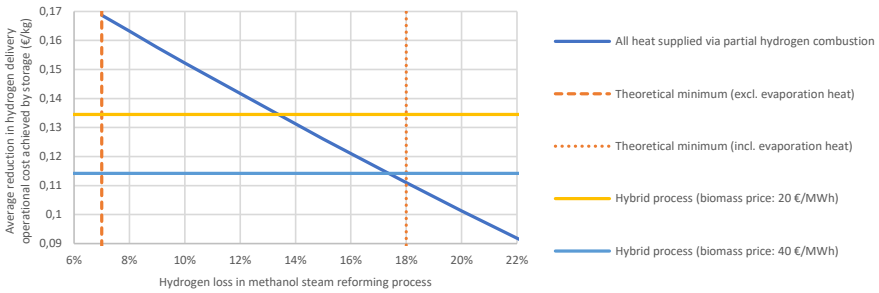

Figure 35: Correlation between hydrogen losses in methanol steam reforming process and the average reduction in operational cost of hydrogen delivery achieved by storage in methanol across 2013–2020 in SE1, SE4, and DK1.

The impact of MSR H_2 loss on the economics of CH_3OH-based H_2 storage is clearly rather substantial. The average difference in the achievable reduction in H_2 delivery operational cost between a 10% and 20% H_2 loss is around 50%. For the electricity prices considered here, the hybrid heat supply approach appears competitive with partial H_2 combustion, especially if the CH_3OH and H_2O preheating and evaporation heat must also be supplied via combustion of H_2, i.e., if integration with the H-DR-EAF plant (as described in section 6.1.2.1) cannot provide this heat. This also applies to the higher biomass price of 40 €/MWh. As mentioned previously, biomass for this type of large-scale industrial use may be sourced at even lower prices than 20 €/MWh in Sweden or Finland, which would further increase the attractiveness of the hybrid heat supply approach [91].

MSR reactor electrification has been suggested and appears technically feasible. Such electrification could allow for more flexible MSR reactor operation and is associated with more efficient heat transfer compared to when a fuel is combusted to provide the reaction heat [428]. Assuming optimistically that a 99% H_2 recovery separation method can be realized yields the results seen in Figure 36 for an electrified MSR process:

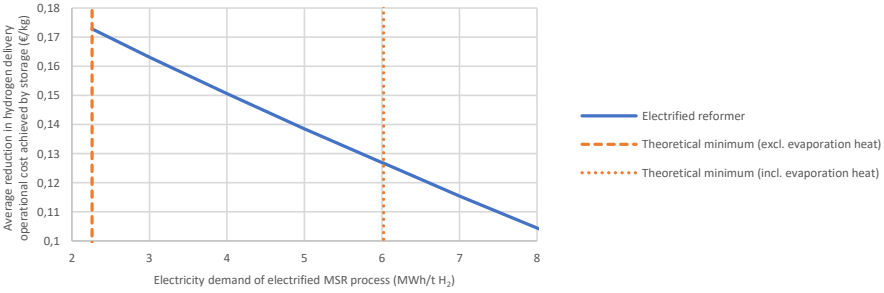

Figure 36: Correlation between electricity demand of electrified methanol steam reforming process and the average reduction in operational cost of hydrogen delivery achieved by storage in methanol across 2013–2020 in SE1, SE4, and DK1. Assumed hydrogen recovery: 99%.

At the minimum theoretical heat demand (excluding evaporation of CH_3OH and H_2O), the electrified MSR performs achieves only a 2% larger reduction in H_2 delivery operational cost compared to the partial H_2 combustion option, despite the very high assumed H_2 recovery in the electrified MSR case. The difference increases to 11% if it is assumed that 10% of released H_2 must be combusted in the non-electrified case. As expected, these results are sensitive towards the electricity price scenario and more volatile electricity prices favor the partial H_2 combustion approach. As an example, for SE1 2020, partial H_2 combustion results in less than a 3% small reduction in H_2 delivery operational cost

compared to MSR electrification (in the case that heat for CH_3OH and H_2O evaporation is not freely available), despite the optimistic H_2 recovery assumed for electrified MSR. Consequently, MSR electrification does not appear particularly attractive in the context of H_2 storage for an H-DR-EAF plant. Out of the considered MSR heat supply options, the hybrid approach appears the most promising option for the considered electricity price scenarios if heat integration with the H-DR-EAF plant is not possible, particularly for low biomass fuel prices.

8.5 INTEGRATION OF METHANOL SALES IN THE OPTIMIZATION PROCEDURE

Introducing the possibility to sell off CH_3OH has the potential to significantly improve the economic prospect of a CH_3OH-based H_2 storage system for an H-DR process. As mentioned previously, two cases for sales integration are considered: one where H_2 storage in CH_3OH is prioritized for grid balancing reasons and one where CH_3OH is sold off whenever a positive CM higher than that of H_2 storage can be achieved. The hybrid MSR heat supply process has been assumed in all cases with a biomass price of 20 €/MWh.

8.5.1 Prioritizing storage

If utilization of the CH_3OH production process for storage is prioritized, the effect of CH_3OH sales on the operational cost of H_2 delivery depends on the extent to which the EOC and the CH_3OH production process are already utilized for storage purposes. If there is excess EOC available at electricity prices below the equivalent CH_3OH price, CH_3OH can be sold off with a positive CM. Excess EOC is available when the system is in the neutral or reforming operating modes. If electricity prices are sufficiently low during the reforming operating mode to allow for CH_3OH to be sold off with a positive CM, CH_3OH will be both produced to be sold off and withdrawn from the storage to be reformed. Note that the overall electrolyzer load will still be well below 100% (e.g., 50% in the case of 50% EOC) in such scenarios. It is also feasible that electricity prices are too high during neutral or reforming operating modes to allow for any CH_3OH to be sold off with a positive CM. In such cases, introducing the possibility to sell off CH_3OH has no effect on the cost of H_2 delivery. Results for the storage-prioritized case are seen in Figure 37.

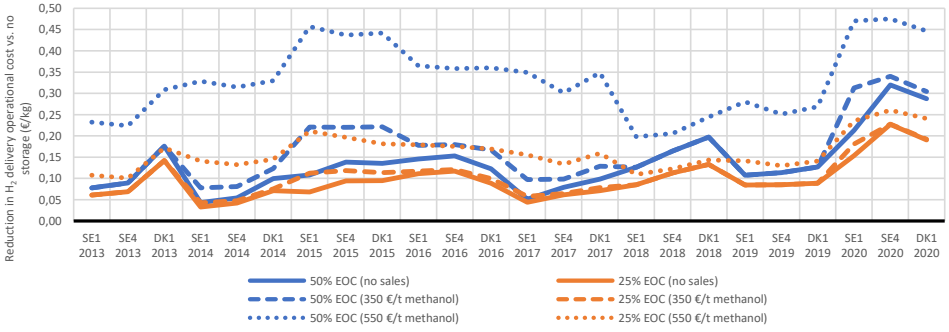

Figure 37: Effect of electrolyzer overcapacity and methanol sales price on the achievable reduction of the operational costs of hydrogen delivery to a hydrogen direct reduction process by the integration of a methanol-based hydrogen storage.

The positive economic effect of introducing CH_3OH sales is, as expected, most noticeable for higher EOCs and CH_3OH sales prices. In the 550 €/t, 50% EOC case, an average reduction of the operational cost of H_2 delivery to the H-DR process of 0.33 €/kg H_2 can be achieved, an improvement of over 140% compared to the case without CH_3OH sales. This renders the storage profitable on average for an EOC investment cost of 500 €/kW. Cases with lower EOCs or CH_3OH sales prices or both see smaller but still significant average improvements in H_2 delivery operational costs compared to the

storage-only case (67% improvement for 25% EOC, 550 €/t; 22% for 50% EOC, 350 €/t; 8% for 25% EOC, 350 €/t).

Scenarios where H_2 storage in CH_3OH is most beneficial do not necessarily coincide with those where the largest effect of introducing CH_3OH sales occurs. The largest reductions in the operational cost of H_2 delivery without CH_3OH sales are achieved for the SE4 and DK1 2020 scenarios as these feature the most volatile electricity prices. Allowing CH_3OH is most economically beneficial in scenarios with low average electricity prices, e.g., in all considered pricing regions during 2015, which can be seen in Figure 38 for cases with 50% EOC. This indicates that the ideas of selling off CH_3OH and utilizing it as a H_2 storage medium can indeed essentially be considered complimentary, which then confirms the hypothesis stated at the start of this chapter.

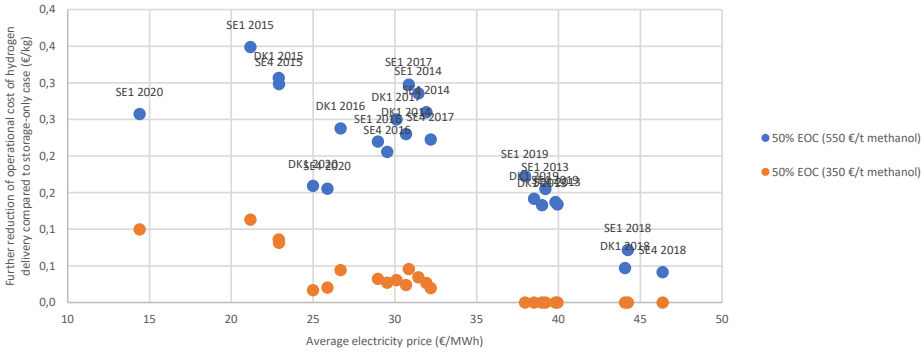

Figure 38: Correlation between year-long average electricity price of scenarios and the economic effect of introducing the possibility to sell of methanol for the case that storage is prioritized over methanol sales. Each dot represents a year in SE1, SE4 or DK1 during the period 2013–2020.

The CH_3OH price has a major effect on the added value of including the possibility for CH_3OH sales. At 350 €/t CH_3OH, the added value of CH_3OH sales is never above 0.11 €/kg H_2 in any scenario and always zero for average electricity prices above 37 €/MWh. The SE1 2020 case is notable as the added value of including CH_3OH sales is relatively low despite the low average electricity price. The reason for this is that electricity prices were also very volatile during 2020 in SE1, which means that a large part of the EOC is already occupied with H_2 storage, leaving little room for additional CH_3OH sales.

8.5.2 Maximizing the contribution margin of methanol production

When storage is not prioritized over selling CH_3OH, larger reductions in the operational cost of H_2 delivery can be achieved, especially for larger EOCs, as seen in Figure 39. This is to be expected given the structure of the applied calculation model. As previously, the effect of CH_3OH sales is more significant for higher CH_3OH prices (leading to larger CMs) and higher EOCs (leading to larger achievable sales volumes).

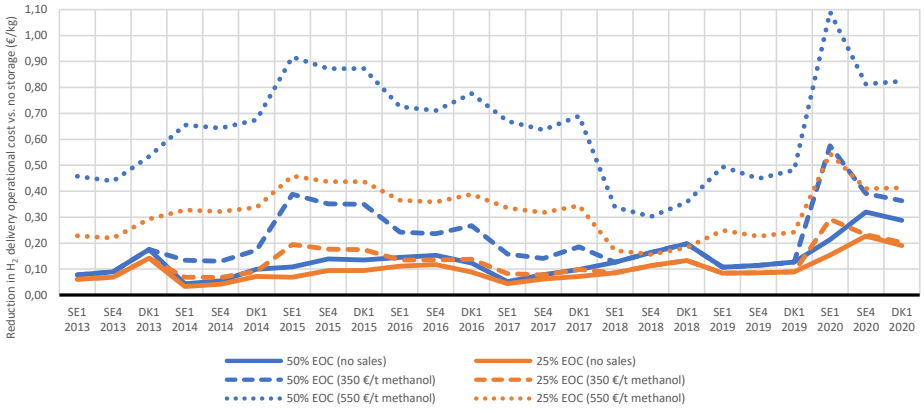

Figure 39: Effect of electrolyzer overcapacity and methanol sales price on the achievable reduction of the operational costs of hydrogen delivery to a hydrogen direct reduction process by the integration of a methanol-based hydrogen storage.

A CH_3OH sales price of 350 €/t is still not sufficient to allow for significant sales volumes in certain considered scenarios. This occurs for years with relatively high average electricity prices. Nevertheless, the average improvement of the reduction of operational cost of H_2 delivery compared to when sales are not allowed is noticeable even for this lower assumed CH_3OH price, particularly for the 50% EOC case (average improvement is 0.09 €/kg H_2). For the higher CH_3OH price, a noticeable improvement compared to the case without sales is always seen. For 50% EOC, the average improvement compared to the storage-only case is 0.50 €/kg H_2 across all considered scenarios, with a maximum of 0.88 €/kg H_2 for SE1 2020 (the total reduction in operational cost of H_2 delivery is 1.09 €/kg H_2). Nevertheless, the amount of CH_3OH sold off varies considerably from scenario to scenario even for 550 €/t CH_3OH depending on the profitability of storage during scenarios (see paper VI).

As noted previously for the case when H_2 storage is prioritized over CH_3OH sales, there is a correlation between the average electricity price and the economic improvement compared to the case considering only H_2 storage also when storage is not prioritized, as seen in Figure 40. This correlation is stronger when storage is not prioritized over sales, particularly for the higher 550 €/t CH_3OH sales price, which can be seen when comparing results in Figure 40 and Figure 38,

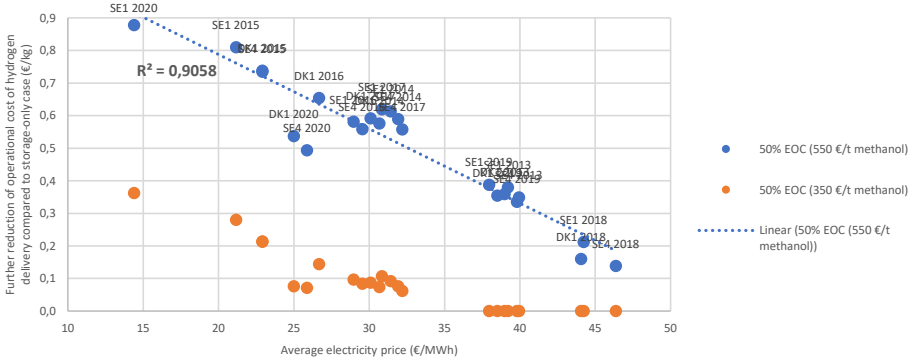

Figure 40: Correlation between average electricity price of scenarios and the economic effect of introducing the possibility to sell of methanol for the case that the contribution margin of methanol production is maximized. Each dot represents a year in SE1, SE4 or DK1 during the period 2013–2020.

When the average electricity price is relatively high and the CH_3OH sales price is low, it is not possible to sell off significant amounts of CH_3OH. In the opposite case, the CH_3OH production plant is essentially exclusively producing CH_3OH for export while the MSR process is operated very sparingly. This is sensible as H_2 production for the H-DR process is also inexpensive during such electricity price conditions, rendering the demand for H_2 storage to cover electricity price peaks low. This kind of complete switch to CH_3OH production for sales is not feasible in the storage-prioritized case considered previously, resulting in lower CH_3OH sales volumes in low-average electricity price scenarios.

SE1 2020 is the scenario for which the largest difference in economic performance to the storage-prioritized approach is seen (around 0.6 €/kg). As mentioned previously, when storage is prioritized due to price volatility, a large portion of EOC is locked up for this purpose, which leads to lower achievable CH_3OH volumes for sale.

9 DISCUSSION AND CONCLUSIONS

This work presents the first investigation of the techno-economic viability of non-geological H_2 storage for fossil-free H-DR steelmaking. The integration of a H_2 storage in such plants allows for flexible H_2 production so that more can be produced when electricity prices are low and vice versa. This flexibility may improve the economic prospects of fossil-free H-DR steelmaking considerably, particularly if a large part of the sizeable electricity demand of such plants is planned to be met by additional wind or solar power. The analysis of non-geological H_2 storage alternatives presented here is useful as there are currently many uncertainties regarding the techno-economic viability and operational limitations of geological H_2 storages, especially for those not of the salt cavern kind. The geological formations necessary for the construction of geological H_2 storages are also far from ubiquitous, rendering such storages not an option in many important steelmaking regions. This may be particularly relevant for the conversion of existing BF-BOF steel plants to fossil-free H-DR-EAF as these were not originally situated with such geological considerations in mind.

Two research questions were posed at the start of this thesis:

- What non-geological H_2 storage technologies are most promising for integration with a fossil-free H-DR steelmaking process from a techno-economic perspective?
- Could the identified most promising technologies be competitive with geological H_2 storage, particularly in LRCs, from a techno-economic perspective?

Both of these questions can be answered based on the material presented in this thesis. The H_2 storage technologies most suitable for integration with a fossil-free H-DR steelmaking process from a techno-economic perspective are in all likelihood the liquid H_2 carriers. All other non-geological alternatives, e.g., aboveground gaseous storage, H_2 liquefaction, adsorption-based storage, and solid hydride-based storage, are associated with high storage energy demands or prohibitively high investment costs or some combination thereof, even with optimistic cost development projections. In addition, these H_2 storage technologies are also currently at a too low technological maturity for integration with large-scale H-DR plants in the mid to late 2020s.

Among the liquid H_2 carriers, CH_3OH appears particularly promising for integration into an H-DR-EAF plant for several reasons: it can store H_2 at a high volumetric density in liquid form and atmospheric pressure in conventional floating roof tanks; plants for both CH_3OH production from CO_2 and MSR are commercialized, mature technologies and both processes also operate at relatively mild pressures and temperatures; the heat demand of MSR is relatively moderate compared to the dehydrogenation of other liquid H_2 carriers; both the CH_3OH production and dehydrogenation processes can also be operated dynamically in response to changes in the electricity price, although such operation has not yet been demonstrated for large-scale plants.

Nevertheless, the viability of CH_3OH as a liquid H_2 carrier depends to a large extent on the access to low-cost CO_2 for its production. Therefore, a concept based on biomass oxy-fuel combustion to provide both H-DR reducing gas preheating and CO_2 for CH_3OH production was developed in this work. The O_2 required for oxy-fuel combustion can be sourced from the H-DR electrolyzers. If the oxy-fuel combustion process is sized based on the preheating demand of the H-DR process, it can provide enough CO_2 to allow for CH_3OH production equivalent to an electrolyzer overcapacity in excess of 50% and its O_2 demand is less than half of that generated by the H-DR electrolyzers. Biomass oxy-fuel combustion in combination with CH_3OH-based H_2 storage may be a particularly attractive option in regions with relatively low biomass prices, e.g., Sweden or Finland.

Another critical aspect for the implementation of liquid H_2 carrier-based storages is the cost-effective supply of heat to the dehydrogenation process. For this purpose, a hybrid MSR heat supply process was developed and simulated in this work. In this heat supply process, biomass combustion is utilized to provide the necessary heat for CH_3OH and H_2O evaporation and preheating, while the MSR reaction heat demand is supplied via combustion of the off-gas from the downstream PSA gas separation process. The biomass combustion process is based on an oversizing of the H-DR preheating furnace so that it is capable of supplying heat for both reducing gas preheating and also MSR feed evaporation and preheating when this is needed. The H-DR biomass demand increases by around 40% when the MSR process is operated. This hybrid heat supply process reduces the share of stored H_2 that must be combusted to provide heat for the MSR process, which is essential for the economic prospect of CH_3OH-based H_2 storage. It was also found to be a more economical MSR heat supply option than reactor electrification in regions with access to relatively low-cost biomass.

The second research question above must be answered with a "yes" considering the techno-economic results for the CH_3OH-based H_2 storage concept, including biomass oxy-fuel combustion and the hybrid MSR heat supply process, developed in this work. CH_3OH-based H_2 storage can achieve similar, or in some scenarios superior, reductions in the operational cost of H-DR H_2 delivery as an LRC-based storage but at lower investment costs. CH_3OH-based storage is particularly competitive in scenarios with prolonged periods of high electricity prices due to the low storage capacity cost, which then tends to outweigh H_2 losses during the storage cycle. The flexibility of CH_3OH storage component sizing is also a potential advantage over LRC-based storage. Finally, synergies between the CH_3OH-based H_2 storage concept and SOEL CO_2 and H_2O co-electrolysis to produce carburized DRI have been noted, e.g., in terms of CO_2 supply.

If a CH_3OH-based H_2 storage is integrated into an H-DR-EAF plant, it is feasible that there will be periods where the full CH_3OH production capacity cannot be utilized for storage purposes, e.g., due to a lack of long periods of high electricity prices. In such scenarios, the plant operator may potentially allow for excess CH_3OH to be sold off to external customers to provide additional revenue and improve the utilization of the CH_3OH production plant. Therefore, allowing for such CH_3OH sales from the H-DR-EAF plant was investigated and was found to have the potential to improve the economic performance of CH_3OH-based storage further under a wide variety of electricity market conditions. Integrating the possibility to sell off accumulated CH_3OH is particularly beneficial in scenarios with low average electricity prices where a H_2 storage is not needed to ensure cost-effective H_2 delivery to the H-DR-EAF plant. The idea of also selling off excess CH_3OH can, thus, be seen as a complementary function to its use for H_2 storage. This approach appears especially promising considering the expected increases in fossil-free CH_3OH demand for, e.g., fuel applications, plastics, and chemicals production. Nevertheless, implementation of a CH_3OH-based H_2 storage process of this kind in an industrial-scale H-DR-EAF plant requires not only technical innovation but also the development of business models that allow for the value of the CH_3OH-based storage system flexibility to be maximized under realistic, uncertain electricity, steel, H_2, and CH_3OH market conditions. It should be noted that this kind of flexible utilization of H_2 storage assets is not feasible for geological H_2 storages, where the storage capacity makes up the vast majority of investment costs.

A general challenge in terms of identifying the optimal integration of a CH_3OH-based H_2 storage in an H-DR plant is the current wide range of possible H-DR process design options. Some open questions include:

- Will the H-DR plant be stand-alone or integrated with an EAF?
- Will there exist possibilities for dynamic DRI production with storage?
- How will the reducing gas be heated?
- Will produced DRI be carburized and, if so, how?
- Which choice of electrolyzer technology is to prefer, low-temperature (AEL, PEM) or high-temperature electrolysis (SOEL)? In the case of SOEL, is steam or steam and CO_2 co-electrolysis the better choice?

The answer to all these questions will affect the optimal choice of CH_3OH-based H_2 storage system layout for the H-DR plant. Therefore, if a H_2 storage is to be part of the H-DR process, integration aspects ought to be included in the early stages of development.

9.1 RECOMMENDATIONS FOR FURTHER STUDIES

Several aspects of the CH_3OH-based H_2 storage suggested here are currently uncertain, including what storage investment costs can be expected upon integration of such a storage with an H-DR-EAF plant. Further detailed exploration of potential cost synergies is warranted, particularly regarding the possibilities for process integration of the H-DR-EAF plant and the CH_3OH-based H_2 storage investigated in this thesis. The identification of cost synergies between CO_2-based CH_3OH production plants and MSR plants is also of interest. Nevertheless, a large part of the investment cost of any large-scale H_2 storage will be that of electrolyzer overcapacity unless unexpectedly significant electrolyzer cost reductions are achieved over the coming years.

The practically achievable performance of the CH_3OH-based storage suggested in this thesis is presently not entirely certain. Although all components of the storage system are essentially fully mature processes on their own, the combination is new and requires further process design optimization considering the intended application. Dynamic operation of the storage system is also a particularly important aspect that requires further investigation, e.g., determination of allowable load cycling rates, start-up times, and minimum process loads. If more dynamic performance of the CH_3OH-based storage than assumed in this thesis turns out to be achievable, it may be feasible to optimize its operation for participation in intraday (hourly resolution) or balancing services in electricity markets.

A critical aspect of CH_3OH-based H_2 storage is the sourcing of CO_2. Supplying CO_2 via biomass oxy-fuel combustion by utilizing the electrolysis byproduct O_2 was identified as a potentially attractive option in this thesis. Such oxy-fuel combustion also allows for the integration of DRI carburization via rWGS or SOEL co-electrolysis, which may potentially be valuable in certain contexts, e.g., for stand-alone H-DR plants. However, no large-scale biomass oxy-fuel process is currently known and further research is needed to evaluate the feasibility of such a process, particularly for woody biomass fuels. Other heat integration possibilities, particularly for providing part of the heat needed for CH_3OH steam reforming via, e.g., EAF off-gas or DRI cooling heat recovery, were also discussed, but more research is needed here also to determine the potential of such approaches. Generally, the identification of the optimal way of integrating a CH_3OH-based storage in an H-DR-EAF plant under realistic operating conditions requires further work.

Combinations of different storage technologies have not been explored in this thesis but could have certain advantages, depending, e.g., on the achievable dynamic performance of the CH_3OH-based storage. As an example, a relatively small LRC could be utilized to handle smaller day-to-day variations in H_2 production demand while a CH_3OH-based storage handles variations over longer durations, i.e., across seasons. The small amounts of H_2 needed to maintain the minimum load of the CH_3OH production process when in the reforming operating mode could then also be sourced from the LRC to allow for H_2 production via electrolysis to be completely halted. In a similar vein, an investigation of the potential operational and economic consequences of connecting the H-DR plant with the associated H_2 storage to a prospective extensive H_2 pipeline network, which may potentially also be connected to other storages, could be of interest.

Finally, wider electricity market-level effects of the integration of different H_2 storage technologies with H-DR plants should be investigated in more detail. This thesis has centered on the perspective of the H-DR-EAF plant operator as an electricity price taker, reacting to changes in electricity price by varying the electrolysis H_2 production rate enabled by large-scale H_2 storage. In practice, the H-DR-EAF plant will affect the electricity price and the electricity market in which it operates. One such effect on the electricity market that was just briefly been discussed in this thesis is the positive effect that large-scale H_2 storage may have on the profitability of wind and solar power, which could potentially increase the probability of lower overall electricity prices for the H-DR-EAF operator. The value of this synergy is complex to quantify, and this was not attempted herein, but is possibly important for the overall profitability of investment into a H_2 storage as part of an H-DR-EAF plant. Considering the results presented in this thesis, it would be useful to know whether this synergy effect may be more significant for, e.g., a CH_3OH-based H_2 storage than for geological H_2 storage. This is not inconceivable considering differences in the operational characteristics and limitations of these kinds of H_2 storages, e.g., the lower cost of storage capacity for a CH_3OH-based storage.

REFERENCES

1. IEA, *Iron and Steel Technology Roadmap: Towards more sustainable steelmaking*. 2020.
2. Pauliuk, S., et al., *The steel scrap age.* Environmental science & technology, 2013. **47**(7): p. 3448-3454.
3. Allen, M., et al., *Technical Summary: Global warming of 1.5° C. An IPCC Special Report on the impacts of global warming of 1.5° C above pre-industrial levels and related global greenhouse gas emission pathways, in the context of strengthening the global response to the threat of climate change, sustainable development, and efforts to eradicate poverty.* 2019.
4. Rogelj, J., et al., *Mitigation pathways compatible with 1.5 °C in the context of sustainable development*, in *Global warming of 1.5 °C*. 2018, Intergovernmental Panel on Climate Change. p. 93-174.
5. IEA, *Net Zero by 2050: A Roadmap for the Global Energy Sector*. 2021.
6. Bataille, C., *Low and zero emissions in the steel and cement industries: Barriers, technologies and policies.* 2020.
7. Bataille, C., et al., *A review of technology and policy deep decarbonization pathway options for making energy-intensive industry production consistent with the Paris Agreement.* Journal of Cleaner Production, 2018. **187**: p. 960-973.
8. Hoffmann, C., M. Van Hoey, and B. Zeumer, *Decarbonization challenge for steel.* 2020, McKinsey.
9. Vogl, V., et al., *Green Steel Tracker.* 2021.
10. Wido K. Witecka, O.v.E.T., Jesse Scott, Helen Burmeister, Li Wang, Prof. Dr. Stefan Lechtenböhmer, Clemens Schneider, Ole Zelt, Prof. Dr. Max Åhman, *Global Steel at a Crossroads*. 2021, Agora Energiwende, Wuppertal Institut, Lund University.
11. Gielen, D., et al., *Renewables-based decarbonization and relocation of iron and steel making: A case study.* Journal of Industrial Ecology, 2020.
12. Holttinen, H., et al., *Design and operation of energy systems with large amounts of variable generation: Final summary report, IEA Wind TCP Task 25*. 2021, VTT Technical Research Centre of Finland.
13. Åhman, M., et al., *Hydrogen steelmaking for a low-carbon economy: A joint LU-SEI working paper for the HYBRIT project.* EESS report 109, 2018.
14. Jaraite, J., et al., *Intermittency and Pricing Flexibility in Electricity Markets*, in *Intermittency and Pricing Flexibility in Electricity Markets (2019), CERE Working Paper*. 2019, Energforsk.
15. Liebscher, A., J. Wackerl, and M. Streibel, *Geologic Storage of Hydrogen–Fundamentals, Processing, and Projects.* Hydrogen Science and Engineering: Materials, Processes, Systems and Technology, 2016: p. 629-658.
16. Kruck, O., et al., *Overview on all known underground storage technologies for hydrogen.* HyUnder (2013 August) Deliverable, 2013(3.1).
17. Johansson, F., et al., *Investigation of research needs regarding the storage of hydrogen gas in lined rock caverns: Prestudy for Work Package 2.3 in HYBRIT Research Program 1*. 2018, KTH Royal Institute of Technology.
18. Sofregaz, U. and C. Gustafsväg, *Commercial potential of natural gas storage in lined rock caverns (LRC).* US Department of Energy, 1999.
19. Hévin, G. *Underground storage of Hydrogen in salt caverns*. in *European Workshop on Underground Energy Storage November 7th–8th*. 2019.
20. Wijk, O., et al., *Slutrapport HYBRIT – Hydrogen Breakthrough Ironmaking Technology* 2018, Energimyndigheten.
21. Papadias, D. and R. Ahluwalia, *Bulk storage of hydrogen.* International Journal of Hydrogen Energy, 2021. **46**(70): p. 34527-34541.
22. Pei, M., et al., *Toward a Fossil Free Future with HYBRIT: Development of Iron and Steelmaking Technology in Sweden and Finland.* Metals, 2020. **10**(7): p. 972.
23. *World steel in figures*, in *World Steel Association: Brussels, Belgium*. 2021, World Steel Association.
24. Söderholm, P. and T. Ejdemo, *Steel scrap markets in Europe and the USA.* Minerals & Energy-Raw Materials Report, 2008. **23**(2): p. 57-73.
25. Dworak, S. and J. Fellner, *Steel scrap generation in the EU-28 since 1946 – Sources and composition.* Resources, Conservation and Recycling, 2021. **173**: p. 105692.
26. Wang, P., et al., *Efficiency stagnation in global steel production urges joint supply-and demand-side mitigation efforts.* Nature communications, 2021. **12**(1): p. 1-11.
27. Cooper, D.R., et al., *The potential for material circularity and independence in the US steel sector.* Journal of Industrial Ecology, 2020. **24**(4): p. 748-762.
28. Mandova, H., *Assessment of Bioenergy as a CO_2 Emission Reduction Strategy for European Iron and Steelmaking*. 2019, University of Leeds.
29. Carpenter, A., *CO_2 abatement in the iron and steel industry.* IEA Clean Coal Centre, 2012. **25**.
30. Hasanbeigi, A., C. Springer, and E. Global, *How Clean Is the US Steel Industry.* An International Benchmarking of Energy and CO2 Intensities.(Global Efficiency Intelligence, 2019), 2019.
31. Draxler, M., et al., *Technology Assessment and Roadmapping (Deliverable 1.2)*. 2021, Green Steel for Europe.
32. Fan, Z. and S.J. Friedmann. *Low-carbon production of iron and steel: Technology options, economic assessment, and policy*. Joule 2021.
33. Xylia, M., et al., *Weighing regional scrap availability in global pathways for steel production processes.* Energy Efficiency, 2018. **11**(5): p. 1135-1159.
34. Bataille, C., S. Stiebert, and F.G.N. Li, *Global Facility Level Net-zero Steel Pathways*. 2021, IDDRI.
35. Material Economics, *Industrial Transformation 2050: Pathways to Net-Zero Emissions from EU Heavy Industry*. 2019.
36. Mission Possible Partnership, *The Net Zero Steel Sector Transition Strategy*. 2021.
37. Sefidari, H., et al., *The Feasibility of Replacing Coal with Biomass in Iron-Ore Pelletizing Plants with Respect to Melt-Induced Slagging.* Energies, 2020. **13**(20): p. 5386.
38. Medarac, H., J. Moya, and J. Somers, *Production costs from iron and steel industry in the EU and third countries.* 2020.
39. *World Direct Reduction Statistics*. 2020, Midrex.

40. Babich, A. and D. Senk, *Recent developments in blast furnace iron-making technology*, in *Iron Ore*. 2015, Elsevier. p. 505-547.
41. Roudier, S., et al., *Best Available Techniques (BAT) reference document for iron and steel production: Industrial emissions directive 2010/75/EU: integrated pollution prevention and control*. 2013, Joint Research Centre (Seville site).
42. Babich, A., et al., *Handbook of ironmaking.* Wissenschaftsverlag Mainz, Aachen, 2008: p. 72-75.
43. Suopajärvi, H., et al., *Use of biomass in integrated steelmaking–Status quo, future needs and comparison to other low-CO2 steel production technologies.* Applied Energy, 2018. **213**: p. 384-407.
44. Jernkontoret, *Klimatfärdplan för en Fossilfri och Konkurrenskraftig Stålindustri i Sverige*. 2018, Jernkontoret Stockholm, Sweden.
45. De Maré, C., *Why Both Hydrogen and Carbon Are Key for Net-Zero Steelmaking.* IRON & STEEL TECHNOLOGY, 2021. **1**.
46. Hakala, J., et al., *Replacing Coal Used in Steelmaking with Biocarbon from Forest Industry Side Streams.* 2019.
47. IEAGHG, *Cost of CO_2 Capture in the Industrial Sector: Cement and Iron and Steel Industries*. 2018.
48. Deerberg, G., M. Oles, and R. Schlögl, *The Project Carbon2Chem®.* Chemie Ingenieur Technik, 2018. **90**(10): p. 1365-1368.
49. Hooey, L., et al., *Iron and steel CCS study (techno-economics integrated steel mill)*. International Energy Agency (IEAGHG), 2013.
50. Heikkilä, A., et al., *Reduction of iron ore pellets, sinter, and lump ore under simulated blast furnace conditions.* steel research international, 2020. **91**(11): p. 2000047.
51. Harvey, D., *From Iron Ore to Crude Steel: Mass Flows Associated with Lump, Pellet, Sinter and Scrap Iron Inputs.* ISIJ International, 2020. **60**(6): p. 1159-1171.
52. Gyllenram, R., et al., *Driving investments in ore beneficiation and scrap upgrading to meet an increased demand from the direct reduction-EAF route.* Mineral Economics, 2021: p. 1-18.
53. Battle, T., et al., *The direct reduction of iron*, in *Treatise on process metallurgy*. 2014, Elsevier. p. 89-176.
54. Zervas, T., J. McMullan, and B. Williams, *Gas-based direct reduction processes for iron and steel production.* International Journal of Energy Research, 1996. **20**(2): p. 157-185.
55. *DRI Products & Applications Providing flexibility for steelmaking*. 2018, Midrex.
56. Anderson, S.H. *Educated use of DRI/HBI improves EAF energy efficiency and yield and downstream operating results*. in *7th European Electric Steelmaking Conference & Expo, AIDM, Venice*. 2002.
57. Memoli, F., J. Jones, and F. Picciolo, *The use of DRI in a consteel® EAF process.* Iron and Steel Technology, 2015. **12**: p. 72-80.
58. Chatterjee, A., *Sponge iron production by direct reduction of iron oxide*. 2010: PHI Learning Pvt. Ltd.
59. Rechberger, K., et al., *Green Hydrogen-Based Direct Reduction for Low-Carbon Steelmaking.* steel research international, 2020(91): p. 2000110.
60. Chevrier, V., *Transitioning to the Hydrogen Economy.* Direct from MIDREX, 2021. **Q1**.
61. Anameric, B. and S.K. Kawatra, *Properties and features of direct reduced iron.* Mineral processing and extractive metallurgy review, 2007. **28**(1): p. 59-116.
62. J.A. Lepinski, J.C.M., Gordon H. Geiger, *Iron*, in *Kirk-Othmer Encyclopedia of Chemical Technology*. 2005.
63. Hunter, R. and C. Ravenscroft, *Is too much carbon a problem.* Direct from Midrex, 2014: p. 4-8.
64. Müller, N., et al., *Assessment of fossil-free steelmaking based on direct reduction applying high-temperature electrolysis.* Cleaner Engineering and Technology, 2021. **4**: p. 100158.
65. Hornby, S., et al., *Myths and Realities of Charging DRI/HBI in Electric Arc Furnaces.* Iron & Steel Technology, 2016.
66. Kim, G., Y. Kacar, and P.C. Pistorius, *Carbon Bonding State Has a Small Effect on Melting of Direct-Reduced Iron.* Metallurgical and Materials Transactions B, 2019. **50**(6): p. 2508-2516.
67. Morris, A.E., *Iron Resources and Direct Iron Production*, in *Encyclopedia of Materials: Science and Technology*, K.H.J. Buschow, et al., Editors. 2001, Elsevier: Oxford. p. 4302-4310.
68. Memoli, F., *Behavior and benefits of high-Fe_3C DRI in the EAF*. Vol. 2. 2015. 1928-1945.
69. Brooks, S.H.G., *Impact of Hydrogen DRI on EAF Steelmaking* Direct from MIDREX, 2021. **Q2**.
70. Duarte, P. and D. Pauluzzi, *Premium Quality DRI Products from ENERGIRON*. 2019, Tech. rep. Energiron.
71. Chevrier, V. and C. Ravenscroft, *Direct reduced ironmaking technology: hot briquetting trials of DRI with higher carbon levels.* Midrex Technol Incorporation, Charlotte, 2018.
72. Luz, A.P., et al., *Slag foaming practice in the steelmaking process.* Ceramics International, 2018. **44**(8): p. 8727-8741.
73. Odenthal, H.J., et al., *Review on modeling and simulation of the electric arc furnace (EAF).* steel research international, 2018. **89**(1): p. 1700098.
74. Echterhof, T., *Review on the Use of Alternative Carbon Sources in EAF Steelmaking.* Metals, 2021. **11**(2): p. 222.
75. Sichen, D., et al., *The Laboratory Study of Metallurgical Slags and the Reality.* steel research international. **n/a**(n/a): p. 2100132.
76. *HOTLINK® SYSTEM: BENEFITS OF CHARGING HOT DRI (HDRI)*. 2021, Midrex Technologies.
77. Lungen, H., K. Mulheims, and R. Steffen, *State of the art of direct reduction and smelting reduction of iron ores.* Stahl und Eisen(Germany), 2001. **121**(5): p. 35-47.
78. Atsushi, M., H. Uemura, and T. Sakaguchi, *MIDREX processes.* 2010.
79. Sane, A., et al., *Enhancing Direct Reduced Iron (DRI) for Use in Electric Steelmaking*. 2020, Air Products and Chemicals, Inc., Allentown, PA, USA.
80. *The MIDREX® Process - The world's most reliable and productive Direct Reduction Technology*. 2018, Midrex Technologies.
81. Pousette, H., *Investigation into Melting Characteristics of Hydrogen-Reduced Iron Ore Pellets*. 2019.
82. Kim, G. and P.C. Pistorius, *Strength of Direct Reduced Iron Following Gas-Based Reduction and Carburization.* Metallurgical and Materials Transactions B, 2020. **51**(6): p. 2628-2641.
83. Monsen, B.E., et al. *Characterization of DR Pellets for DRI Applications*. in *Proceedings of the Association for Iron and Steel Technology Conference Proceedings*. 2015.

84. Kirschen, M., T. Hay, and T. Echterhof, *Process Improvements for Direct Reduced Iron Melting in the Electric Arc Furnace with Emphasis on Slag Operation.* Processes, 2021. **9**(2): p. 402.
85. Pauluzzi, D. and A. Martinis, *Sustainable decrease of CO2 emissions in the steelmaking industry by means of the Energiron direct reduction technology.* AISTech 2018, 2018.
86. Formanek, L., et al., *Iron, 3. Direct Reduction Processes*, in *Ullmann's Encyclopedia of Industrial Chemistry*. 2019. p. 1-21.
87. Dutta, S.K. and R. Sah, *Direct Reduced Iron: Production.* Encyclopedia of Iron, Steel, and Their Alloys; Colás, R., Totten, GE, Eds, 2016: p. 1082-1108.
88. *MIDREX Plants*. 2021 [cited 2021 1/12]; Available from: https://www.midrex.com/about/midrex-plants/.
89. De Santis, M., et al., *Green Steel for Europe: Investment Needs.* 2021.
90. Béchara, R., et al., *Optimization of the iron ore direct reduction process through multiscale process modeling.* Materials, 2018. **11**(7): p. 1094.
91. Pissot, S., et al., *Production of Negative-Emissions Steel Using a Reducing Gas Derived from DFB Gasification.* Energies, 2021. **14**(16): p. 4835.
92. Parisi, D.R. and M.A. Laborde, *Modeling of counter current moving bed gas-solid reactor used in direct reduction of iron ore.* Chemical Engineering Journal, 2004. **104**(1-3): p. 35-43.
93. Cano, J.A.M., F. Wendling, and G.M. Peixoto, *Sulfur in iron ore pellets and its liberation in the Midrex direct reduction process.* Mining, Metallurgy & Exploration, 1990. **7**(3): p. 141-143.
94. Lu, L., J. Pan, and D. Zhu, *Quality requirements of iron ore for iron production*, in *Iron Ore*. 2015, Elsevier. p. 475-504.
95. Morales, R.G. and M. Prenzel. *Flexible and Reliable direct reduction plants the key for economic DRI/HBI production*. in *XXXII ABM Ironmaking Seminar*. 2002.
96. *Energy use in the Steel Industry*. 2014, World Steel Association.
97. *ENERGIRON: DRI Technology by Tenova and Danieli*. 2021 [cited 2021 1/12]; Available from: https://www.energiron.com/.
98. *HYL/ENERGIRON PROJECTS REFERENCE LIST*. 2021 [cited 2021 27/1]; Available from: https://www.google.com/url?sa=t&rct=j&q=&esrc=s&source=web&cd=&ved=2ahUKEwjqvZy60dH1AhUcQ_EDHSi2AaEQFnoECAQQAQ&url=https%3A%2F%2Fwww.energiron.com%2Fwp-content%2Fuploads%2F2020%2F12%2FENERGIRON-REFERENCE-LIST-1.pdf&usg=AOvVaw06CXhx0l_fy9lqCyzc8wzo.
99. Duarte, P.E., A. Tavano, and E. Zendejas. *Achieving carbon-free emissions via the ENERGIRON DR process*. in *AISTech 2010 Conference Proceedings. Pittsburgh: American Iron and Steel Society*. 2010.
100. Martinez, P.D.J., *By-products and emissions in an Energiron DR plant.* HYL News, 2015.
101. *Tenova HYL Continues Emphasis on Environmental Iron & Steel Making with Energiron Technology*. 2007, Tenova HYL.
102. Zugliano, A., et al., *Online modelling of energiron direct reduction shaft furnaces.* IFAC Proceedings Volumes, 2013. **46**(16): p. 346-351.
103. Liu, W., et al., *The production and application of hydrogen in steel industry.* International Journal of Hydrogen Energy, 2021.
104. Duarte, P., *Effect of high Pressure in the design of ENERGIRON DR Plants*, in *3rd World DRI & Pellet Congress*. 2015: Abu Dhabi.
105. Muscolino, F., et al., *Introduction to direct reduction technology and outlook for its use.* Metallurgia Italiana, 2016. **4**: p. 25-31.
106. Bui, M., et al., *Carbon capture and storage (CCS): the way forward.* Energy & Environmental Science, 2018. **11**(5): p. 1062-1176.
107. Marchetti, C., *On geoengineering and the CO_2 problem.* Climatic change, 1977. **1**(1): p. 59-68.
108. Hansson, A., *Kolets återkomst: Koldioxidavskiljning och lagring i vetenskap och politik*. 2008, Linköping University Electronic Press.
109. Loria, P. and M.B. Bright, *Lessons captured from 50 years of CCS projects.* The Electricity Journal, 2021. **34**(7): p. 106998.
110. Reiner, D., et al., *Carbon Capture and Storage*. 2019, Cambridge, UNITED KINGDOM: Royal Society of Chemistry.
111. Jacobasch, E., et al., *Economic evaluation of low-carbon steelmaking via coupling of electrolysis and direct reduction.* Journal of Cleaner Production, 2021: p. 129502.
112. Martin-Roberts, E., et al., *Carbon capture and storage at the end of a lost decade.* One Earth, 2021.
113. Eurofer, *Low carbon roadmap: Pathways to a CO2-neutral European steel industry*. 2019.
114. Grant, N., et al., *Cost reductions in renewables can substantially erode the value of carbon capture and storage in mitigation pathways.* One Earth, 2021. **4**(11): p. 1588-1601.
115. Van Der Stel, J., et al., *ULCOS top gas recycling blast furnace process (ULCOS TGRBF).* Research fund for coal and steel (EC), EUR, 2014. **26414**.
116. Danloy, G., et al., *ULCOS-Pilot testing of the low-CO2 Blast Furnace process at the experimental BF in Luleå.* Metallurgical Research & Technology, 2009. **106**(1): p. 1-8.
117. Fischedick, M., et al., *Techno-economic evaluation of innovative steel production technologies.* Journal of Cleaner Production, 2014. **84**: p. 563-580.
118. Birat, J.P., *16 - Carbon dioxide (CO_2) capture and storage technology in the iron and steel industry*, in *Developments and Innovation in Carbon Dioxide (CO_2) Capture and Storage Technology*, M.M. Maroto-Valer, Editor. 2010, Woodhead Publishing. p. 492-521.
119. Leeson, D., et al., *A Techno-economic analysis and systematic review of carbon capture and storage (CCS) applied to the iron and steel, cement, oil refining and pulp and paper industries, as well as other high purity sources.* International Journal of Greenhouse Gas Control, 2017. **61**: p. 71-84.
120. Wörtler, M., et al., *Steel's contribution to a low-carbon Europe 2050: Technical and economic analysis of the sector's CO_2 abatement potential.* London: BCG. Retrieved April, 2013. **20**: p. 2015.
121. Bataille, C., L.J. Nilsson, and F. Jotzo, *Industry in a net-zero emissions world: New mitigation pathways, new supply chains, modelling needs and policy implications.* Energy and Climate Change, 2021. **2**: p. 100059.

122. Dorndorf, M., *GrInHy 2.0 - Another step towards hydrogen based steelmaking.* 2020.
123. Liu, H., C. Consoli, and A. Zapantis. *Overview of Carbon Capture and Storage (CCS) facilities globally*. in *14th Greenhouse Gas Control Technologies Conference Melbourne*. 2018.
124. *CCS facilities database*. 2019, Global CCS Institute.
125. *Fact sheet: Carbon capture and storage (CCS)*. 2021, World Steel Association.
126. Jaramillo, P., W.M. Griffin, and S.T. McCoy, *Life cycle inventory of CO_2 in an enhanced oil recovery system*. 2009, ACS Publications.
127. Babich, A. and D. Senk, *Biomass use in the steel industry: back to the future.* stahl und eisen, 2013. **133**(5): p. 57-67.
128. Smil, V., *Still the iron age: iron and steel in the modern world*. 2016: Butterworth-Heinemann.
129. Mandova, H., et al., *Global assessment of biomass suitability for ironmaking–Opportunities for co-location of sustainable biomass, iron and steel production and supportive policies.* Sustainable Energy Technologies and Assessments, 2018. **27**: p. 23-39.
130. Angelstam, P., et al., *Knowledge production and learning for sustainable forest management on the ground: Pan-European landscapes as a time machine.* Forestry: An International Journal of Forest Research, 2011. **84**(5): p. 581-596.
131. Nwachukwu, C.M., C. Wang, and E. Wetterlund, *Exploring the role of forest biomass in abating fossil CO_2 emissions in the iron and steel industry–The case of Sweden.* Applied Energy, 2021. **288**: p. 116558.
132. Norgate, T., et al., *Biomass as a source of renewable carbon for iron and steelmaking.* ISIJ international, 2012. **52**(8): p. 1472-1481.
133. Hanrot, F., et al., *Short term CO_2 mitigation for steelmaking (SHOCOM).* European Commission, Luxembourg, 2011. **108**(10.2777): p. 8592.
134. Tanzer, S.E., K. Blok, and A. Ramírez, *Can bioenergy with carbon capture and storage result in carbon negative steel?* International Journal of Greenhouse Gas Control, 2020. **100**: p. 103104.
135. Mandova, H., et al., *Possibilities for CO2 emission reduction using biomass in European integrated steel plants.* Biomass and Bioenergy, 2018. **115**: p. 231-243.
136. Grip, C.-E., et al. *Forestry meets steel: a technoeconomic study of the possible DRI production using biomass*. in *European Steel Technology and Application Days: METEC 16/06/2015-19/06/2015*. 2015.
137. Nwachukwu, C.M., *Utilising forest biomass in iron and steel production: investigating supply chain and competition aspects*. 2021, Luleå University of Technology.
138. Lösch, O., et al., *Bewertung der Direktreduktion von Eisenerz mittels Elektrolyse-Wasserstoff*. 2020, IREES GmbH.
139. Wiencke, J., et al., *Electrolysis of iron in a molten oxide electrolyte.* Journal of Applied Electrochemistry, 2018. **48**(1): p. 115-126.
140. Paramore, J.D., *Candidate anode materials for iron production by molten oxide electrolysis*. 2010, Massachusetts Institute of Technology.
141. Thonstad, J., et al., *Aluminium Electrolysis: Fundamentals of the Hall-Herault Process.* 2001.
142. Judge, W.D. and G. Azimi. *Thermodynamic and Kinetic Modelling of Molten Oxide Electrolysis Cells*. in *TMS 2020 149th Annual Meeting & Exhibition Supplemental Proceedings*. 2020. Springer.
143. Allanore, A., *Electrochemical engineering for commodity metals extraction.* The Electrochemical Society Interface, 2017. **26**(2): p. 63.
144. Witte, K., *Social acceptance of carbon capture and storage (CCS) from industrial applications.* Sustainability, 2021. **13**(21): p. 12278.
145. NIST, *Standard Reference Database 69: NIST Chemistry WebBook*. 2010, National Institute of Standards and Technology.
146. Andersson, J., A. Krüger, and S. Grönkvist, *Methanol as a carrier of hydrogen and carbon in fossil-free production of direct reduced iron.* Energy Conversion and Management: X, 2020. **7**: p. 100051.
147. March, L., *Introduction to pinch technology.* Targeting House, Gadbrook Park, Northwich, Cheshire, CW9 7UZ, England, 1998.
148. Nordpool, *Historical Market Data*. 2022.
149. Parkinson, B., et al., *Hydrogen production using methane: Techno-economics of decarbonizing fuels and chemicals.* International Journal of Hydrogen Energy, 2018. **43**(5): p. 2540-2555.
150. Holladay, J.D., et al., *An overview of hydrogen production technologies.* Catalysis today, 2009. **139**(4): p. 244-260.
151. IEA, *Global Hydrogen Review 2021*, IEA, Editor. 2021, IEA: Paris.
152. *Nel ASA: Receives 4.5 MW electrolyzer purchase order for fossil free steel production*. 2019, Nel ASA.
153. Nuber, D., H. Eichberger, and B. Rollinger, *Circored fine ore direct reduction.* Millen. Steel, 2006. **2006**: p. 37-40.
154. H. Loch, C.D., Arnoud; T. Pich, Michael ;, *Chapter 2: The Limits of Established PRM: The Circored Project*, in *Managing the Unknown: A New Approach to Managing High Uncertainty and Risk in Projects*. 2006.
155. Hölling, M. and S. Gellert, *Direct Reduction: Transition from Natural Gas to Hydrogen?* 2018.
156. Manocha, S. and F. Ponchon, *Management of Lime in Steel.* Metals, 2018. **8**(9): p. 686.
157. Echterhof, T. and H. Pfeifer. *Study on biochar usage in the electric arc furnace*. in *2nd International Conference Clean Technologies in the Steel Industry*. 2014.
158. Robinson, R., et al., *An Empirical Comparative Study of Renewable Biochar and Fossil Carbon as Carburizer in Steelmaking.* ISIJ International, 2020: p. ISIJINT-2020-135.
159. Kirschen, M., K. Badr, and H. Pfeifer, *Influence of direct reduced iron on the energy balance of the electric arc furnace in steel industry.* Energy, 2011. **36**(10): p. 6146-6155.
160. Kirschen, M., V. Risonarta, and H. Pfeifer, *Energy efficiency and the influence of gas burners to the energy related carbon dioxide emissions of electric arc furnaces in steel industry.* Energy, 2009. **34**(9): p. 1065-1072.
161. Patisson, F. and O. Mirgaux, *Hydrogen Ironmaking: How it Works.* Metals, 2020. **10**(7): p. 922.
162. Hall, W.M., Robert; Rothberger, Johannes; Singh, Amar; K Shah, Chirag, *Green Steel through Hydrogen Direct Reduction: A Study in the Role of Hydrogen in the Indian Iron and Steel Sector*. 2021, TERI, Primetals Technologies, Siemens.
163. Remus, R., et al., *Best available techniques (BAT) reference document for iron and steel production.* Luxembourg: Publications Office of the European Union, 2013: p. 621.

164. Lee, B. and I. Sohn, *Review of innovative energy savings technology for the electric arc furnace.* Jom, 2014. **66**(9): p. 1581-1594.
165. Jiemin, T., M.B. Ferri, and P. Argenta, *EAF technology evolution by continuous charging.* Ironmaking & steelmaking, 2005. **32**(3): p. 191-194.
166. Müller, N., et al., *Assessment of fossil-free steelmaking based on direct reduction applying high-temperature electrolysis.* Cleaner Engineering and Technology, 2021: p. 100158.
167. Kühn, R., *Untersuchungen zum Energieumsatz in einem Gleichstromlichtbogenofen zur Stahlerzeugung*. 2003: Shaker.
168. *Public policy paper: Steel industry co-products*. 2020, World Steel Association.
169. Yang, F., H. Meerman, and A. Faaij, *Harmonized comparison of virgin steel production using biomass with carbon capture and storage for negative emissions.* International Journal of Greenhouse Gas Control, 2021. **112**: p. 103519.
170. *Study on Early Business Cases for H_2 in Energy Storage and More Broadly Power to H_2 Applications*. 2017, Fuel Cells and Hydrogen Joint Undertaking.
171. Hurskainen, M., *Industrial oxygen demand in Finland.* VTT, Jyväskylä, 2017.
172. Finke, C.E., et al., *Economically advantageous pathways for reducing greenhouse gas emissions from industrial hydrogen under common, current economic conditions.* Energy & Environmental Science, 2021. **14**(3): p. 1517-1529.
173. Hannula, I., *Co-production of synthetic fuels and district heat from biomass residues, carbon dioxide and electricity: Performance and cost analysis.* Biomass and Bioenergy, 2015. **74**: p. 26-46.
174. *Standard plants fully-packaged modular solutions*. 2017, Air Liquide. p. 1-16.
175. Kato, T., et al., *Effective utilization of by-product oxygen from electrolysis hydrogen production.* Energy, 2005. **30**(14): p. 2580-2595.
176. Buttler, A. and H. Spliethoff, *Current status of water electrolysis for energy storage, grid balancing and sector coupling via power-to-gas and power-to-liquids: A review.* Renewable and Sustainable Energy Reviews, 2018. **82**: p. 2440-2454.
177. MIDREX, *MIDREX® Direct Reduction Plants: 2020 Operation Summary*, in *Direct from Midrex*. 2021.
178. BloombergNEF, *2H 2021 Hydrogen Market Outlook: China Drives a Gigawatt*. 2021.
179. Taibi, E., et al., *Green Hydrogen Cost Reduction*. 2020, IRENA.
180. Badgett, A., M. Ruth, and B. Pivovar, *Chapter 10 - Economic considerations for hydrogen production with a focus on polymer electrolyte membrane electrolysis*, in *Electrochemical Power Sources: Fundamentals, Systems, and Applications*, T. Smolinka and J. Garche, Editors. 2022, Elsevier. p. 327-364.
181. IRENA. *Green Hydrogen Cost Reduction: Scaling up electrolysers to meet the 1.5 ^{o}C climate goal*. 2020.
182. Hans van't Noordende, P.R., *Baseline design and total installed costs of a GW green hydrogen plant*. 2020, Institute for Sustainable Process Technology (ISPT),.
183. Ikäheimo, J., et al., *Power-to-ammonia in future North European 100 % renewable power and heat system.* International Journal of Hydrogen Energy, 2018. **43**(36): p. 17295-17308.
184. Böhm, H., et al., *Projecting cost development for future large-scale power-to-gas implementations by scaling effects.* Applied Energy, 2020. **264**: p. 114780.
185. Proost, J., *Critical assessment of the production scale required for fossil parity of green electrolytic hydrogen.* International Journal of Hydrogen Energy, 2020.
186. van 't Noordende, H. and P. Ripson, *A One-GigaWatt Green-Hydrogen Plant: Advanced Design and Total Installed-Capital Costs*. 2022, Institute for Sustainable Process Technology (ISPT).
187. Rizwan, M., V. Alstad, and J. Jäschke, *Design considerations for industrial water electrolyzer plants.* International Journal of Hydrogen Energy, 2021. **46**(75): p. 37120-37136.
188. Nguyen, T., et al., *Grid-connected hydrogen production via large-scale water electrolysis.* Energy Conversion and Management, 2019. **200**: p. 112108.
189. IEA, *The Future of Hydrogen*. 2019.
190. BloombergNEF, *Hydrogen Economy Outlook: Key messages*. 2020.
191. Hauch, A., et al., *Recent advances in solid oxide cell technology for electrolysis.* Science, 2020. **370**(6513).
192. Wang, A., et al., *Analysing Future Demand, Supply, and Transport of Hydrogen*. 2021, Guidehouse.
193. Tenhumberg, N. and K. Büker, *Ecological and Economic Evaluation of Hydrogen Production by Different Water Electrolysis Technologies.* Chemie Ingenieur Technik, 2020.
194. Lazard, *Lazard's Levelized Cost of Hydrogen Analysis – Version 2.0*. 2021.
195. Suermann, M., et al., *Electrochemical Hydrogen Compression: Efficient Pressurization Concept Derived from an Energetic Evaluation.* Journal of The Electrochemical Society, 2017. **164**(12): p. F1187-F1195.
196. Hamilton, R.T. and D. McLarty. *A System Analysis of Pressurized Electrolysis for Compressed Hydrogen Production*. in *Energy Sustainability*. 2019. American Society of Mechanical Engineers.
197. Rivera-Tinoco, R., et al., *Investigation of power-to-methanol processes coupling electrolytic hydrogen production and catalytic CO2 reduction.* International journal of hydrogen energy, 2016. **41**(8): p. 4546-4559.
198. Zheng, Y., et al., *Optimal day-ahead dispatch of an alkaline electrolyser system concerning thermal–electric properties and state-transitional dynamics.* Applied Energy, 2021: p. 118091.
199. Schulte Beerbühl, S., M. Fröhling, and F. Schultmann, *Combined scheduling and capacity planning of electricity-based ammonia production to integrate renewable energies.* European Journal of Operational Research, 2015. **241**(3): p. 851-862.
200. Krishnan, S., et al., *Chapter 10 - Power to gas (H_2): alkaline electrolysis*, in *Technological Learning in the Transition to a Low-Carbon Energy System*, M. Junginger and A. Louwen, Editors. 2020, Academic Press. p. 165-187.
201. Häussinger, P., R. Lohmüller, and A.M. Watson, *Hydrogen, 2. Production*, in *Ullmann's Encyclopedia of Industrial Chemistry*.
202. Ali Habib, M.O., *Egypt's Low Carbon Hydrogen Development Prospects* 2021, The Oxford Institute for Energy Studies (OIES).
203. Choksi, A., A. Meeraus, and A. Stoutjesdijk, *The planning of investment programs. v. 2: The planning of investment programs in the fertilizer industry:[methodology and its application to the Egyptian fertilizer sector].* World Bank Research Publication (IBRD). 1980.

204. Brauns, J. and T. Turek, *Alkaline water electrolysis powered by renewable energy: A review.* Processes, 2020. **8**(2): p. 248.
205. Grubb, W.T. and L.W. Niedrach, *Batteries with Solid Ion-Exchange Membrane Electrolytes.* Journal of The Electrochemical Society, 1960. **107**(2): p. 131.
206. Ayers, K., *The potential of proton exchange membrane–based electrolysis technology.* Current Opinion in Electrochemistry, 2019. **18**: p. 9-15.
207. Smolinka, T., et al., *Chapter 4 - The history of water electrolysis from its beginnings to the present*, in *Electrochemical Power Sources: Fundamentals, Systems, and Applications*, T. Smolinka and J. Garche, Editors. 2022, Elsevier. p. 83-164.
208. Grot, W., *Perfluorierte Ionenaustauscher-Membrane von hoher chemischer und thermischer Stabilität.* Chemie Ingenieur Technik, 1972. **44**(4): p. 167-169.
209. Carmo, M., et al., *A comprehensive review on PEM water electrolysis.* International Journal of Hydrogen Energy, 2013. **38**(12): p. 4901-4934.
210. Ayers, K., *High efficiency PEM water electrolysis: Enabled by advanced catalysts, membranes, and processes.* Current Opinion in Chemical Engineering, 2021. **33**: p. 100719.
211. *Fueling the Transition: Accelerating Cost-Competitive Green Hydrogen*. 2021, RMI, Green Hydrogen Catapult.
212. Isenberg, A., *Energy conversion via solid oxide electrolyte electrochemical cells at high temperatures.* Solid State Ionics, 1981. **3**: p. 431-437.
213. Elikan, L., J. Morris, and C. Wu, *Development of a solid electrolyte carbon dioxide and water reduction system for oxygen recovery.* 1972.
214. Posdziech, O., K. Schwarze, and J. Brabandt, *Efficient hydrogen production for industry and electricity storage via high-temperature electrolysis.* International Journal of Hydrogen Energy, 2019. **44**(35): p. 19089-19101.
215. Frøhlke, U., *Haldor Topsoe to build large-scale SOEC electrolyzer manufacturing facility to meet customer needs for green hydrogen production*. 2021, Haldor Topsoe.
216. Buttler, A., et al., *A detailed techno-economic analysis of heat integration in high temperature electrolysis for efficient hydrogen production.* International journal of hydrogen energy, 2015. **40**(1): p. 38-50.
217. Hansen, J.B., *Solid oxide electrolysis–a key enabling technology for sustainable energy scenarios.* Faraday discussions, 2015. **182**: p. 9-48.
218. Peterson, D. and E. Miller, *Hydrogen Production Cost from Solid Oxide Electrolysis.* Department of Energy-USA, 2016.
219. Küngas, R., et al., *Progress in SOEC Development Activities at Haldor Topsøe.* ECS Transactions, 2019. **91**(1): p. 215-223.
220. Ebbesen, S.D., et al., *High Temperature Electrolysis in Alkaline Cells, Solid Proton Conducting Cells, and Solid Oxide Cells.* Chemical Reviews, 2014. **114**(21): p. 10697-10734.
221. Schäfer, D., et al., *System-supporting operation of solid-oxide electrolysis stacks.* Energies, 2021. **14**(3): p. 544.
222. *SUNFIRE-HYLINK SOEC – Technical Data*. 2021, Sunfire GmbH.
223. *SUNFIRE-SYNLINK SOEC – Technical Data*. 2021, Sunfire GmbH.
224. *SOEC high-temperature electrolysis: the future of green hydrogen production*. 2021, Haldor Topøe A/S.
225. Graves, C., et al., *Sustainable hydrocarbon fuels by recycling CO_2 and H_2O with renewable or nuclear energy.* Renewable and Sustainable Energy Reviews, 2011. **15**(1): p. 1-23.
226. Zheng, Y., et al., *A review of high temperature co-electrolysis of H_2O and CO_2 to produce sustainable fuels using solid oxide electrolysis cells (SOECs): advanced materials and technology.* Chemical Society Reviews, 2017. **46**(5): p. 1427-1463.
227. Sala, E.M., et al., *Current understanding of ceria surfaces for CO_2 reduction in SOECs and future prospects–A review.* Solid State Ionics, 2022. **375**: p. 115833.
228. Krüger, A., et al., *Integration of water electrolysis for fossil-free steel production.* International journal of hydrogen energy, 2020. **45**(55): p. 29966-29977.
229. Böhm, H., et al., *Power-to-hydrogen & district heating: Technology-based and infrastructure-oriented analysis of (future) sector coupling potentials.* International Journal of Hydrogen Energy, 2021. **46**(63): p. 31938-31951.
230. Karjunen, H., E. Inkeri, and T. Tynjälä, *Mapping Bio-CO_2 and Wind Resources for Decarbonized Steel, E-Methanol and District Heat Production in the Bothnian Bay.* Energies, 2021. **14**(24): p. 8518.
231. Linda, D.P.-M., Bondesson; Håkan, Sköldberg; Johan, Holm; Magnus, Brolin; Sofia, Nyström; Rebecca, Samuelsson, *Sektorkoppling för ett mer effektivt energisystem: Förstudie gas tillsammans med el och fjärrvärme*. 2021, Energiforsk.
232. Patronen, J., E. Kaura, and C. Torvestad, *Nordic heating and cooling: Nordic approach to EU's Heating and Cooling Strategy*. 2017: Nordic Council of Ministers.
233. Cárdenas, J., A. Conejo, and G. Gnechi, *Optimization of energy consumption in electric arc furnaces operated with 100% DRI*.
234. Vogl, V., M. Åhman, and L.J. Nilsson, *Assessment of hydrogen direct reduction for fossil-free steelmaking.* Journal of cleaner production, 2018. **203**: p. 736-745.
235. Sikström, P., *ULCORED Direct Reduction Concept for ULCOS: a brief introduction* 2013, LKAB.
236. Zugliano, A., et al., *CFD Study of an Energiron Reactor Fed With Different Concentrations of Hydrogen.* AISTech2020 Proceedings of the Iron and Steel Technology Conference, 2020.
237. Xu, C., et al. *Effect of H_2/CO Ratio on Gas Consumption and Energy Utilization Rate of Gas-Based Direct Reduction Process*. in *10th International Symposium on High-Temperature Metallurgical Processing*. 2019. Springer.
238. Wu, J., S.-Q. Guo, and W.-Z. Ding, *Investigation on the application of reformed coke oven gas in direct reduction iron production with a mathematical model.* Advances in Manufacturing, 2013. **1**(3): p. 276-283.
239. Dalle Nogare, D., et al., *Multiphysics simulation of a DRP shaft furnace.* gas, 2013. **7**: p. 2.
240. Shams, A. and F. Moazeni, *Modeling and simulation of the MIDREX shaft furnace: reduction, transition and cooling Zones.* JOM, 2015. **67**(11): p. 2681-2689.
241. Sarkar, S., et al., *Modeling MIDREX based process configurations for energy and emission analysis.* steel research international, 2018. **89**(2): p. 1700248.

242. Bhaskar, A., et al., *Decarbonization of the Iron and Steel Industry with Direct Reduction of Iron Ore with Green Hydrogen.* Energies, 2020. **13**(3): p. 758.
243. Toktarova, A., et al., *Pathways for low-carbon transition of the steel industry—a Swedish case study.* Energies, 2020. **13**(15): p. 3840.
244. Yadav, D., A. Guhan, and T. Biswas, *Greening Steel: Moving to Clean Steelmaking Using Hydrogen and Renewable Energy*. 2021, Council on Energy, Environment and Water (CEEW); : New Delhi.
245. Vogl, V., O. Olsson, and B. Nykvist, *Phasing out the blast furnace to meet global climate targets.* Joule, 2021. **5**(10): p. 2646-2662.
246. Hübner, T., et al., *European Steel with Hydrogen*. 2020.
247. Werner, S., *European district heating price series*. 2016, Energiforsk.
248. Barecka, M.H., J.W. Ager, and A.A. Lapkin, *Carbon neutral manufacturing via on-site CO_2 recycling.* Iscience, 2021. **24**(6): p. 102514.
249. Skafte, T.L., et al., *Carbon deposition and sulfur poisoning during CO_2 electrolysis in nickel-based solid oxide cell electrodes.* Journal of Power Sources, 2018. **373**: p. 54-60.
250. Cheah, S., D.L. Carpenter, and K.A. Magrini-Bair, *Review of mid-to high-temperature sulfur sorbents for desulfurization of biomass-and coal-derived syngas.* Energy & Fuels, 2009. **23**(11): p. 5291-5307.
251. Simon, K.A., Redenius; Ralph, Schaper, *Method and device for operating a direct reduction reactor for the production of directly reduced iron from iron ore*. 2016, Salzgitter Flachstahl GmbH Germany.
252. Matthias, J.G., Herz; Aniko, Walther; Erik, Reichelt;Nils, Müller, *Process for producing sponge iron, in particular in a direct reduction process*. 2018, Fraunhofer Gesellschaft zur Forderung der Angewandten Forschung eV.
253. Rezaei, E. and S. Dzuryk, *Techno-economic comparison of reverse water gas shift reaction to steam and dry methane reforming reactions for syngas production.* Chemical engineering research and design, 2019. **144**: p. 354-369.
254. Daza, Y.A. and J.N. Kuhn, *CO_2 conversion by reverse water gas shift catalysis: comparison of catalysts, mechanisms and their consequences for CO_2 conversion to liquid fuels.* RSC advances, 2016. **6**(55): p. 49675-49691.
255. Kaiser, P., et al., *Production of liquid hydrocarbons with CO_2 as carbon source based on reverse water-gas shift and Fischer-Tropsch synthesis.* Chemie Ingenieur Technik, 2013. **85**(4): p. 489-499.
256. Wolf, A., A. Jess, and C. Kern, *Syngas Production via Reverse Water-Gas Shift Reaction over a Ni-Al_2O_3 Catalyst: Catalyst Stability, Reaction Kinetics, and Modeling.* Chemical Engineering & Technology, 2016. **39**(6): p. 1040-1048.
257. Joo, O.-S., et al., *Carbon dioxide hydrogenation to form methanol via a reverse-water-gas-shift reaction (the CAMERE process).* Industrial & engineering chemistry research, 1999. **38**(5): p. 1808-1812.
258. Thor Wismann, S., K.-E. Larsen, and P. Mølgaard Mortensen, *Electrical Reverse Shift: Sustainable CO_2 Valorization for Industrial Scale.* Angewandte Chemie International Edition. **61**(8): p. e202109696.
259. Yi, L.-y., et al., *Action rules of H_2 and CO in gas-based direct reduction of iron ore pellets.* Journal of Central South University, 2012. **19**(8): p. 2291-2296.
260. Duarte, P., *Trends in H_2-based steelmaking.* Steel Times International, 2019. **43**(1): p. 27-32.
261. Chevrier, V., *MIDREX H2 and the transition to the hydrogen economy*, in *Hydrogen and low-CO_2 iron and steelmaking webinar*. 2020, AIST - DRI Technology Committee.
262. Nezamoddini, N. and Y. Wang, *Real-time electricity pricing for industrial customers: Survey and case studies in the United States.* Applied Energy, 2017. **195**: p. 1023-1037.
263. Toktarova, A., et al., *Interaction between electrified steel production and the north European electricity system.* Applied Energy, 2022. **310**: p. 118584.
264. Pimm, A.J., T.T. Cockerill, and W.F. Gale, *Energy system requirements of fossil-free steelmaking using hydrogen direct reduction.* Journal of Cleaner Production, 2021: p. 127665.
265. Ziel, F. and R. Steinert, *Probabilistic mid- and long-term electricity price forecasting.* Renewable and Sustainable Energy Reviews, 2018. **94**: p. 251-266.
266. Andersson, J., *Application of Liquid Hydrogen Carriers in Hydrogen Steelmaking.* Energies, 2021. **14**(5): p. 1392.
267. Rehnholm, T., *HYBRIT – System integration and flexibility*. 2021, Vattenfall AB.
268. Foh, S., et al., *Underground hydrogen storage. final report.[salt caverns, excavated caverns, aquifers and depleted fields]*. 1979, Brookhaven National Lab., Upton, NY (USA).
269. Bond, D.C., *Underground storage of natural gas.* Illinois petroleum no. 104, 1975.
270. Crotogino, F., *Larger Scale Hydrogen Storage*, in *Storing Energy*. 2016, Elsevier. p. 411-429.
271. Jan Cihlar, D.M., Kees van der Leun, *Picturing the value of underground gas storage to the European hydrogen system*, G.I.E. Guidehouse, Editor. 2021.
272. Hajibeygi, H., *Underground Hydrogen Storage: A Multiscale Experimental and Numerical Study*. 2021, MIT Earth Resources Laboratory.
273. Heinemann, N., et al., *Enabling large-scale hydrogen storage in porous media–the scientific challenges.* Energy & Environmental Science, 2021. **14**(2): p. 853-864.
274. Heinemann, N., et al., *Hydrogen storage in porous geological formations – onshore play opportunities in the midland valley (Scotland, UK).* International Journal of Hydrogen Energy, 2018. **43**(45): p. 20861-20874.
275. Lord, A.S., *Overview of geologic storage of natural gas with an emphasis on assessing the feasibility of storing hydrogen.* SAND2009-5878, Sandia Natl. Lab. Albuquerque, NM, 2009.
276. Le Fevre, C.N., *Gas storage in Great Britain*. 2013: Oxford institute for energy studies.
277. US Energy Information Administration, *Underground Natural Gas Storage Capacity*. 2021.
278. Lankof, L. and R. Tarkowski, *Assessment of the potential for underground hydrogen storage in bedded salt formation.* International Journal of Hydrogen Energy, 2020. **45**(38): p. 19479-19492.
279. Grgic, D., et al., *Evolution of Gas Permeability of Rock Salt Under Different Loading Conditions and Implications on the Underground Hydrogen Storage in Salt Caverns.* Rock Mechanics and Rock Engineering, 2021.
280. Torquet, H.J.M., *Conceptual design of salt cavern and porous media underground storage site*. 2021, Hydrogen Storage in European Subsurfaces (hystories).
281. Liu, X., et al., *Maximum gas production rate for salt cavern gas storages.* Energy, 2021. **234**: p. 121211.

282. Lux, K.-H., *Design of salt caverns for the storage of natural gas, crude oil and compressed air: geomechanical aspects of construction, operation and abandonment.* Geological Society, London, Special Publications, 2009. **313**(1): p. 93-128.
283. Wallace, R.L., et al., *Utility-scale subsurface hydrogen storage: UK perspectives and technology.* International Journal of Hydrogen Energy, 2021. **46**(49): p. 25137-25159.
284. Sadler, D., et al., *H21 North of England*. 2018, Report, Northern Gas Networks, Leeds.
285. Schlichtenmayer, M. and M. Klafki. *Differences and challenges in salt cavern design for hydrogen, air and natural gas storage*. in *Energy Geotechnics: Proceedings of the 1st International Conference on Energy Geotechnics, ICEGT 2016, Kiel, Germany, 29-31 August 2016*. 2016. CRC Press.
286. Laban, M.P., *Hydrogen Storage in Salt Caverns: Chemical modelling and analysis of large-scale hydrogen storage in underground salt caverns.* 2020.
287. Bérest, P., *Heat transfer in salt caverns.* International Journal of Rock Mechanics and Mining Sciences, 2019. **120**: p. 82-95.
288. Crotogino, F., K.-U. Mohmeyer, and R. Scharf. *Huntorf CAES: More than 20 years of successful operation*. in *SMRI Spring meeting*. 2001.
289. Tengborg, P., J. Johansson, and G. Durup. *Storage of highly compressed gases in underground lined rock caverns–more than 10 years of experience*. in *Proceedings of the World Tunnel Congress 2014–tunnels for a better Life*. 2014.
290. Caglayan, D.G., et al., *Technical potential of salt caverns for hydrogen storage in Europe.* International Journal of Hydrogen Energy, 2020. **45**(11): p. 6793-6805.
291. Muhammed, N.S., et al., *A review on underground hydrogen storage: Insight into geological sites, influencing factors and future outlook.* Energy Reports, 2022. **8**: p. 461-499.
292. Wang, G., et al., *Scaling analysis of hydrogen flow with carbon dioxide cushion gas in subsurface heterogeneous porous media.* International Journal of Hydrogen Energy, 2022. **47**(3): p. 1752-1764.
293. Gabrielli, P., et al., *Seasonal energy storage for zero-emissions multi-energy systems via underground hydrogen storage.* Renewable and Sustainable Energy Reviews, 2020. **121**: p. 109629.
294. Crotogino, F., G.-S. Schneider, and D.J. Evans, *Renewable energy storage in geological formations.* Proceedings of the Institution of Mechanical Engineers, Part A: Journal of Power and Energy, 2018. **232**(1): p. 100-114.
295. Portarapillo, M. and A. Di Benedetto, *Risk Assessment of the Large-Scale Hydrogen Storage in Salt Caverns.* Energies, 2021. **14**(10): p. 2856.
296. Dopffel, N., S. Jansen, and J. Gerritse, *Microbial side effects of underground hydrogen storage–Knowledge gaps, risks and opportunities for successful implementation.* International Journal of Hydrogen Energy, 2021.
297. Michalski, J., et al., *Hydrogen generation by electrolysis and storage in salt caverns: Potentials, economics and systems aspects with regard to the German energy transition.* International Journal of Hydrogen Energy, 2017. **42**(19): p. 13427-13443.
298. Siddiqui, R.A. and H.A. Abdullah, *Hydrogen embrittlement in 0.31% carbon steel used for petrochemical applications.* Journal of Materials Processing Technology, 2005. **170**(1): p. 430-435.
299. Woods, S. and J.A. Lee, *Hydrogen Embrittlement*. 2016, NASA.
300. Khare, A., M. Vishwakarma, and V. Parashar, *A review on failures of industrial components due to hydrogen embrittlement & techniques for damage prevention.* International Journal of Applied Engineering Research, 2017. **12**(8): p. 1784-1792.
301. Reitenbach, V., et al., *Influence of added hydrogen on underground gas storage: a review of key issues.* Environmental Earth Sciences, 2015. **73**(11): p. 6927-6937.
302. *LKAB and Vattenfall building unique pilot project in Luleå for large-scale hydrogen storage investing a quarter of a billion Swedish kronor*. 2021, Hybrit Development AB.
303. Lord, A.S., P.H. Kobos, and D.J. Borns, *Geologic storage of hydrogen: Scaling up to meet city transportation demands.* International Journal of Hydrogen Energy, 2014. **39**(28): p. 15570-15582.
304. Bünger, U., et al., *7 - Large-scale underground storage of hydrogen for the grid integration of renewable energy and other applications*, in *Compendium of Hydrogen Energy*, M. Ball, A. Basile, and T.N. Veziroğlu, Editors. 2016, Woodhead Publishing: Oxford. p. 133-163.
305. Aghahosseini, A. and C. Breyer, *Assessment of geological resource potential for compressed air energy storage in global electricity supply.* Energy conversion and management, 2018. **169**: p. 161-173.
306. Papadias, D.D., J.-K. Peng, and R.K. Ahluwalia, *Hydrogen carriers: Production, transmission, decomposition, and storage.* International Journal of Hydrogen Energy, 2021.
307. Andersson, J. and S. Grönkvist, *Large-scale storage of hydrogen.* International Journal of Hydrogen Energy, 2019. **44**(23): p. 11901-11919.
308. *Hydrogen and Fuel Cell Technologies Office Multi-Year Research, Development, and Demonstration Plan, Section 3.2, Hydrogen Delivery*. 2015, US Department of Energy.
309. Tietze, V. and S. Luhr, *Near-Surface Bulk Storage of Hydrogen*, in *Transition to Renewable Energy Systems*. 2013, Wiley-VCH Verlag GmbH & Co. KGaA. p. 659-690.
310. Tietze, V., S. Luhr, and D. Stolten, *Bulk Storage Vessels for Compressed and Liquid Hydrogen*, in *Hydrogen Science and Engineering : Materials, Processes, Systems and Technology*. 2016, Wiley-VCH Verlag GmbH & Co. KGaA. p. 659-690.
311. Valenti, G., *2 - Hydrogen liquefaction and liquid hydrogen storage A2 - Gupta, Ram B*, in *Compendium of Hydrogen Energy*, A. Basile and T.N. Veziroğlu, Editors. 2016, Woodhead Publishing. p. 27-51.
312. Cardella, U.F., *Large-scale hydrogen liquefaction under the aspect of economic viability*. 2018, Technische Universität München.
313. Stolzenburg, K., et al., *Efficient liquefaction of hydrogen: results of the IDEALHY project.* Energi symposium, Stralsund/Germany, 2013.
314. Cardella, U., L. Decker, and H. Klein, *Roadmap to economically viable hydrogen liquefaction.* International Journal of Hydrogen Energy, 2017. **42**(19): p. 13329-13338.
315. Reuß, M., et al., *Seasonal storage and alternative carriers: A flexible hydrogen supply chain model.* Applied Energy, 2017. **200**(Supplement C): p. 290-302.

316. Connelly, E., et al., *Current Status of Hydrogen Liquefaction Costs.* DOE Hydrogen and Fuel Cells Program Record, 2019.
317. Berstad, D., et al., *Liquid hydrogen as prospective energy carrier: A brief review and discussion of underlying assumptions applied in value chain analysis.* Renewable and Sustainable Energy Reviews, 2022. **154**: p. 111772.
318. Peschka, W., *Thermal Insulation, Storage and Transportation of Liquid Hydrogen*, in *Liquid Hydrogen*, W. Peschka, Editor. 1992, Springer Vienna: Vienna. p. 71-103.
319. Heuser, P.-M., et al., *Techno-economic analysis of a potential energy trading link between Patagonia and Japan based on CO2 free hydrogen.* International Journal of Hydrogen Energy, 2019. **44**(25): p. 12733-12747.
320. Hank, C., et al., *Energy efficiency and economic assessment of imported energy carriers based on renewable electricity.* Sustainable Energy & Fuels, 2020. **4**(5): p. 2256-2273.
321. Ramirez-Vidal, P., et al., *Modeling High-Pressure Hydrogen Uptake by Nanoporous Metal–Organic Frameworks: Implications for Hydrogen Storage and Delivery.* ACS Applied Nano Materials, 2022.
322. Chahine, R. and T.K. Bose, *Low-pressure adsorption storage of hydrogen.* International Journal of Hydrogen Energy, 1994. **19**(2): p. 161-164.
323. Samantaray, S.S., S.T. Putnam, and N.P. Stadie, *Volumetrics of Hydrogen Storage by Physical Adsorption.* Inorganics, 2021. **9**(6).
324. Allendorf, M.D., et al., *An assessment of strategies for the development of solid-state adsorbents for vehicular hydrogen storage.* Energy & Environmental Science, 2018.
325. Adametz, P., K. Muller, and W. Arlt, *Efficiency of low-temperature adsorptive hydrogen storage systems.* International Journal of Hydrogen Energy, 2014. **39**(28): p. 15604-15613.
326. Müller, K., *Technologies for the Storage of Hydrogen Part 1: Hydrogen Storage in the Narrower Sense.* ChemBioEng Reviews, 2019. **6**(3): p. 72-80.
327. Schlichtenmayer, M. and M. Hirscher, *The usable capacity of porous materials for hydrogen storage.* Applied Physics a-Materials Science & Processing, 2016. **122**(4): p. 379.
328. Anastasopoulou, A., et al., *Technoeconomic analysis of metal–organic frameworks for bulk hydrogen transportation.* Energy & Environmental Science, 2021. **14**(3): p. 1083-1094.
329. Cardella, U., et al., *Process optimization for large-scale hydrogen liquefaction.* International Journal of Hydrogen Energy, 2017. **42**(17): p. 12339-12354.
330. Eberle, U., M. Felderhoff, and F. Schuth, *Chemical and physical solutions for hydrogen storage.* Angew Chem Int Ed Engl, 2009. **48**(36): p. 6608-30.
331. Ahluwalia, R.K., J.K. Peng, and T.Q. Hua, *Sorbent material property requirements for on-board hydrogen storage for automotive fuel cell systems.* International Journal of Hydrogen Energy, 2015. **40**(19): p. 6373-6390.
332. Bazzanella, A. and F. Ausfelder, *DECHEMA Low Carbon Energy and Feedstock for the European Chemical Industry.* The European Chemical Industry Council: Brussels, Belgium, 2017.
333. Matzen, M.J., M.H. Alhajji, and Y. Demirel, *Technoeconomics and sustainability of renewable methanol and ammonia productions using wind power-based hydrogen.* 2015.
334. White, S., et al. *Integrated Insulation System for Automotive Cryogenic Storage Tanks*. in *US Dept. of Energy (DOE) Annual Merit Review and Peer Evaluation Meeting (AMR) 2017*. 2017.
335. Grande, C., *PSA Technology for H_2 Separation*, in *Hydrogen Science and Engineering : Materials, Processes, Systems and Technology*. 2016.
336. Broom, D.P., et al., *Concepts for improving hydrogen storage in nanoporous materials.* International Journal of Hydrogen Energy, 2019. **44**(15): p. 7768-7779.
337. DeSantis, D., et al., *Techno-economic Analysis of Metal–Organic Frameworks for Hydrogen and Natural Gas Storage.* Energy & Fuels, 2017. **31**(2): p. 2024-2032.
338. Neves, M.I.S., et al., *MOF industrialization: a complete assessment of production costs.* Faraday Discussions, 2021.
339. Law, K., et al., *US Department of Energy Hydrogen Storage Cost Analysis*. 2013, TIAX LLC.
340. Sandrock, G. and S. Suda, *Applications.–Hydrogen in Intermetallic Compounds. II. Surface and Dynamic Properties, Applications, Ed. by L. Schlapbach*. 1992, Springer-Verlag.
341. Cummings, D.L. and G.J. Powers, *The storage of hydrogen as metal hydrides.* Industrial & Engineering Chemistry Process Design and Development, 1974. **13**(2): p. 182-192.
342. Hirscher, M., et al., *Materials for hydrogen-based energy storage–Past, recent progress and future outlook.* Journal of Alloys and Compounds, 2019: p. 153548.
343. Preuster, P., A. Alekseev, and P. Wasserscheid, *Hydrogen storage technologies for future energy systems.* Annual review of chemical and biomolecular engineering, 2017. **8**: p. 445-471.
344. Ouyang, L., et al., *Magnesium-based hydrogen storage compounds: A review.* Journal of Alloys and Compounds, 2020. **832**: p. 154865.
345. Dornheim, M., et al., *Hydrogen storage in magnesium-based hydrides and hydride composites.* Scripta Materialia, 2007. **56**(10): p. 841-846.
346. Shang, Y., et al., *Mg-based materials for hydrogen storage.* Journal of Magnesium and Alloys, 2021.
347. Shao, H., et al., *Progress and Trends in Magnesium-Based Materials for Energy-Storage Research: A Review.* Energy Technology, 2018. **6**(3): p. 445-458.
348. de Rango, P., P. Marty, and D. Fruchart, *Hydrogen storage systems based on magnesium hydride: from laboratory tests to fuel cell integration.* Applied Physics A, 2016. **122**(2): p. 126.
349. Stampfer, J.F., C.E. Holley, and J.F. Suttle, *The Magnesium-Hydrogen System.* Journal of the American Chemical Society, 1960. **82**(14): p. 3504-3508.
350. Paskevicius, M., D.A. Sheppard, and C.E. Buckley, *Thermodynamic Changes in Mechanochemically Synthesized Magnesium Hydride Nanoparticles.* Journal of the American Chemical Society, 2010. **132**(14): p. 5077-5083.
351. Crema, L., *High energy density Mg-Based metal hydrides storage system (EDEN) Final Report*. 2016, Fondazione Bruno Kessler.
352. Van Vucht, J.H., F. Kuijpers, and H.C. Bruning, *Reversible room-temperature absorption of large quantities of hydrogen by intermetallic compounds.* Philips Res. Rep. 25: 133-40 (Apr 1970). 1970.
353. Reilly, J. and R. Wiswall, *Formation and properties of iron titanium hydride.* Inorganic Chemistry, 1974. **13**(1): p. 218-222.

354. Sandrock, G., *A panoramic overview of hydrogen storage alloys from a gas reaction point of view.* Journal of Alloys and Compounds, 1999. **293**(Supplement C): p. 877-888.
355. Lai, Q., et al., *How to design hydrogen storage materials? Fundamentals, synthesis, and storage tanks.* Advanced Sustainable Systems, 2019. **3**(9): p. 1900043.
356. Harries, D.N., et al., *Concentrating Solar Thermal Heat Storage Using Metal Hydrides.* Proceedings of the Ieee, 2012. **100**(2): p. 539-549.
357. Orimo, S., et al., *Complex hydrides for hydrogen storage.* Chem Rev, 2007. **107**(10): p. 4111-32.
358. Milanese, C., et al., *Complex hydrides for energy storage.* international journal of hydrogen energy, 2019. **44**(15): p. 7860-7874.
359. Møller, K., et al., *Complex Metal Hydrides for Hydrogen, Thermal and Electrochemical Energy Storage.* Energies, 2017. **10**(10).
360. Pistidda, C., *Solid-State Hydrogen Storage for a Decarbonized Society.* Hydrogen, 2021. **2**(4).
361. Bogdanović, B. and M. Schwickardi, *Ti-doped alkali metal aluminium hydrides as potential novel reversible hydrogen storage materials.* Journal of alloys and compounds, 1997. **253**: p. 1-9.
362. Ley, M.B., et al., *Development of hydrogen storage tank systems based on complex metal hydrides.* Materials, 2015. **8**(9): p. 5891-5921.
363. Swisher, J.H. and E.D. Johnson, *Hydrides versus competing options for storing hydrogen in energy systems.* Journal of the Less Common Metals, 1980. **74**(2): p. 301-320.
364. Carpetis, C., *A system consideration of alternative hydrogen storage facilities for estimation of storage costs.* International Journal of Hydrogen Energy, 1980. **5**(4): p. 423-437.
365. Padro, C.E. and V. Putsche, *Survey of the economics of hydrogen technologies*. 1999, National Renewable Energy Lab., Golden, CO (US).
366. Meille, V. and I. Pitault, *Liquid Organic Hydrogen Carriers or Organic Liquid Hydrides: 40 Years of History.* Reactions, 2021. **2**(2): p. 94-101.
367. Bockris, J.O.M., *The hydrogen economy: Its history.* International Journal of Hydrogen Energy, 2013. **38**(6): p. 2579-2588.
368. Sultan, O. and H. Shaw, *Study of automotive storage of hydrogen using recyclable liquid chemical carriers.* NASA STI/Recon Technical Report N, 1975. **76**.
369. Preuster, P., C. Papp, and P. Wasserscheid, *Liquid Organic Hydrogen Carriers (LOHCs): Toward a Hydrogen-free Hydrogen Economy.* Acc Chem Res, 2017. **50**(1): p. 74-85.
370. Newson, E., et al., *Seasonal storage of hydrogen in stationary systems with liquid organic hydrides.* International Journal of Hydrogen Energy, 1998. **23**(10): p. 905-909.
371. Aakko-Saksa, P.T., et al., *Liquid organic hydrogen carriers for transportation and storing of renewable energy–Review and discussion.* Journal of Power Sources, 2018. **396**: p. 803-823.
372. Makepeace, J.W., et al., *Reversible ammonia-based and liquid organic hydrogen carriers for high-density hydrogen storage: Recent progress.* international journal of hydrogen energy, 2019. **44**(15): p. 7746-7767.
373. Modisha, P.M., et al., *The prospect of hydrogen storage using liquid organic hydrogen carriers.* Energy & fuels, 2019. **33**(4): p. 2778-2796.
374. Esche, E. and J.U. Repke, *Dynamic Process Operation Under Demand Response–A Review of Methods and Tools.* Chemie Ingenieur Technik, 2020. **92**(12): p. 1898-1909.
375. Cui, X., S.K. Kær, and M.P. Nielsen, *Energy analysis and surrogate modeling for the green methanol production under dynamic operating conditions.* Fuel, 2022. **307**: p. 121924.
376. Riese, J. and M. Grünewald, *Challenges and Opportunities to Enhance Flexibility in Design and Operation of Chemical Processes.* Chemie Ingenieur Technik, 2020.
377. Swartz, C.L.E. and Y. Kawajiri, *Design for dynamic operation - A review and new perspectives for an increasingly dynamic plant operating environment.* Computers & Chemical Engineering, 2019. **128**: p. 329-339.
378. Stankiewicz, A. and M. Kuczynski, *An industrial view on the dynamic operation of chemical converters.* Chemical Engineering and Processing: Process Intensification, 1995. **34**(4): p. 367-377.
379. Wei, M., C.A. McMillan, and S. de la Rue du Can, *Electrification of Industry: Potential, Challenges and Outlook.* Current Sustainable/Renewable Energy Reports, 2019. **6**(4): p. 140-148.
380. Burre, J., et al., *Power-to-X: Between Electricity Storage, e-Production, and Demand Side Management.* Chemie Ingenieur Technik, 2020. **92**(1-2): p. 74-84.
381. Daiyan, R., I. MacGill, and R. Amal, *Opportunities and Challenges for Renewable Power-to-X.* ACS Energy Letters, 2020. **5**(12): p. 3843-3847.
382. IEA, *Ammonia Technology Roadmap*. 2021, IEA: Paris.
383. Morgan, E., J. Manwell, and J. McGowan, *Wind-powered ammonia fuel production for remote islands: A case study.* Renewable Energy, 2014. **72**: p. 51-61.
384. Bañares-Alcántara, R., et al., *Analysis of islanded ammonia-based energy storage systems.* University of Oxford, 2015.
385. Klerke, A., et al., *Ammonia for hydrogen storage: challenges and opportunities.* Journal of Materials Chemistry, 2008. **18**(20): p. 2304-2310.
386. Morgan, E.R., *Techno-economic feasibility study of ammonia plants powered by offshore wind*. 2013: University of Massachusetts Amherst.
387. Appl, M., *Ammonia, 2. Production Processes*, in *Ullmann's Encyclopedia of Industrial Chemistry*. 2011.
388. Rouwenhorst, K.H., et al., *Islanded ammonia power systems: Technology review & conceptual process design.* Renewable and Sustainable Energy Reviews, 2019. **114**: p. 109339.
389. Rouwenhorst, K.H.R., et al., *Ammonia, 4. Green Ammonia Production*, in *Ullmann's Encyclopedia of Industrial Chemistry*. p. 1-20.
390. Hellman, A., et al., *Ammonia synthesis: state of the bellwether reaction*, in *Comprehensive Inorganic Chemistry II (Second Edition): From Elements to Applications*. 2013, Elsevier. p. 459-474.
391. Mittasch, A. and W. Frankenburg, *Early Studies of Multicomponent Catalysts*, in *Advances in Catalysis*, W.G. Frankenburg, V.I. Komarewsky, and E.K. Rideal, Editors. 1950, Academic Press. p. 81-104.

392. Fasihi, M., O. Efimova, and C. Breyer, *Techno-economic assessment of CO2 direct air capture plants.* Journal of cleaner production, 2019. **224**: p. 957-980.
393. Frattini, D., et al., *A system approach in energy evaluation of different renewable energies sources integration in ammonia production plants.* Renewable Energy, 2016. **99**: p. 472-482.
394. Smith, C., A.K. Hill, and L. Torrente-Murciano, *Current and future role of Haber–Bosch ammonia in a carbon-free energy landscape.* Energy & Environmental Science, 2020. **13**(2): p. 331-344.
395. Cinti, G., et al., *Coupling Solid Oxide Electrolyser (SOE) and ammonia production plant.* Applied energy, 2017. **192**: p. 466-476.
396. MacFarlane, D.R., et al., *A roadmap to the ammonia economy.* Joule, 2020. **4**(6): p. 1186-1205.
397. Cheema, I.I. and U. Krewer, *Operating envelope of Haber–Bosch process design for power-to-ammonia.* RSC advances, 2018. **8**(61): p. 34926-34936.
398. Castle, W., *Air separation and liquefaction: recent developments and prospects for the beginning of the new millennium.* International Journal of Refrigeration, 2002. **25**(1): p. 158-172.
399. Smith, A. and J. Klosek, *A review of air separation technologies and their integration with energy conversion processes.* Fuel processing technology, 2001. **70**(2): p. 115-134.
400. Sánchez, A. and M. Martín, *Scale up and scale down issues of renewable ammonia plants: Towards modular design.* Sustainable Production and Consumption, 2018. **16**: p. 176-192.
401. Wang, M., et al., *Can sustainable ammonia synthesis pathways compete with fossil-fuel based Haber–Bosch processes?* Energy & Environmental Science, 2021. **14**(5): p. 2535-2548.
402. Aneke, M. and M. Wang, *Potential for improving the energy efficiency of cryogenic air separation unit (ASU) using binary heat recovery cycles.* Applied thermal engineering, 2015. **81**: p. 223-231.
403. Palys, M.J. and P. Daoutidis, *Using hydrogen and ammonia for renewable energy storage: A geographically comprehensive techno-economic study.* Computers & Chemical Engineering, 2020: p. 106785.
404. Grinberg Dana, A., et al., *Nitrogen-Based Fuels: A Power-to-Fuel-to-Power Analysis.* Angew Chem Int Ed Engl, 2016. **55**(31): p. 8798-805.
405. Hardenburger, T.L., M. Ennis, and U.b. Staff, *Nitrogen*, in *Kirk-Othmer Encyclopedia of Chemical Technology*. 2005.
406. Osman, O., S. Sgouridis, and A. Sleptchenko, *Scaling the production of renewable ammonia: A techno-economic optimization applied in regions with high insolation.* Journal of Cleaner Production, 2020. **271**: p. 121627.
407. Giddey, S., et al., *Ammonia as a Renewable Energy Transportation Media.* Acs Sustainable Chemistry & Engineering, 2017. **5**(11): p. 10231-10239.
408. Nayak-Luke, R., R. Bañares-Alcántara, and I. Wilkinson, *"Green" ammonia: impact of renewable energy intermittency on plant sizing and levelized cost of ammonia.* Industrial & Engineering Chemistry Research, 2018. **57**(43): p. 14607-14616.
409. Fuhrmann, J., M. Hülsebrock, and U. Krewer, *Energy storage based on electrochemical conversion of ammonia.* Transition to Renewable Energy Systems, 2013: p. 691-706.
410. Ostuni, R. and F. Zardi, *Method for load regulation of an ammonia plant*. 2016, Google Patents.
411. Armijo, J. and C. Philibert, *Flexible production of green hydrogen and ammonia from variable solar and wind energy: Case study of Chile and Argentina.* International Journal of Hydrogen Energy, 2020. **45**(3): p. 1541-1558.
412. Verleysen, K., A. Parente, and F. Contino, *How sensitive is a dynamic ammonia synthesis process? Global sensitivity analysis of a dynamic Haber-Bosch process (for flexible seasonal energy storage).* Energy, 2021: p. 121016.
413. Gullberg, R.M.B., *Controllability Analysis of Ammonia Synthesis Loops*. 2018, NTNU.
414. Corbetta, R.O.M.B.M., *Dynamic Analysis of Casale Green Ammonia Synthesis Process*. 2021, Casale.
415. Nielsen, R., *Topsoes Ammonia cracking technology – Delivering green Hydrogen*. 2021, Haldor Topsoe.
416. Bagga, K., *Flexible green ammonia synthesis and large scale ammonia cracking technology by Uhde®* 2021, thyssenkrupp Uhde: AEA conference.
417. *D2.2: Public report on industrial requirements*, ENGIE, Editor. 2021, Advanced Materials and Reactors for Energy Storage Through Ammonia.
418. Klein, H., et al., *Flexible Operation of Air Separation Units.* ChemBioEng Reviews, 2021. **8**(4): p. 357-374.
419. Caspari, A., et al., *Economic nonlinear model predictive control for flexible operation of air separation units.* IFAC-PapersOnLine, 2018. **51**(20): p. 295-300.
420. Caspari, A., et al., *A flexible air separation process: 1. Design and steady-state optimizations.* AIChE Journal, 2019. **65**(11): p. e16705.
421. Caspari, A., et al., *A flexible air separation process: 2. Optimal operation using economic model predictive control.* AIChE Journal, 2019. **65**(11): p. e16721.
422. Cesaro, Z., et al., *Ammonia to power: Forecasting the levelized cost of electricity from green ammonia in large-scale power plants.* Applied Energy, 2021. **282**: p. 116009.
423. Jackson, C., et al., *Ammonia to Green Hydrogen Project: Feasibility Study*. 2020.
424. Makhloufi, C. and N. Kezibri, *Large-scale decomposition of green ammonia for pure hydrogen production.* International Journal of Hydrogen Energy, 2021. **46**(70): p. 34777-34787.
425. Lucentini, I., et al., *Review of the Decomposition of Ammonia to Generate Hydrogen.* Industrial & Engineering Chemistry Research, 2021.
426. Nasharuddin, R., et al., *A techno-economic analysis of centralised and distributed processes of ammonia dissociation to hydrogen for fuel cell vehicle applications.* International Journal of Hydrogen Energy, 2019. **44**(28): p. 14445-14455.
427. Ishimoto, Y., et al., *Large-scale production and transport of hydrogen from Norway to Europe and Japan: Value chain analysis and comparison of liquid hydrogen and ammonia as energy carriers.* International Journal of Hydrogen Energy, 2020. **45**(58): p. 32865-32883.
428. Wismann, S.T., *Electrically heated steam methane reforming*, in *Department of Physics*. 2019, Technical University of Denmark (DTU).
429. Wismann, S.T., et al., *Electrified methane reforming: A compact approach to greener industrial hydrogen production.* Science, 2019. **364**(6442): p. 756-759.

430. Wismann, S.T., et al., *Electrified methane reforming: Elucidating transient phenomena.* Chemical Engineering Journal, 2021. **425**: p. 131509.
431. Mølgaard Mortensen, P., et al., *On Demand Hydrogen From Methanol*, W.I.P. Organization, Editor. 2020, Haldor Topsøe A/S.
432. Jorschick, H., et al., *Hydrogenation of aromatic and heteroaromatic compounds–a key process for future logistics of green hydrogen using liquid organic hydrogen carrier systems.* Sustainable Energy & Fuels, 2021. **5**(5): p. 1311-1346.
433. Bulgarin, A., et al., *Purity of hydrogen released from the Liquid Organic Hydrogen Carrier compound perhydro dibenzyltoluene by catalytic dehydrogenation.* International Journal of Hydrogen Energy, 2020. **45**(1): p. 712-720.
434. Müller, K., J. Völkl, and W. Arlt, *Thermodynamic evaluation of potential organic hydrogen carriers.* Energy Technology, 2013. **1**(1): p. 20-24.
435. Hurskainen, M., *Liquid organic hydrogen carriers (LOHC): Concept evaluation and techno-economics.* 2019.
436. Brückner, N., et al., *Evaluation of Industrially Applied Heat-Transfer Fluids as Liquid Organic Hydrogen Carrier Systems.* ChemSusChem, 2014. **7**(1): p. 229-235.
437. Okada, Y. and M. Shimura. *Development of large-scale H_2 storage and transportation technology with Liquid Organic Hydrogen Carrier (LOHC)*. in *The 21st joint GCC-Japan environment symposium*. 2013.
438. Teichmann, D., et al., *A future energy supply based on liquid organic hydrogen carriers (LOHC).* Energy & Environmental Science, 2011. **4**(8): p. 2767-2773.
439. Müller, K., et al., *Experimental assessment of the degree of hydrogen loading for the dibenzyl toluene based LOHC system.* International Journal of Hydrogen Energy, 2016. **41**(47): p. 22097-22103.
440. Wulf, C. and P. Zapp, *Assessment of system variations for hydrogen transport by liquid organic hydrogen carriers.* International Journal of Hydrogen Energy, 2018.
441. *LOHC production cost estimation study*, in *Hydrogen Supply and Transportation Using Liquid Organic Hydrogen Carriers (HYSTOC)*. 2020, VTT.
442. Teichmann, D., et al., *Transport and Storage of Hydrogen via Liquid Organic Hydrogen Carrier (LOHC) Systems*, in *Hydrogen Science and Engineering : Materials, Processes, Systems and Technology*. 2016, Wiley-VCH Verlag GmbH & Co. KGaA. p. 811-830.
443. Gianotti, E., et al., *High-Purity Hydrogen Generation via Dehydrogenation of Organic Carriers: A Review on the Catalytic Process.* ACS Catalysis, 2018. **8**(5): p. 4660-4680.
444. Geißelbrecht, M., et al., *Highly efficient, low-temperature hydrogen release from perhydro-benzyltoluene using reactive distillation.* Energy & Environmental Science, 2020. **13**(9): p. 3119-3128.
445. Müller, K., T. Skeledzic, and P. Wasserscheid, *Strategies for Low-Temperature Liquid Organic Hydrogen Carrier Dehydrogenation.* Energy & Fuels, 2021.
446. Kwak, Y., et al., *Hydrogen production from homocyclic liquid organic hydrogen carriers (LOHCs): Benchmarking studies and energy-economic analyses.* Energy Conversion and Management, 2021. **239**: p. 114124.
447. Raab, M., S. Maier, and R.-U. Dietrich, *Comparative techno-economic assessment of a large-scale hydrogen transport via liquid transport media.* International Journal of Hydrogen Energy, 2021. **46**(21): p. 11956-11968.
448. Olah, G.A., *Beyond oil and gas: the methanol economy.* Angewandte Chemie International Edition, 2005. **44**(18): p. 2636-2639.
449. Palo, D.R., R.A. Dagle, and J.D. Holladay, *Methanol steam reforming for hydrogen production.* Chem Rev, 2007. **107**(10): p. 3992-4021.
450. Jaggai, C., et al., *Towards greater sustainable development within current Mega-Methanol (MM) production.* Green Chemistry, 2020. **22**(13): p. 4279-4294.
451. *Innovation Outlook: Renewable Methanol*. 2021, IRENA and Methanol Institute: Abu Dhabi.
452. Sheldon, D., *Methanol Production-A Technical History*. Johnson Matthey Technology Review, 2017. **61**(3): p. 172-182.
453. Goeppert, A., et al., *Recycling of carbon dioxide to methanol and derived products–closing the loop.* Chemical Society Reviews, 2014. **43**(23): p. 7995-8048.
454. Bergins, C., et al., *A Technology Review and Cost Analysis of the Production of Low Carbon Methanol and Following Methanol to Gasoline Process*, in *Zukünftige Kraftstoffe*. 2019, Springer. p. 433-463.
455. Dieterich, V., et al., *Power-to-liquid via synthesis of methanol, DME or Fischer–Tropsch-fuels: a review.* Energy & Environmental Science, 2020.
456. Ott, J., et al., *Methanol.* Ullmann's Encyclopedia of Industrial Chemistry, 2000.
457. Schittkowski, J., et al., *Methanol Synthesis from Steel Mill Exhaust Gases: Challenges for the Industrial $Cu/ZnO/Al_2O_3$ Catalyst.* Chemie Ingenieur Technik, 2018.
458. Frei, M.S., et al., *Methanol as a Hydrogen Carrier: Kinetic and Thermodynamic Drivers for its CO_2-Based Synthesis and Reforming over Heterogeneous Catalysts.* ChemSusChem, 2020.
459. Behrens, M., *Chemical hydrogen storage by methanol: Challenges for the catalytic methanol synthesis from CO_2.* Recyclable Catalysis, 2015. **2**(1).
460. Marlin, D.S., E. Sarron, and Ó. Sigurbjörnsson, *Process Advantages of Direct CO_2 to Methanol Synthesis.* Frontiers in chemistry, 2018. **6**.
461. Pontzen, F., et al., *CO_2-based methanol and DME–Efficient technologies for industrial scale production.* Catalysis Today, 2011. **171**(1): p. 242-250.
462. Schemme, S., et al., *H2-based synthetic fuels: a techno-economic comparison of alcohol, ether and hydrocarbon production.* International journal of hydrogen energy, 2020. **45**(8): p. 5395-5414.
463. Schorn, F., et al., *Methanol as a renewable energy carrier: An assessment of production and transportation costs for selected global locations.* Advances in Applied Energy, 2021. **3**: p. 100050.
464. Cheng, W.H. and H.H. Kung, *Methanol production and use*. 1994, New York, NY (United States): Marcel Dekker Inc.
465. Kastens, M., J. Dudley, and J. Troeltzsch, *Synthetic Methanol Manufacture.* Industrial & Engineering Chemistry, 1948. **40**(12): p. 2230-2240.

466. Sarp, S., et al., *Alcohol production from carbon dioxide: methanol as a fuel and chemical feedstock.* Joule, 2021. **5**(1): p. 59-76.
467. Perez-Fortes, M., et al., *Methanol synthesis using captured CO_2 as raw material: Techno-economic and environmental assessment.* Applied Energy, 2016. **161**: p. 718-732.
468. Nyári, J., et al., *Techno-economic barriers of an industrial-scale methanol CCU-plant.* Journal of CO_2 Utilization, 2020. **39**: p. 101166.
469. Hensel, C.S.F.K.S.W.R., *Methanol Production at Waste to Energy Plants*, in *Waste Management, Volume 9: Waste-to-Energy*, S.T.E. Thomé-Kozmiensky, Editor. 2019, Thomé-Kozmiensky Verlag GmbH: Neuruppin.
470. Otto, A., *Chemische, verfahrenstechnische und ökonomische Bewertung von Kohlendioxid als Rohstoff in der chemischen Industrie*. 2015: Forschungszentrum Jülich GmbH, Zentralbibliothek.
471. Bergins, C., et al. *Power to Methanol Solutions for Flexible and Sustainable Operations in Power and Process Industries*. in *Power-Gen Europe*. 2015.
472. Atsonios, K., K.D. Panopoulos, and E. Kakaras, *Investigation of technical and economic aspects for methanol production through CO_2 hydrogenation.* International Journal of Hydrogen Energy, 2016. **41**(4): p. 2202-2214.
473. Hank, C., et al., *Economics & carbon dioxide avoidance cost of methanol production based on renewable hydrogen and recycled carbon dioxide–power-to-methanol.* 2018. **2**(6): p. 1244-1261.
474. Schweitzer, C. *Small scale Methanol Plants: a chance for re-industrialisation*. in *International Methanol Conference*. 2017. Copenhagen.
475. Ruland, H., et al., *CO_2 hydrogenation with Cu/ZnO/Al_2O_3: A benchmark study.* ChemCatChem, 2020.
476. Zurbel, A., et al., *Methanol synthesis by CO_2 Hydrogenation over Cu/ZnO/Al_2O_3 catalysts under fluctuating conditions.* Chemie Ingenieur Technik, 2018. **90**(5): p. 721-724.
477. Chen, C. and A. Yang, *Power-to-methanol: The role of process flexibility in the integration of variable renewable energy into chemical production.* Energy Conversion and Management, 2021. **228**: p. 113673.
478. Varela, C., et al., *Agile Operation of Renewable Methanol Synthesis under Fluctuating Power Inputs*, in *Computer Aided Chemical Engineering*, S. Pierucci, et al., Editors. 2020, Elsevier. p. 1381-1386.
479. Stießel, S., et al., *Methodology for the Evaluation of CO_2-Based Syntheses by Coupling Steel Industry with Chemical Industry.* Chemie Ingenieur Technik, 2018. **90**(10): p. 1392-1408.
480. Subramani, V., et al., *Catalytic steam reforming technology for the production of hydrogen and syngas*. 2010: John Wiley and Sons: Hoboken, NY, USA.
481. Agrell, J., et al., *Catalytic hydrogen generation from methanol.* Catalysis, 2002. **16**(67): p. 1-2.
482. Haid, J. and U. Koss, *Lurgi's Mega-Methanol technology opens the door for a new era in down-stream applications*, in *Studies in Surface Science and Catalysis*. 2001, Elsevier. p. 399-404.
483. Bertau, M., et al., *Methanol Utilisation Technologies*, in *Methanol: The Basic Chemical and Energy Feedstock of the Future: Asinger's Vision Today*, M. Bertau, et al., Editors. 2014, Springer Berlin Heidelberg: Berlin, Heidelberg. p. 327-601.
484. Neumann, P. and F. von Linde, *Options for economical supply of hydrogen.* Metallurgical Plant and Technology International, 2003(2): p. 72-75.
485. Iulianelli, A., et al., *Methanol steam reforming for hydrogen generation via conventional and membrane reactors: A review.* Renewable & Sustainable Energy Reviews, 2014. **29**: p. 355-368.
486. Heo, J., et al., *Deterministic and stochastic economic analysis based on historical natural gas and CO_2 allowance prices for steam reforming of methanol.* Energy Conversion and Management, 2019. **193**: p. 140-148.
487. Rostrup-Nielsen, J. and L. Christiansen, *Catalytic Science Series: Concepts in Syngas Manufacture*. 2011, Imperial College Press, Singapore, US, US.
488. Voldsund, M., K. Jordal, and R. Anantharaman, *Hydrogen production with CO_2 capture.* International Journal of Hydrogen Energy, 2016. **41**(9): p. 4969-4992.
489. Sircar, S. and T.C. Golden, *Pressure swing adsorption technology for hydrogen production.* Hydrogen and syngas production and purification technologies, 2009. **10**: p. 414-450.
490. Ritter, J.A. and A.D. Ebner, *State-of-the-Art Adsorption and Membrane Separation Processes for Hydrogen Production in the Chemical and Petrochemical Industries.* Separation Science and Technology, 2007. **42**(6): p. 1123-1193.
491. Mortensen, P.M., M. Østberg, and P.E.H. Nielsen, *Process for producing hydrogen or syngas by methanol cracking*. 2021, Google Patents.
492. Durusut, E. and M. Joos, *Shipping CO2–UK Cost Estimation Study.* Final Report for BEIS (Department for Business, Energy & Industrial Strategy, Hrsg.). Cambridge: Element Energy Limited, 2018.
493. Brynolf, S., et al., *Electrofuels for the transport sector: A review of production costs.* Renewable and Sustainable Energy Reviews, 2018. **81**: p. 1887-1905.
494. Irlam, L., *Global costs of carbon capture and storage.* Global CCS institute, 2017.
495. Tottie, J.A.G.H.M., *Process for the production of carburized sponge iron*. 2020, Hybrit Development AB.
496. Angelidaki, I., et al., *Biogas upgrading and utilization: Current status and perspectives.* Biotechnol Adv, 2018. **36**(2): p. 452-466.
497. Bäcklin, Å., *HYBRIT: Fossil free gas heating – an important step towards fossil free steel*. 2021, Hybrit Development AB.
498. Brown, A., et al., *Advanced Biofuels—Potential for Cost Reduction.* IEA Bioenergy, 2020. **88**.
499. Thunman, H., et al., *Economic assessment of advanced biofuel production via gasification using cost data from the GoBiGas plant.* Energy Science & Engineering, 2019. **7**(1): p. 217-229.
500. Energimyndigheten. *Trädbränsle- och torvpriser*. 2019; Available from: https://www.energimyndigheten.se/statistik/den-officiella-statistiken/statistikprodukter/tradbransle--och-torvpriser/?currentTab=2#mainheading.
501. Lindroos, T.J., et al., *Replacing fossil fuels with bioenergy in district heating – Comparison of technology options.* Energy, 2021. **231**: p. 120799.
502. Friedmann, B., Z. FAN, and K. Tang, *Low-Carbon heat solutions for heavy industry: sources, options, and costs today*. 2019, New York, New York.

503. Thiel, G.P. and A.K. Stark, *To decarbonize industry, we must decarbonize heat.* Joule, 2021.
504. Toftegaard, M.B., et al., *Oxy-fuel combustion of solid fuels.* Progress in Energy and Combustion Science, 2010. **36**(5): p. 581-625.
505. Landälv, I., et al., *Two years experience of the BioDME project—A complete wood to wheel concept.* Environmental Progress & Sustainable Energy, 2014. **33**(3): p. 744-750.
506. Eriksson, A., et al., *Effect of Varied Oxygen Levels on the Oxidation of a Magnetite Pellet Bed during Pot Furnace Induration.* ISIJ International, 2021: p. ISIJINT-2020-469.
507. Saxe, M. and P. Alvfors, *Advantages of integration with industry for electrolytic hydrogen production.* Energy, 2007. **32**(1): p. 42-50.
508. Becerra-Novoa, J.O., et al., *Integrated steel plant with production of hot or cold DRI*. 2015, Google Patents.
509. Gandt, K., et al., *Heat recovery from EAF off-gas for steam generation: analytical exergy study of a sample EAF batch.* Ironmaking & Steelmaking, 2016. **43**(8): p. 581-587.
510. Steinparzer, T., et al., *Electric Arc Furnace Off-Gas Heat Recovery and Experience with a Testing Plant.* steel research international, 2014. **85**(4): p. 519-526.
511. Vance, D., et al., *Estimation of and barriers to waste heat recovery from harsh environments in industrial processes.* Journal of Cleaner Production, 2019. **222**: p. 539-549.
512. Keplinger, T., et al., *Dynamic simulation of an electric arc furnace waste heat recovery system for steam production.* Applied Thermal Engineering, 2018. **135**: p. 188-196.
513. Keplinger, T., et al., *Modeling, simulation, and validation with measurements of a heat recovery hot gas cooling line for electric arc furnaces.* steel research international, 2018. **89**(6): p. 1800009.
514. Herz, G., et al., *High Temperature Co-Electrolysis as a Key Technology for CO_2 Emission Mitigation–A Model-Based Assessment of CDA and CCU.* Chemie Ingenieur Technik, 2020. **92**(8): p. 1044-1058.
515. Eypasch, M., et al., *Model-based techno-economic evaluation of an electricity storage system based on Liquid Organic Hydrogen Carriers.* Applied Energy, 2017. **185**(Part 1): p. 320-330.
516. Sircar, S., et al., *Hydrogen production by hybrid SMR–PSA–SSF membrane system.* Separation and Purification Technology, 1999. **17**(1): p. 11-20.
517. Kim, S., et al., *Steam reforming of methanol for ultra-pure H_2 production in a membrane reactor: Techno-economic analysis.* International Journal of Hydrogen Energy, 2019. **44**(4): p. 2330-2339.
518. Zhang, H., et al., *Techno-economic optimization of CO_2-to-methanol with solid-oxide electrolyzer.* Energies, 2019. **12**(19): p. 3742.
519. Wang, L., et al., *Power-to-fuels via solid-oxide electrolyzer: Operating window and techno-economics.* Renewable and Sustainable Energy Reviews, 2019. **110**: p. 174-187.
520. Andika, R., et al., *Co-electrolysis for power-to-methanol applications.* Renewable and Sustainable Energy Reviews, 2018. **95**: p. 227-241.
521. Abdin, Z., et al., *Large-scale stationary hydrogen storage via liquid organic hydrogen carriers.* Iscience, 2021. **24**(9): p. 102966.
522. Towler, G. and R. Sinnott, *Chemical engineering design: principles, practice and economics of plant and process design*. 2012: Elsevier.
523. Tribe, M.A. and R.L.W. Alpine, *Scale economies and the "0.6 rule".* Engineering Costs and Production Economics, 1986. **10**(4): p. 271-278.
524. Peters, M.S., K.D. Timmerhaus, and R.E. West, *Plant design and economics for chemical engineers*. Vol. 4. 2003: McGraw-Hill New York.
525. Tremel, A., et al., *Techno-economic analysis for the synthesis of liquid and gaseous fuels based on hydrogen production via electrolysis.* International Journal of Hydrogen Energy, 2015. **40**(35): p. 11457-11464.
526. Turton, R.B., Richard C.; Whiting, Wallace B.: Shaeiwitz, Joseph A.; Bhattacharyya, Debangsu *Analysis, synthesis, and design of chemical processes*. 4th ed, ed. R. Turton. 2012: Place of publication not identified Prentice Hall.
527. Fasihi, M., et al., *Global potential of green ammonia based on hybrid PV-wind power plants.* Applied Energy, 2021. **294**: p. 116170.
528. Loh, H., J. Lyons, and C.W. White, *Process equipment cost estimation, final report*. 2002, National Energy Technology Lab.(NETL), Morgantown, WV (United States).
529. Langefeld, J. *Construction of Large Crude Oil Storage Tanks Utilizing High Tensile Steel*. in *7th World Petroleum Congress*. 1967. OnePetro.
530. Pouyakian, M., et al., *A comprehensive approach to analyze the risk of floating roof storage tanks.* Process Safety and Environmental Protection, 2021. **146**: p. 811-836.
531. de Wit, J., *Steel Vertical Cylindrical Storage Tanks*, in *Mechanical Engineer's Reference Book (Eleventh Edition)*, A. Parrish, Editor. 1973, Butterworth-Heinemann. p. 11-2-11-14.
532. Müller, K., et al., *Liquid organic hydrogen carriers: thermophysical and thermochemical studies of benzyl-and dibenzyl-toluene derivatives.* Industrial & Engineering Chemistry Research, 2015. **54**(32): p. 7967-7976.
533. *Methanol-Water Density: Datasheet from "Dortmund Data Bank (DDB) – Thermophysical Properties Edition 2014" in SpringerMaterials (https://materials.springer.com/thermophysical/docs/ve1_c110c174)*. Springer-Verlag Berlin Heidelberg & DDBST GmbH, Oldenburg, Germany.
534. Khodadadi, A., et al. *Nordic balancing markets: Overview of market rules*. in *2020 17th International Conference on the European Energy Market (EEM)*. 2020. IEEE.
535. Stenqvist, C. and L.J. Nilsson, *Energy efficiency in energy-intensive industries—an evaluation of the Swedish voluntary agreement PFE.* Energy Efficiency, 2012. **5**(2): p. 225-241.
536. Edfeldt, E. and E. Wiesner, *Industrins elkostnader – ligger Sverige så lågt som många säger?* 2018, Sweco.
537. Andersson, J. and S. Grönkvist, *A comparison of two hydrogen storages in a fossil-free direct reduced iron process.* International Journal of Hydrogen Energy, 2021. **46**(56): p. 28657-28674.
538. Zong, Y., et al. *Identifying the System-related Conditions and Consequences of Power-to-X Solutions for a High Renewables Penetration in Denmark*. in *2020 IEEE 4th Conference on Energy Internet and Energy System Integration (EI2)*. 2020. IEEE.
539. Spodniak, P., K. Ollikka, and S. Honkapuro, *The impact of wind power and electricity demand on the relevance of different short-term electricity markets: The Nordic case.* Applied Energy, 2021. **283**: p. 116063.

540. Bosma, R.v.G.M.E.T., *Hydrogen in the Electricity Value Chain*, in *Position paper*. 2019, DNV GL.
541. Eichman, J., A. Townsend, and M. Melaina, *Economic assessment of hydrogen technologies participating in California electricity markets*. 2016, National Renewable Energy Lab.(NREL), Golden, CO (United States).
542. SCB, *Elförsörjning 2021*. 2022.
543. Forsberg, C., *Addressing the low-carbon million-gigawatt-hour energy storage challenge.* The Electricity Journal, 2021. **34**(10): p. 107042.
544. Ruhnau, O., *How flexible electricity demand stabilizes wind and solar market values: the case of hydrogen electrolyzers.* 2021.
545. He, G., et al., *Sector coupling via hydrogen to lower the cost of energy system decarbonization.* arXiv preprint arXiv:2103.03442, 2021.
546. Witkowski, A., et al., *Comprehensive analysis of hydrogen compression and pipeline transportation from thermodynamics and safety aspects.* Energy, 2017. **141**: p. 2508-2518.
547. Haldor Topsoe A/S, *Energy Efficient Production of Pressurized Hydrogen - Final Report*. 2016.
548. Brinkman, L., B. Bulfin, and A. Steinfeld, *Thermochemical Hydrogen Storage via the Reversible Reduction and Oxidation of Metal Oxides.* Energy & Fuels, 2021. **35**(22): p. 18756-18767.
549. Meys, R., et al., *Achieving net-zero greenhouse gas emission plastics by a circular carbon economy.* Science, 2021. **374**(6563): p. 71-76.
550. Korberg, A.D., et al., *Techno-economic assessment of advanced fuels and propulsion systems in future fossil-free ships.* Renewable and Sustainable Energy Reviews, 2021. **142**: p. 110861.
551. González-Aparicio, I., Z. Kapetaki, and E. Tzimas, *Wind energy and carbon dioxide utilisation as an alternative business model for energy producers: A case study in Spain.* Applied Energy, 2018. **222**: p. 216-227.
552. Energinet, *PtX in Denmark Before 2030: Short term potential of PtX in Denmark from a system perspective* 2019, Energinet.
553. Blumberg, T., G. Tsatsaronis, and T. Morosuk, *On the economics of methanol production from natural gas.* Fuel, 2019. **256**: p. 115824.
554. Methanex Corporation. *Historical Methanex Posted Price*. [cited 2022 25/1]; Available from: https://www.methanex.com/.
555. Bos, M., S. Kersten, and D. Brilman, *Wind power to methanol: Renewable methanol production using electricity, electrolysis of water and CO2 air capture.* Applied Energy, 2020. **264**: p. 114672.

ACKNOWLEDGMENTS

The work presented in this thesis would not have been possible without the help and support of countless people. I would first like to thank my main supervisor, Stefan Grönkvist, for allowing me to pursue this project. I do not think that I can even begin to list all the things I have learned from you, so I will avoid it. Thanks for the many amusing and interesting discussions on various non-work-related topics over the years.

I would also like to thank Nicklas Simonson and Per Holmberg at Vattenfall for their excellent guidance throughout the project. Thanks to Andries Krüger for the enjoyable and fruitful collaborations on papers II and III. Thanks also to Henrik, Christer, Volker, and Farzad at Hybrit Development for all the productive discussions and support, in particular when it came to questions about iron and steelmaking. I am grateful to all involved in HYBRIT RP1 for making all project conferences, meetings, and study visits so much fun. I also want to thank Joakim Lundgren for his very helpful review of this thesis.

I also have to mention all colleagues and friends at the division of Energy Processes and the division of Applied Electrochemistry. Thanks for the many laughs and, at times, bizarre lunch and fika conversations. Special thanks go out to my longest-time roommate Yang Zhang for welcoming me to Energy Processes with such warmth and Adrian Lefvert for fabulous drumming and fun times during travels.

Thank you Ludde and Mårten for the Thursday dinners. Let´s keep that tradition going. I would like to thank mention Kaj och Kanoterna for all the magnificent canoeing trips over the last couple of years.

Tack Mamma och Pappa för allt stöd genom åren.

Finally, thank you Caroline, mainly for being you, but also for everything you have done for me over the last more than three years and for accepting me for who I am. I could not have done this without you.